UNITED STATES
NAVAL POSTGRADUATE SCHOOL

AN INVESTIGATION OF THE EFFECT OF ACCELERATION ON THE BURNING RATE OF COMPOSITE PROPELLANTS

by

J. B. ANDERSON

and

R. E. REICHENBACH

NPS-57RV7071A
28 July 1967

AN INVESTIGATION OF THE EFFECT OF ACCELERATION ON THE BURNING RATE OF COMPOSITE PROPELLANTS

by

J. B. Anderson

and

R. E. Reichenbach

NAVAL POSTGRADUATE SCHOOL

Monterey, California

AN INVESTIGATION OF THE EFFECT OF ACCELERATION ON THE BURNING RATE OF COMPOSITE PROPELLANTS*

by

J. B. Anderson

and

R. E. Reichenbach

1967

ABSTRACT

The average burning rates of composite solid rocket propellant were measured in acceleration fields up to 2000 times the standard acceleration of gravity. The acceleration vector was perpendicular to and into the burning surface. Propellant strands were burned in a combustion bomb mounted on a centrifuge, and surge tanks were employed to ensure essentially constant pressure burning at 500, 1000, and 1500 psia. The burning rates of both aluminized and non-aluminized composite propellants were found to depend on acceleration. The effect of acceleration on burning rate was found to depend on the burning rate of the propellant without acceleration, aluminum mass loading, and aluminum mass median particle size. The relative burning rate increase was found to be greater for slow burning propellant than for faster burning propellants. The experimental results are compared to the analytical models proposed by Crowe for aluminized propellants and by Glick for non-aluminized propellants. The results indicate that these models do not adequately predict the observed relative burning rate increase with acceleration, and hence that more complex modeling will be required to explain the observed acceleration effect.

TABLE OF CONTENTS

LIST OF TABLES

LIST OF FIGURES

I. INTRODUCTION

Development programs involving spin-stabilized vehicles propelled by solid propellant rocket motors have shown that a motor spinning about its longitudinal axis performs differently than does a similar motor at rest. Typically, spinning motor performance is characterized by a shorter burning time, higher chamber pressure, and lower total impulse. In addition, inspections of motors fired on spin-test rigs have revealed residues in the motor cases comprising several per cent of the initial propellant mass. The review and abstracting of reference material pertinent to the effects of acceleration on solid propellant performance is presented in Refs. 1 and 2.

The investigation reported here was concerned with one probable cause for the burning rate increase observed in spinning rocket motors with internal burning grains - radial acceleration. The objectives of the investigation were threefold. The first objective was to determine the quantitative effect of acceleration on the burning rate at constant pressure. The second objective was to find the effect of pressure level on the burning rate increase at given acceleration. The third objective was to find the effect of changing aluminum mass loading and mass median particle size on the sensitivity of the propellant burning rate to acceleration.

In order to study the effect of acceleration alone on propellant burning rate, conventional strand burning techniques were used in conjunction with a centrifuge. A 1565 cubic inch combustion bomb and surge tank volume ensured

essentially constant pressure during burning and the use of relatively short, two and one-quarter inch long, propellant strands at a centrifuge radius of three feet limited the total acceleration change during burning to less than seven per cent of the initial value.

The experimental equipment is described in the first section, and the propellants utilized in the burning rate experiments are described in the second section. Experimental results for both non-aluminized and aluminized composite propellants are presented in the third section and in the fourth section these results are compared to the analytical models proposed by Crowe for aluminized propellants, and Glick for non-aluminized propellants.

II. EXPERIMENTAL EQUIPMENT

The centrifuge used in the investigation reported here is shown in Figure 1. The machine is located at the U. S. Naval Postgraduate School, Monterey, California, and is capable of subjecting the combustion bomb at the end of the centrifuge arm to radial accelerations up to 2000G. The centrifuge is driven by an automobile engine and has a maximum speed of 1450 rpm. The two surge tanks, mounted close to the axis of rotation, and the combustion bomb may be pressurized to 3000 psig by means of a flexible hose fitted with a quick-connect, disconnect coupler. Valves are provided for isolating the bomb from the surge tanks and depressurizing

the system. A schematic diagram of the bomb -- surge tank system is shown in Figure 2.

The propellant strand holders consisted of a machined aluminum plug, canvas phenolic strand support, and a commercial gland seal for the ignition wire (Figure 3). The aluminum plug was a slip-fit in an access port in the combustion bomb, and was locked in place with an aluminum collar. The installation is shown schematically in Figure 4.

Instrumentation was provided to determine centrifuge speed, pressure in the combustion bomb, and propellant burning rate. A magnetic pickup was used to determine centrifuge rpm, and the pressure in the combustion bomb was sensed by a zero to 2000 psig variable reluctance pressure transducer. The transducer was mounted at the centrifuge axis of rotation in order to minimize the effect of acceleration on the instrument. Three bourdon-tube type pressure gauges were located between a nitrogen supply and the charging hose to aid in pressurizing the combustion bomb and surge tanks to the desired level. Repeated comparisons between the gauges and the pressure transducer output indicated that the combustion bomb and surge tanks were pressurized to within one percent of the desired value at pressures above 500 psig.

As propellant strands burned in the combustion bomb, the internal pressure increased 15 to 30 psig depending on strand length and cross-sectional area. This pressure rise

was sensed by the pressure transducer and was recorded on an oscillograph chart. Oscillograph recordings of combustion bomb pressure were used to determine average propellant strand burning rate within $\pm$ 2.1%. Ignition was assumed to coincide with the initial rise in pressure, and it was assumed that burning terminated when the pressure stopped rising. Dividing the initial strand length by the total burning time gave the average burning rate.

Timing wires and electric timers were also used to determine burning rate early in the experimental program. However, this method was abandoned due to excessive sample preparation time and frequent timing circuit malfunctions caused by conducting residue remaining in the propellant inhibitor cases. A more complete description of the experimental equipment may be found in References 3 and 4.

III. PROPELLANT SPECIMENS

Composite propellants having ammonium perchlorate oxidizer (AP) and various amounts of spheroidal aluminum powder were utilized in this investigation. Three binders were used, and to facilitate discussion in the next section they are designated as follows: X100 series - polyurethane binder, X200 - carboxy-terminated polybutadiene binder, and X300 series - PBAN binder.

The compositions (by mass percent) of the four polyurethane propellants were as follows: X101: 30% binder,

70% AP, no aluminum. X102: 27% binder, 63% AP, 10% H-3 aluminum. X103: 25% binder, 57% AP, 18% H-3 aluminum. X104: 25% binder, 57% AP, 18% Al(123) aluminum. The unimodal AP had a mass median diameter of 195 microns (Tyler sieve), and the H-3 and Al(123) aluminum powders had mass median diameters of 6.3 and 31 microns, respectively (micromerograph).

Only one carboxy-terminated polybutadiene propellant (X200) was used. It contained 14% binder, 69% AP, and 17% H-5 aluminum. The AP was a tri-modal blend consisting generally of 25% 600 micron spheres, 50% as received, and 25% ground. The mass median diameter was 195 microns (micromerograph). The H-5 aluminum powder had a mass median diameter of 7.1 microns (micromerograph).

The formulations of the four PBAN propellants were as follows: X301: 20% binder, 80% AP, no aluminum. X302: 19% binder, 77% AP, 4% H-10 aluminum. X303: 16% binder, 68% AP, 16% H-10 aluminum. X304: 16% binder, 68% AP, 16% H-322 aluminum. The AP was a bi-modal blend consisting of 2/3 as received (190 micron mass median diameter) and 1/3 ground (9 micron mass median diameter). The H-10 and H-322 aluminum powders had mass median diameters of 14 microns and 47 microns respectively.

The X104 and X200 propellants were cut from a slab into 0.2 inch x 0.2 inch or 0.4 inch x 0.4 inch square strands

after which they were molded in polyester resin inhibitor. The wall of the inhibitor material was approximately 1/8 inch thick. The X101, X102, and X103 propellants were prepared as above, except that only 0.2 inch x 0.2 inch strands were used. The X300 series propellants were cast directly into paper phenolic tubes having an inside diameter of 1/4 inch. Some of the X304 propellant was also cast in 3/8 inch inside diameter tubes. In all cases, a cap of high-temperature epoxy was cast on one end of the sample. The propellant samples were prepared with a rigid inhibitor and and end-closure for two reasons: to provide support for the visco-elastic propellant in the anticipated high acceleration environment, and to retain any non-gaseous residue that might remain at the end of burning. The finished propellant strands were 2 1/4 inches long except in the case of some timing wire experiments where 2 3/4 inch strands were used.

Propellant samples were placed on the strand holders with the end of the sample resting on the base of the strand support (see Figure 4) and were secured with masking tape. The propellant was ignited with a nichrome resistance wire, and flame propagation across the propellant surface was aided by a thin layer (approximately 50 mg) of FFFg black rifle powder.

IV. EXPERIMENTAL RESULTS

Burning Rate Experiments

Experimental results are presented for burning rate change with acceleration and pressure for the propellants described in the preceding section. Results are presented in the form of burning rate augmentation (r/r_o) and actual burning rate (r) as a function of acceleration (G). Burning rate augmentation (r/r_o) is defined as the actual burning rate (r) at a given pressure and acceleration divided by the burning rate at the same pressure with the centrifuge at rest (r_o). Combustion bomb pressure, either 500, 1000, or 1500 psia, is the parameter.

Radial acceleration levels varied from zero with the centrifuge at rest to a maximum of 2000 times standard gravity (2000G). With the exception of the zero radial acceleration condition, the acceleration vector was always normal to and directed into the burning surface. That is, the burning end of the strand was toward the centrifuge axis of rotation. With the centrifuge at rest, the one G field due to the gravitational field of the earth was parallel to the burning surface.

Each datum point is the result of one experiment. Curves are drawn to indicate the apparent trend of the data. These curves are used to facilitate comparison of results.

Results for the X100 series propellants are shown in Figures 5 through 28. The X200 propellant results are

shown in Figure 29, and the X300 series are shown in Figures 30 through 49.

X100 Series - Polyurethane Binder

X101 - no aluminum. Experimental results for the X101 propellant are shown in Figures 5 through 12. The Figures show data points with and without an asterisk (*). An asterisk by a datum point indicates that the ignition wire did not break or melt and was still intact after the experiment. In these instances the ignition wire was placed on the edge of the inhibitor case so that it would not melt in the flame. The lack of an asterisk by a datum point indicates that the ignition wire was placed across the face of the propellant strand and was not intact at the completion of the experiment. The length of the missing segment was about 0.2 inch; and its mass was about 1.34 mg. If the wire melted and formed two equal size spheres*, they would have been about 540 microns in diameter. These spheres, if held against the burning surface by centrifugal force, would have been immersed in the gas-phase reaction zone. Thus they could have served as good conductors of energy to the propellant.

Figures 5 through 12 show considerable burning rate augmentation when the ignition wire was allowed to burn through. At all three pressures the burning rate increased rapidly with acceleration up to about 100G. Above 100G the

* High speed pictures of aluminum wires burning in oxygen indicate that when the wires break, molten spheres form on the wire ends and travel outward toward the wire suspension points. See Ref. 5.

burning rate continued to increase, but at a much slower rate. At 1000 psia and above 350G, the propellant strands stopped burning after ignition. In some cases extinguishment was near the beginning, and in some cases near the end. At 1983G ignition took place, but extinguishment followed after burning about 1/16 inch in the immediate vicinity of the ignition wire. This same strand subsequently burned normally at 1500 psia, zero G. At 1500 psia, the propellants burned normally up to 500 G. At 1500G the propellant would not ignite without black powder, and at 1980G only about 1/16 inch of the strand burned. At 1000 and 1500G the strands burned completely, but the pressure traces indicated voids in the propellant.

A comparison of the burning rate augmentation at different pressures in Figure 12 shows that for a given acceleration, the augmentation increased with pressure.

When the ignition wire was placed on the edge of the inhibitor case so that it would not melt in the flame, much different results were obtained. At 500 and 1000 psia, there was an increase in burning rate at 100G. At 200G there was a decrease; that is, the burning rate was lower than with zero G. At 300G the strands stopped burning after about 3/8 inch. No such experiments were run at 1500 psia.

Considerable deposition of a black powdery substance, believed to be condensed phase combustion products, occurred

on the inside walls of the inhibitor case at zero G. The amount of deposition decreased rapidly with increasing acceleration, and the material was not accumulated in the capped end of the case after the experiment. It is believed that at the higher burning rates caused by the presence of the nichrome at the burning surface, the gas velocity was sufficient to reduce the deposition of material on the inhibitor case walls.

X102 - 9.7% 6.3 micron aluminum. The X102 propellant was investigated at 1500 psia only for comparison with other variations in the X100 series. Figures 13 and 14 indicate that the presence of the ignition wire had an insignificant effect on the burning rate augmentation. The Figures show a rapid increase in burning rate up to 25G, after which the slope of the curve is much lower. However, the slope increases again above 500 G. It is interesting to note that the only other formulations showing increasing acceleration sensitivity above 500G were the X302 and X303, both PBAN formulations with 14 micron aluminum.

X103 - 17.7% 6.3 micron aluminum. The X103 propellant was investigated at both 500 and 1500 psia. As shown in Figures 15 through 19, the initial augmentation is not as rapid as with the X101 and X102, and the rather abrupt change in slope is also not present. It should be noted that particularly below 100G the curve indicates only the general trend. It may be that additional data points in the low

acceleration range would reveal a rapid augmentation increase up to about 10G, a leveling off, and then another increase in the 50 to 100G range.

X104 - 17.7% 31 micron aluminum. Both 0.2 inch x 0.2 inch and 0.4 inch x 0.4 inch X104 strands were used. From the results shown in Figures 20 through 24, it was concluded that within the range of sizes used, the burning rate and burning rate augmentation are not significantly affected by size.

Four 0.2 inch x 0.2 inch strands inhibited with 40X415 Plastisol Primer (Stanley Chemical Co., East Berlin, Connecticut) were burned at 500 psia. Two were burned at zero G and two were burned at 20G. The average burning rate at zero G was used to calculate burning rate augmentation at 20G. Figures 20 and 21 show that while burning rate is affected by the inhibitor material, burning rate augmentation apparently is not.

Figure 26 shows that burning rate augmentation increased with pressure (500, 1000 and 1500 psia) at all accelerations up to 1000G.

Comparison between X100 series formulations. Figures 27 and 28 show the comparative burning rate change for the X100 series propellants at 1500 psia. Figure 27 shows actual burning rate and Figure 28 shows burning rate augmentation. Of particular interest is the behavior of the non-aluminized propellant, in which the augmentation is attributed to the

1.34 mg. nichrome ignition wire. Except possibly for $G < 15$, it showed greater augmentation than any of the aluminized formulations. If it is assumed that the ignition wire, which was by mass 60% Ni, 25% Fe, and 15% Cr, reacted with the oxidizer to produce NiO, Fe_2O_3, and CrO_3, it can be shown that the energy released would have been only about 1/800 that released by the formation of γ-Al_2O_3 from all of the aluminum in the X102 propellant. This suggests that an increase in thermal conductivity between the reaction zone and the solid may be an important mechanism. It further indicates that the observed increases in burning rate shown by the aluminized propellants were not due simply to the release of additional energy close to the propellant surface.

Also of interest is the comparison of the X102 and the X103 in Figure 28. The X102, which had half as much aluminum showed more sensitivity to acceleration below 90G and above 925G. It was anticipated that the X103 would be more sensitive to acceleration at all values of G.

The X104, which had the larger aluminum particle size, was more sensitive than the X103 up to 525G. From that point on, the X103 augmentation was greater. Above 800G, the X104 showed less augmentation than either the X102 or X103.

X200 - Carboxy-terminated Polybutadiene Binder, 17.7%

7.1 Micron Aluminum

Figure 29 shows log $(r/r_o - 1)$ as a function of log G for 500, 1000, and 1500 psia. Unlike the X100 series, there was little pressure dependence associated with acceleration sensitivity. Also, the augmentation at 1000G was only 1.23, while the X103 showed an augmentation of 3.8. This indicates strong dependence of augmentation on oxidizer particle size distribution and/or binder material.

X300 Series - PBAN Binder

X301 - no aluminum. Figures 30, 31, and 32 show burning rate augmentation as a function of G at pressures of 500, 1000, and 1500 psia respectively. The asterisk (*) denotes that the ignition wire was still intact after the strand holder was removed from the bomb. The Figures show this to be a significant factor below 200G. When the wire remained intact, the propellant burning rate was insensitive to acceleration up to about 100G. At 1000 psia this threshold appears to lie between 75 and 100G. As acceleration was increased, the augmentation increased rapidly and then leveled off. This is in sharp contrast to the X101 where acceleration resulted in propellant extinguishment at 300G and greater.

At about 300G and greater, the disposition of the ignition wire appears to be insignificant. i.e., there was

little difference, if any, between the points with and without (*). This indicates that the mechanism responsible for the augmentation increase remained rate controlling in spite of the presence of the ignition wire. This also is in contrast with the X101.

It is of interest to note that the pairs of data points on Figure 30 marked 1 and 2, 3 and 4, and 5 and 6 are in the same acceleration ranges, yet show quite different burning rate augmentation. Ambient temperature and bomb temperature for these experiments were:

Datum Point	Ambient ^{o}C.	Bomb ^{o}C.
1	17	19
2	19	20
3	23	25
4	24	25
5	22	23
6	23	24

Experiments 3 and 4, and 5 and 6 were done in sequence on two different days. Experiments 1 and 2 were done on the same day, but not in sequence. Both the strand holder and propellant sample were in all six instances at a uniform temperature of 20^{o}C. when removed from the refrigerated oven. Elapsed time from removal from the oven to installation in the bomb was about 30 seconds, and elapsed time from installation in the bomb to ignition was two to three minutes. Hence the propellant temperature at the time of

ignition should have been close to 20°C. The spread in the data points marked 1 through 6 indicates the possibility of significant temperature dependence of acceleration sensitivity in the threshold range.

Figure 34 shows the comparative augmentation for 500, 1000, and 1500 psia. The curves are essentially the same up to 300G. At higher accelerations the augmentation decreased with increasing pressure. This trend is opposite to that shown by the X101 propellant.

X302 - 4% 14 micron aluminum. Results for the X302 propellant at 1000 psia are shown in Figures 35 and 36. The shape of the curve is similar to the X102, also a lightly loaded propellant. The high burning rates at 1500G and greater suggest voids in the propellants, but in all three runs the pressure traces indicated even burning.

X303 - 16% 14 micron aluminum. Results for the X303 are shown in Figures 37 and 38. The data show a rapid increase in burning rate up to about 50G where there is an abrupt decrease in slope. At higher acceleration approaching 2000G a gradual increase in slope is indicated. However, the increase is not nearly so great as with the X302.

X304 - 16% 47 micron aluminum. Results for the X304 propellant are shown in Figures 39 through 46. Both 3/8 inch and 1/4 inch diameter strands were used. As with the X104, the results indicate no apparent difference in burning rates for the two sizes. The burning rate augmentation at 500,

1000, and 1500 psia is shown in Figure 46. A comparison of the curves shows the augmentation to be greatest at 1000 psia, the least at 1500 psia with the 500 psia curve lying approximately midway between. This behavior is different than either of the two propellants (X100 series and X200) previously discussed.

Comparison between X300 series formulations. Figures 47 and 48 show curves for all four formulations at 1000 psia. In Figure 48 it appears that up to 50G the augmentation of the X302 and the X304 were the same. Above 50G the X304 was greater, but it appears that this situation would have reversed at about 1500G.

The X303 showed the highest augmentation up to 100G where the X303 and X304 curves cross. From 200 to 1400G the X303 and X302 were about the same with the X303 higher. Above 1400G the X302, with 4% aluminum, showed greater augmentation than the X303, with 16% aluminum.

A comparison of the X301 and X304 shows that the increase in augmentation was due entirely to the presence of aluminum up to about 100G. As acceleration was increased, the contribution from the aluminum became less and less important.

Of special interest is the comparison between the X301 and the propellants with small aluminum particles (X302 and X303). As with the X304, the increase in augmentation appears to have been caused by the aluminum up to 100G.

Above 200G however, the augmentation was greater for the non-aluminized X301. Between 1500 and 1700G the curves cross, so that again the aluminized propellants show the greater acceleration sensitivity.

The curves in Figure 49 are presented in order to more clearly show the role of aluminum in acceleration sensitivity. The curves are derived from Figure 48 by subtracting r/r_o for the non-aluminized X301 from the aluminized propellants.

Time Dependence

Spinning motor experiments reported by Crowe, et al., (6) have indicated an apparent time dependence of acceleration effects. Similar behavior was anticipated in the present investigation, but the burning rate summaries shown in Tables II and III do not show any consistent time dependence. This disagreement may be due to the different burning lengths in the two investigations. The spinning motor used by Crowe had a web thickness of 0.6 inch while the strands in Tables II and III were 2 1/4 and 2 3/4 inches long. Hence an initial transient condition would be more apparent in the spinning motor investigation.

The Effect of Acceleration on Propellant Burning Rate Exponent

An empirical relationship commonly used to relate propellant burning rate sensitivity to combustion chamber pressure is $r = aP^n$ where (r) is burning rate and (P) is pressure. The coefficient (a) and the pressure exponent (n)

are constant over a limited range of pressure, the extent of the range being dependent on the propellant. In Figures 50 and 51 it has been assumed that this relationship is valid in the acceleration field environment.

Figure 50 shows the variation of the pressure exponent (n) with G for the X101, X103, and X104 propellants. The burning rate increase in the X101 is attributed to the 1.34 mg of nichrome wire. The general tendency was for (n) to be greater with acceleration than without. With X101 and X103, the value of (n) continued to increase as acceleration was increased. The X104, however, showed a decreasing value of (n) as acceleration was increased beyond 50G.

Figure 51 shows the variation of (n) with G for the X301 and X304 propellants. Both the X301 and X304 showed little change in burning rate pressure dependence with acceleration.

The curves in both Figures 50 and 51 were derived from the smooth curves drawn through the burning rate data.

The X200 propellant burning rate pressure exponent was insensitive to acceleration provided that the curve shown in Figure 29 is taken to be a reasonable fit to the data.

Residue Analysis

Inhibitor cases from the metallized propellant experiments were periodically broken open during the course of the investigation to inspect for possible residue. The residues of all three propellant series, X100, X200, and X300 were

similar in appearance. Deposited on the inside walls of the inhibitor cases was a powdery carbon-like substance. A metallic material was found in the bottom of the inhibitor cases, and the amount of this metallic material appeared to be proportional to the acceleration level at which the propellant had been burned.

Sixteen inhibitor cases were selected for closer inspection. Ten X104 samples and six X200 samples, representing accelerations of zero to 1000G, were inspected. Inside the cases there was found a powdery carbon-like substance clinging to the inside walls and deposited at the closed end of the case. The amount of material deposited at the closed end increased as acceleration increased but its appearance did not change. No measurements of particle size or chemical composition of this material were made.

Also found inside the cases was what appeared to be a metal or metal oxide. Subsequent x-ray diffraction and infrared spectrophotometer analyses indicated this material to be predominantly aluminum oxide. In the case of zero G, these oxide particles were imbedded in the black powder on the case walls. These particles were solid, spherical in shape, and the largest were approximately 1000 microns in diameter. At 8G (X200 propellant) there were a few spherical particles found on the walls but they were considerably smaller than 1000 microns. In the bottom of the case, however, there was found a single spheroidal particle about 1/8

inch in diameter. This particle had a mass of 38.0 milligrams and is shown in Figure 52. The size of the X200 propellant sample in this particular experiment was 0.39 inch x 0.40 inch x 2.283 inches. As acceleration increased, oxide particles ceased to appear on the case walls but the amount of residue found in the bottom of the case increased. From 10G (X104 propellant) to about 300G (X104 and X200 propellants) the oxide in the bottom of the case was in several pieces. The pieces appeared to have come from one or more larger masses which apparently suffered multiple fractures durning cooling. The epoxy cap on which the particles were resting generally had one area of severe charring which increased in size as the acceleration increased.

Above 300G the oxide residue in the bottom could be removed in one piece, although multiple cracks through the material could be observed. The thickness of the layer increased with acceleration. At 1014G (X104 propellant) the solid piece of oxide was about 0.16 inch thick and is shown in Figures 52 and 53. The mass of the oxide shown in Figure 53 is 1.816 grams. The X104 propellant sample was 0.4 inch x 0.4 inch x 2.245 inches.

In some instances there was attached to the periphery of this block of material a wall up to 3/8 inch high. It appeared to be of the same material and was about 1/64 inch thick. This formation occurred more in the X104 than the X200. A wall with a mass of 471 milligrams was attached to the oxide shown in Figure 53. The formation of this wall

is believed to be the result of molten residue material being thrown out of the pool by the combustion gases and then freezing on the walls of the inhibitor case as it runs back toward the propellant surface.

The oxide residue collected from the bottom of each inhibitor case was weighed on an automatic laboratory balance (Mettler Model H15) to determine its mass. The results are shown in Figure 54. In calculating the ordinate it was assumed that the residue consisted entirely of aluminum oxide (Al_2O_3). The aluminum retention ratio is equal to 0.529 x residue mass/total mass of aluminum in the propellant sample. The major portion of the scatter in the lower acceleration range is attributed to the difficulty encountered in separating the small fractured oxide particles from the black powdery residue.

V. COMPARISON OF EXPERIMENTAL RESULTS WITH PROPOSED THEORETICAL MODELS

Two models have been proposed to explain the increase in propellant burning rate associated with acceleration. One model, proposed by Crowe, et al., [6] is for metallized propellants, while the other, Glick's modified granular diffusion flame model, [8] is limited to non-metallized composite propellants. First, Crowe's model is described and compared with the results of the polyurethane and PBAN propellant burning rate experiments. Second, Glick's model

is described and compared with the results of the non-aluminized PBAN (X301) propellant burning rate experiments.

Crowe's Critical Particle Size Model

The model proposed by Crowe, et al., [6] is for propellants containing a spheroidal aluminum fuel additive. With the acceleration vector normal to and into the burning surface, Crowe assumed that sufficiently large aluminum particles remain on the propellant surface while burning to a critical size. This critical size is achieved when the aerodynamic drag force is just equal to the particle weight. Until a particle reaches critical size, the energy released during combustion contributes to the heat transfer to the propellant surface. Having burned to less than critical size, the particle is swept away from the surface. Once a particle leaves the surface its combustion is assumed to contribute nothing to the surface heat transfer rate. Those particles initially less than the critical size leave the surface immediately and hence have no effect on the rate of heat transfer to the propellant. Crowe's expression for the burning rate increase due to acceleration is

$$r/r_o = \frac{1}{1 - (ZQ/h_v)\, f(r_{pc}/r_{pm}, \sigma)} \qquad (1)$$

where

r = burning rate with acceleration (cm/sec)

r_o = burning rate without acceleration (cm/sec)

h_v = heat of vaporization (cal/gm)

Z = mass fraction of aluminum in the propellant

Q = energy released by aluminum combustion (cal/gm)

r_{pc} = critical particle radius (cm)

r_{pm} = mass median particle radius (cm)

σ^2 = variance

$f(r_{pc}/r_{pm}, \sigma)$ = fraction of mass which must be removed to reduce all particles larger than the critical size to the critical size

Equation (1) predicts that the burning rate increase varies with aluminum mass loading, and it predicts that the burning rate of a non-aluminized propellant ($Z=0$) will not be affected by acceleration. Stokes' equation for the drag of a sphere is used for particle drag, hence the burning rate increase is sensitive to pressure only to the extent that gas velocity is affected. Crowe assumed a log-normal particle size distribution and found the function $f(r_{pc}/r_{pm}, \sigma)$. Assuming the burning rate to increase by a factor of two when all particles burn completely on the surface, the factor ZQ/h_v equals one-half. The resultant dependence of burning rate on acceleration is shown in Figure 55 for two particle size distributions.

The results of this investigation are similar to the curves based on Crowe's model which are shown in Figure 55.

That is, the data indicate a fairly rapid initial increase in burning rate as acceleration is increased from zero. At high acceleration the data in the majority of cases appear to approach a limiting value as dictated by Crowe's theory.

The theory predicts no change in burning rate until the critical acceleration of the largest aluminum particles is reached. Using Stokes' equation for the drag of spherical particles, the critical particle diameter (d_{crit}) is given by

$$d_{crit} = \left(\frac{18 \mu_g U_g}{\rho_p a} \right)^{1/2} \qquad (2)$$

Reasonable values of the variables in Equation (2) for a typical aluminized propellant burning at 1000 psia are

$r = 1$ cm/sec

$\rho_s = 1.6$ gm/cm^3 (propellant density)

$Z = 0.2$

$\rho_p = 2.7$ gm/cm^3 (density of aluminum)

$T = 3000^{\circ}K$

$\mu_g = 6.6 \times 10^{-4}$ gm/cm sec (gas viscosity)

$\rho_g = 6.1 \times 10^{-3}$ gm/cm^3 (gas density)

$U_g = r \rho_s (1-Z)/\rho_g = 2.15 \times 10^2$ cm/sec

a = acceleration (cm/sec^2)

The resultant critical particle diameter for a typical aluminized propellant in a one G gravitational field is about 200 microns. Crump's motion pictures [7] taken of propellants burning in a one G field show aluminum agglomerates with

diameters in the 100 to 300 micron range; hence an acceleration of 10G would be expected to have a significant effect on the burning rate. The experimental results of this investigation show that this is the case.

Comparing Crowe's theory with Figure 28, we see that the theory predicts the observed trend with a change in aluminum mass loading between 100 and 900G. Beyond these limits, however, the observed trends are not predicted. The X302 and X303 propellants contain 4% and 16% aluminum, respectively. Hence, according to Crowe's theory the X303 propellant should exhibit greater augmentation than the X302. However, Figure 48 shows approximately the same burning rate augmentation for the X302 and the X303 propellants up to 1400G. Above 1400G, the X302 is higher. Figure 48 also shows the burning rate augmentation for the non-aluminized X301 propellant to be greater than either of the two aluminized propellants from about 200 to 1500G. The critical particle size model predicts that non-aluminized propellant burning rate will be unaffected by acceleration.

Crowe's theory also predicts a change in burning rate augmentation with pressure to the extent that particle drag is affected. Applying Stokes' equation, the drag force F_d on a spherical particle at rest on the propellant surface is

$$F_d = 3\pi \mu_g d U_g$$

where

μ_g = gas viscosity (gm/cm sec)

d = particle diameter (cm)

U_g = gas velocity = $r(1-Z)\ \rho_s / \rho_g$ (cm/sec)

r = propellant burning rate (cm/sec)

ρ_s = density of solid propellant (gm/cm^3)

ρ_g = gas density (gm/cm^3)

Z = aluminum mass fraction

The body force F_b, which opposes the drag force, is

$$F_b = \frac{\pi\ d^3}{6}\ \rho_p\ a$$

where

ρ_p = particle density (gm/cm^3)

a = acceleration (cm/sec^2)

If the acceleration is greater than the critical acceleration for a given particle, then $F_b > F_d$, and the particle will remain on the propellant surface. If the acceleration is less than the critical acceleration, $F_b < F_d$ and the particle will leave the surface. Thus we see that the critical acceleration is dependent on the velocity of the gas leaving the propellant surface. That is, the important parameter is not simply acceleration, but the ratio F_b/F_d. For a given propellant and particle size, $F_b/F_d \propto a/U_g$. Assuming a perfect gas and the flame temperature to be independent of pressure (P),

$$F_b/F_d \propto GP/r$$

Hence, the ratio GP/r should be a correlating parameter for burning rate augmentation data at different accelerations and pressures.

Referring to Figure 46, which shows burning rate augmentation versus acceleration for the X304 propellant, we see that the augmentation is lower at 1500 psia than at 1000 psia or 500 psia. Since increasing pressure by a factor of two results in a corresponding burning rate increase of less than a factor of two, replotting the curves in Figure 46 as r/r_o versus GP/r would move the 1500 psia curve farther away from the 500 and 1000 psia curves. Hence Crowe's model does not predict the observed dependence of burning rate augmentation on pressure.

The foregoing comparisons between Crowe's critical particle size model and the experimental results of this investigation show that the model is inadequate for three reasons. First, the model fails to predict the observed effect of increasing aluminum mass loading at all accelerations. Second, the model predicts that the burning rates of non-aluminized propellants will be unaffected by acceleration, while the burning rates of both non-aluminized propellants investigated were significantly affected by acceleration. Third, the model does not predict the correct dependence of burning rate augmentation on pressure.

Glick's Modified Granular Diffusion Flame Model [8]

Glick extended Summerfield's granular diffusion flame model [9] for non-metallized composite propellants to account for the effect of acceleration on the thickness of the gas phase reaction zone. Glick assumed the fuel gas to be more dense than the oxidizer gas, so that in the presence of an acceleration field the buoyancy force would tend to produce relative motion between fuel pockets and the surrounding oxidizer gas. Glick considered the effect of this relative motion on convective mass transport and the velocity with which a fuel pocket would move away from the surface.

The buoyancy force was assumed to be balanced by a drag force with the drag coefficient proportional to the reciprocal of the Reynold's number (Re). The increased mass transport at the fuel pocket boundary was accounted for by means of an expression involving the Sherwood number (Sh) which may be thought of as the ratio of convective mass transport to diffusive mass transport. The Sherwood number was related to the Schmidt number (Sc) and Re using a relationship for solid spheres.

Glick's resultant equation for the burning rate increase due to acceleration is,

$$r/r_o = C \frac{Gr}{Re_o} \cos\theta + \left[\left(C \frac{Gr}{Re_o} \cos\theta \right)^2 + 0.28 Gr^{1/2} Sc^{0.35} + 1 \right]^{1/2} \quad (3)$$

where

r/r_o = burning rate augmentation as previously defined

C = constant

Gr = $\rho_g a \Delta\rho d^3 / \mu^2$ (Graschoff number)

ρ_g = average gas density (gm/cm^3)

ρ_f = fuel gas density (gm/cm^3)

ρ_o = oxidizer gas density (gm/cm^3)

$\Delta\rho$ = $\rho_f - \rho_o$ (gm/cm^3)

a = acceleration (cm/sec^2)

d = characteristic dimension of fuel pocket (cm)

μ = mean gas viscosity (gm/cm sec)

Re_o = $\rho_s d r_o / \mu$ (a Reynolds number)

ρ_s = density of solid propellant (gm/cm^3)

θ = angle between acceleration vector and an inward-drawn normal to the propellant surface

Sc = $\mu / \rho_g D$ (Schmidt number)

D = diffusion coefficient (cm^2/sec)

The term $C(Gr/Re_o) \cos\theta$ accounts for the fuel pocket velocity, while the term containing Sc accounts for the reduced fuel pocket lifetime due to convective mass transport.

The dimensionless numbers Re_o and Sc are independent of pressure, but Gr is proportional to pressure provided that

the mass of a fuel pocket is independent of pressure as postulated by Summerfield.[9] Hence the right-hand side of Equation (3), expressed in terms of acceleration (G) and pressure (P) with, $\theta = 0$, may be written,

$$r/r_o = \psi GP + \left[(\psi GP)^2 + \chi (GP)^{1/2} + 1\right]^{1/2} \quad (4)$$

where ψ and χ are constants for a particular propellant.

Glick's theory is compared with the burning rate results for the X301 propellant in Figure 56 by fitting Equation (4) to the representative points $r/r_o = 1.228$ at 300G and $r/r_o = 1.36$ at 1500 G. Equation (4) fits these points when $\psi P = -1.195 \times 10^{-4}$ and $\chi P^{1/2} = 3.46 \times 10^{-2}$. Figure 56 indicates good agreement between the theory and the data above 200G.

It should be noted that in fitting Equation (4) to the data in Figure 56, ψP was found to be less than zero. Since the only way ψP can be less than zero is for $\Delta\rho$ to be less than zero, we are led to the conclusion that ρ_o must be greater than ρ_f. If the acceleration vector were away from the propellant surface, the fuel pockets should move slower than without acceleration. Thus Glick's model predicts that the X301 propellant will be affected more by acceleration away than by acceleration toward the burning surface.

Glick's theory also predicts an immediate increase in burning rate as acceleration is increased from zero. However, the experimental results in Figures 34 and 56 indicate that the burning rate is independent of acceleration up to about 100g when the ignition wire remains intact. Moreover, the theory predicts that burning rate augmentation at a given acceleration should increase with increasing pressure, whereas Figure 34 shows that increasing pressure caused the burning rate augmentation to decrease. We may conclude that although Glick's modified granular diffusion flame theory may be fitted to the X301 propellant burning rate data at 1000 psia, the predicted burning rate change at low acceleration and the predicted effect of a change in pressure level are not confirmed. These results cast doubt on the adequacy of the model.

VI. SUMMARY AND DISCUSSION

The burning rates of all propellants investigated were found to change with acceleration. The effect of acceleration depended on propellant ingredients and ranged from an increase in burning rate by a factor of four to propellant extinguishment immediately after ignition. The burning rates of the aluminized propellants increased with acceleration, and the burning rate augmentation was considerably greater for the slow burning propellant than for the two medium burning propellants. The slow burning polyurethane propellant had a uni-modal oxidizer and showed a maximum

burning rate augmentation of 4. The PBAN propellant with a bi-modal oxidizer showed a maximum burning rate augmentation of 1.5, and the carboxy-terminated polybutadiene propellant with a tri-modal oxidizer showed a maximum burning rate augmentation of only 1.2. These results indicate that burning rate augmentation depends to a significant degree on binder composition and/or oxidizer particle size distribution. It further points out that slow burning aluminized propellants should be avoided in rocket motor applications involving acceleration perpendicular to and into the burning surface.

The burning rate augmentation for a given binder - oxidizer system depended on aluminum mass loading and aluminum mass median particle size. The general effects of changing aluminum mass loading or particle size in one binder - oxidizer system were similar to the effects shown in another binder - oxidizer system. However, a change in aluminum mass loading or particle size did not produce the same relative change in burning rate at all acceleration levels. This suggests that the mechanism of the burning rate increase is not the same at all levels of acceleration.

The two non-aluminized propellants, one with a PBAN binder and the other with a polyurethane binder, were each affected differently by acceleration. The PBAN propellant was insensitive to acceleration up to 100G and then displayed approximately the same burning rate augmentation as

the aluminized PBAN propellants. In contrast, the polyurethane propellant showed an increase in burning rate at 100G, but as acceleration was increased, the burning rate decreased, and at 300G the strands stopped burning shortly after ignition. The cause for extinguishment may have been the formation of a polyurethane liquid layer which impeded the heat transfer from the gas-phase reaction or possibly quenched the AP decomposition flame.

The disposition of the ignition wire had a significant effect on the behavior of the non-aluminized propellants. In the PBAN propellant the effect was confined to accelerations up to 300G. When the wire was permitted to fall into the inhibitor case the burning rate increased rapidly as radial acceleration was increased from zero. Above 300G the disposition of the ignition wire had no effect. The non-aluminized polyurethane propellant was affected by the presence of the ignition wire at all accelerations. When the wire was permitted to fall into the case, the response of both the polyurethane and PBAN propellants was similar to the general behavior of the aluminized propellants. In addition, the degree of burning rate augmentation was about the same magnitude as that shown by the aluminized propellants. The disposition of the ignition wire had insignificant effect on the acceleration sensitivity of the aluminized propellants.

The burning rate augmentation at a given acceleration level was found to change with a change in pressure. In some instances the burning rate augmentation increased with increasing pressure, and in other instances the augmentation decreased. The burning rate pressure exponent (n) of the slow burning polyurethane propellant was higher with acceleration than without. On the other hand, the pressure exponents of the two medium burning propellants were relatively unaffected by acceleration.

An aluminum oxide residue was found in the bottom of the aluminized propellant inhibitor cases, and the amount of oxide retained increased as the acceleration level increased. The oxide from burning rate experiments at 400G and above could be removed as a solid block from the inhibitor cases, and at 1000G the mass of aluminum in the oxide block was over one-half the total mass of aluminum which had been contained in the propellant strand.

The two models which have been proposed by other investigators [6,8] to predict the effect of acceleration on propellant burning rate do not adequately predict the behavior of the propellants used in this investigation. Crowe's critical particle size model [6] predicts that acceleration will affect the burning rate of aluminized propellants only. This was not borne out in the present investigation. In addition, the predicted effect of changing aluminum mass loading and pressure were not confirmed. Glick's modified

granular diffusion flame model [8] predicts that the burning rates of non-aluminized propellants will increase with acceleration. Good agreement was found between the theory and the data for the non-aluminized PBAN propellant between 200 and 2000G. A consequence of fitting the theory to the data was to show that the oxidizer gas must be more dense than the fuel gas. However, Glick's model predicts dependence of burning rate augmentation on pressure in a manner opposite to that observed, and it predicts an immediate increase in burning rate as acceleration is increased from zero while the experimental results indicate little or no change in burning rate up to 100G.

The modified granular diffusion flame model leads to an expression for burning rate augmentation which can be written

$$r/r_o = \phi + \left[\phi^2 + KG^{1/2} + 1\right]^{1/2}$$

where ϕ is a relative motion term and the term $KG^{1/2}$ accounts for convective mass transport. It can be shown that $|\phi| \ll KG^{1/2}$ when $\left|\rho_f/\rho_g - \rho_o/\rho_g\right| \leq 1$ and $d \leq 20$ microns. This suggests a simplified form in which the relative motion term ϕ is ignored. The expression for r/r_o is then

$$r/r_o = (1 + KG^n)^{1/2} \qquad (5)$$

The exponent (n) was found from the data in Figure 57 by plotting log $(r^2/r_o^2 - 1)$ versus log G. A straight line with

slope 0.25 proved to be a reasonable fit to the data in the acceleration range of 300 to 2000G. Equation (5) then becomes

$$r/r_o = (1 + KG^{1/4})^{1/2} \qquad (6)$$

The coefficient K was found to be 0.137 by fitting Equation (6) to the point $r/r_o = 1.36$ at 1500G. This solution is shown in Figure 57. A comparison with the data shows good agreement from 300 to 2000G.

The experimental results for the X301 propellant suggest the existence of a critical acceleration below which the propellant burning rate is unaffected. As acceleration is increased above the critical value the burning rate increases and appears to approach a limit. Diffusion flame experiments using gas jets in air and a one G acceleration field indicate that the flame remains laminar with gas get velocities up to 2000 cm/sec. [11] Since the velocity of the gas leaving a burning propellant surface is typically of the order 100 cm/sec, one might conclude that transition to a turbulent flame would not occur. However, the body forces resulting from large accelerations and a difference in density between the fuel gas and oxidizer gas would tend to promote flow instability at the boundaries between fuel rich and oxidizer rich regions. This suggests a modified form of Equation (5) in which the acceleration G is replaced by the difference between the actual acceleration and some critical

acceleration G_c below which the propellant burning rate is the same as without acceleration. In this case, the burning rate augmentation might be described by

$$r/r_o = 1, \quad G \leq G_c$$
$$r/r_o = \left[1 + K'(G-G_c)^n\right]^{1/2}, \quad G \geq G_c \qquad (7)$$

Equation (7) is compared with the experimental results for the X301 propellant at 1000 psia in Figure 57. The curve, for which $K' = 0.105$, $G_c = 100$, and $n = 0.3$, agrees reasonably well with the data.

The observed burning rate increase is attributed to the gas phase reaction occurring closer to the propellant surface. It is believed that in a sufficiently strong acceleration field, the body forces promote increased mixing of the originally separate oxidizer and fuel species. With a propellant containing relatively small oxidizer particles, the original degree of unmixedness would be small, thus decreasing the relative importance of body forces. Hence, a non-aluminized PBAN propellant containing large oxidizer crystals would be expected to show a greater burning rate augmentation with acceleration than one with small oxidizer crystals.

The burning rate augmentation shown by the non-aluminized propellants when the nichrome ignition wire was allowed to fall into the inhibitor case was essentially the same as the augmentation shown by the aluminized propellants. This indicates that the important mechanism of burning rate

augmentation in the aluminized propellants is conduction. In the case of the non-aluminized propellant the nichrome wire is believed to have been in one or more pieces, possibly spherical in shape, lying on the burning propellant surface. In this position they would have contributed to increased localized heat transfer. Thus small pits would have been formed with an attendant increase in burning area.

Increased localized heat transfer at discrete locations may be the predominant mechanism of the burning rate increase shown by aluminized propellants at low acceleration. The aluminum agglomerates may collect in small pools. Pools of both reacting aluminum and completely reacted oxide would be good conductors of energy to the propellant surface. These pools would gradually settle into pits formed by the more rapid pyrolysis of binder and oxidizer. Thus the localized burning rate increase would be augmented by an increase in burning surface area.

On the basis of this hypothesis it would appear that one approach to reducing burning rate augmentation at low accelerations would be to somehow reduce the aluminum agglomerate size. Crump's film [7] indicates that agglomerate size decreases with smaller oxidizer crystal size. Hence in those applications where a medium to high burning rate propellant could be used, acceleration effects might be adequately controlled through the use of small oxidizer particle sizes. A more basic approach would be to prevent the accumulation of aluminum particles which leads to

agglomeration. It might be speculated that the aluminum particles are cemented together by partially decomposed binder residue as they emerge from the regressing binder and oxidizer.

At high accelerations there probably is sufficient oxide retained to cover the burning surface with a molten layer. Hence independent pools causing increased localized heat transfer probably do not exist. Instead, the oxide may be expected to contact the burning surface in a random fashion as the oxide is violently stirred by the gaseous products of combustion flowing through the oxide mass. In this case, the initial aluminum particle size would not be expected to affect the depth of the oxide layer. However, initial aluminum particle size aluminum mass loading, and the dispersion of the aluminum particles in the binder may affect the thermal conductivity at the propellant - oxide interface.

The burning rate of the non-aluminized PBAN propellant increased significantly at high acceleration even though the ignition wire remained intact. Hence the burning rate augmentation shown by the aluminized PBAN propellants at high acceleration cannot be attributed solely to the presence of the aluminum. It is likely that coupling between two or more mechanisms is involved.

An adequate analytical model describing the effect of acceleration on the burning rate of non-aluminized composite propellants must account for the effects of changing pressure

level, oxidizer particle size distribution, and binder composition. A model for aluminized composite propellants must, in addition to the above variables, account for changing aluminum mass loading and aluminum mass median particle size. At this time the mechanisms by which the above parameters affect propellant burning rate in a one G acceleration field are not well understood. Several models have been formulated in an attempt to explain the change of burning rate with pressure, but no one model has gained universal acceptance. Due to the complex nature of the burning mechanism, the formulation of a mathematical model to account for the effect of acceleration on propellant burning rate does not appear to be feasible in the light of present knowledge. An acceptable mathematical model is unlikely to evolve until more of the fundamental mechanisms have been extensively investigated and are understood.

Recommendations for Future Investigation

The results reported here indicate that further investigations are required to gain a better understanding of the mechanisms involved in burning rate augmentation associated with acceleration. High-speed photography of propellants burning in acceleration fields would be a significant contribution.

The relative importance of oxidizer particle size and binder composition on the burning rate augmentation of

aluminized propellants could be studied by using the same two uni-modal oxidizer particle size distributions, one with large particles and one with small particles, in propellants with two different binders. The same aluminum mass loading and particle size distribution should be used in all four propellants. The use of aluminum particle size distributions with small variance but different mass median diameters would help to more clearly define the importance of oxidizer particle size at low accelerations where agglomeration is believed to be important.

The retention of aluminum oxide in the motor combustion chamber is a significant factor in the performance losses experienced with spinning rocket motors. An expression for the mass of oxide retained as a function of propellant burning rate, aluminum mass loading, acceleration and propellant grain web thickness would be of value to the rocket motor designer. Experimental data could be obtained by burning propellant strands similar to those used in the present investigation, but with various lengths.

The non-aluminized propellants merit further investigation. Experiments with the acceleration vector at various angles to the burning surface, including parallel to and away from, may indicate possible reasons for propellant extinction in one instance and burning rate increase in another. Additional evidence to evaluate the basic concepts of the modified granular diffusion flame model proposed by

Glick could be provided by two experiments. First, experiments similar to those reported herein should be conducted at low pressures where chemical reaction rates are believed to be rate controlling. Second, propellants with different oxidizer crystal size should be investigated.

Initial propellant temperature may be an important parameter in burning rate augmentation due to acceleration. Experiments at constant acceleration and constant pressure but with varying initial propellant temperature may show that propellant burning rate temperature coefficients are affected to a significant degree by acceleration.

VII. CONCLUSIONS

The study reported here is a systematic investigation of composite propellant burning rates at high acceleration. Previously reported investigations have been limited to one propellant and 300G, or spinning motor experiments with radial accelerations up to about 100G.

Acceleration perpendicular to and into the burning surface was found to affect the burning rates of both aluminized and non-aluminized composite propellants. Prior to this investigation it was generally believed that acceleration had no effect on the burning rate of non-aluminized composite propellants.

The primary factor affecting the relative amount of burning rate increase with acceleration was found to be oxidizer particle size distribution and/or binder composition. Acceleration effects may be reduced by using an oxidizer with small mass median particle size. The pressure level was found to be a secondary factor. The relative burning rate increase was greater with increasing pressure for some propellants and less for others. Aluminum mass loading and mass median particle size are also important, but the significance of a change in either of these two parameters depends on the acceleration level.

The presence of a small piece of nichrome wire at the burning surface of a non-aluminized composite propellant

results in a relative burning rate increase with acceleration quite similar to that of the same propellant with an aluminum fuel additive.

The burning rate pressure exponent (n) increases with acceleration for some propellants but remains essentially unchanged for other.

No large scale time dependence is indicated by average burning rates over adjacent one-half inch intervals in two and one-quarter inch long propellant strands.

The models proposed by Crowe [6] and Glick [8] do not adequately predict the effect on relative burning rate increase with acceleration of a change in aluminum mass loading or pressure. Moreover, other simplified models do not suggest themselves in the light of present knowledge.

Further investigations are required to gain a deeper insight into the mechanisms involved.

REFERENCES

1. Emerson Electric Co., Compilation of Skin Data Program, Technical Summary No. 1, Emerson Electric Co., St. Louis, Mo., Report No. 2122-1, January, 1967

2. Emerson Electric Co., Compilation of Skin Data Program, Technical Summary No. 2, Reference Bibleography, Emerson Electric Co., St. Louis, Mo., Report No. 2122-2, May, 1967

3. Anderson, J. B., An Investigation of the Effect of Acceleration on the Burning Rate of Composite Propellants, PhD. Thesis, U. S. Naval Postgraduate School, Monterey, California, August, 1966

4. Anderson, J. B., and Reichenbach, R. E., 76-Inch Diameter Centrifuge Facility, Department of Aeronautics, Technical Note 66T-4, U. S. Naval Postgraduate School, Monterey, California, September, 1966

5. Cinémicrographie de la Combustion des Poudres Composites Métallisées (1964), (Dinemicrography of the Combustion of Composite Solid Propellants Containing Metal Additives), Office National d'Etudes et de Recherches Aérospatiales, 29, Avenue de la Division Leclerc, Chatillon-Sous-Bagneux, (Seine) France

6. Crowe, C. T., and Willoughby, P. G., Effect of Skin on the Internal Ballistics of a Solid Propellant Motor, AIAA Paper No. 66-523 presented at the AIAA Fourth Aerospace Sciences Meeting (West Coast), June 27-29, 1966

7. Crump, J. E., Aluminum Combustion in Composite Propellants, Proceedings of the 2nd ICRPG Combustion Conference, Aerospace Corp., El Segundo, Calif., Nov. 1-5, 1965

8. Glick, R. L., The Effect of Acceleration on the Burning Rate of Non-Metallized Composite Propellants, paper presented at the ICRPG 3rd Combustion Conference, John F. Kennedy Space Center, Oct. 17-21, 1966

9. Summerfield, M., et al., "Burning Mechanism of Ammonism Perchlorate Propellants," Progress in Astronautics and Rocketry, Vol. I, p. 142-182, Academic Press, Inc., New York, New York, 1960

10. Propellant Burning Studies, JPL Film 366, Jet Propulsion Laboratory, Pasadena, Calif., 1961

11. Penner, S. S., Chemistry Problems in Jet Propulsion, Pergamon Press, New York, 1957, p. 270

TABLE I

BURNING RATE SUMMARY

X104 PROPELLANT 500 PSIA

Acceleration G	r_1 in/sec	r_2 in/sec	r_3 in/sec	$\bar{r}$ in/sec
0	0.145	0.145	0.143	0.144
0	.132	.141	.140	.137
9	.202	.177	.155	.176
16	.208	.174	.161	.179
32	.188	.188	.179	.185
49	.186	.184	.180	.183
103	.209	.229	.224	.221
106	.203	.201	.202	.202
214	.228	.230	.234	.231
316	.284	.272	.261	.275
622	.316	.318	.326	.320
1034	0.339	0.351	0.351	0.334

r_1 is the average burning rate over the first of three adjacent intervals, each ½ inch long.

$$\bar{r} = (r_1 + r_2 + r_3)/3$$

TABLE II

BURNING RATE SUMMARY

X304 PROPELLANT 500 PSIA

Acceleration G	r_1 in/sec	r_2 in/sec	r_3 in/sec	$\bar{r}$ in/sec
0	0.334	0.345	0.343	0.340
0	.338	.345	.342	.342
0	.317	.317	,316	.317
0	.324	.330	.334	.329
21	.331	.363	.359	.352
39	.382	.370	.338	.363
96	.372	.351	.346	.355
101	.378	.407	.352	.378
101	.380	.376	.367	.378
103	.386	.374	.370	.382
204	.379	.376	.370	.375
207	.434	.384	.393	.402
306	0.414	0.373	0.366	0.384

r_1 is the burning rate over the first of three adjacent intervals, each 3/4 inch long.

$$\bar{r} = (r_1 + r_2 + r_3)/3$$

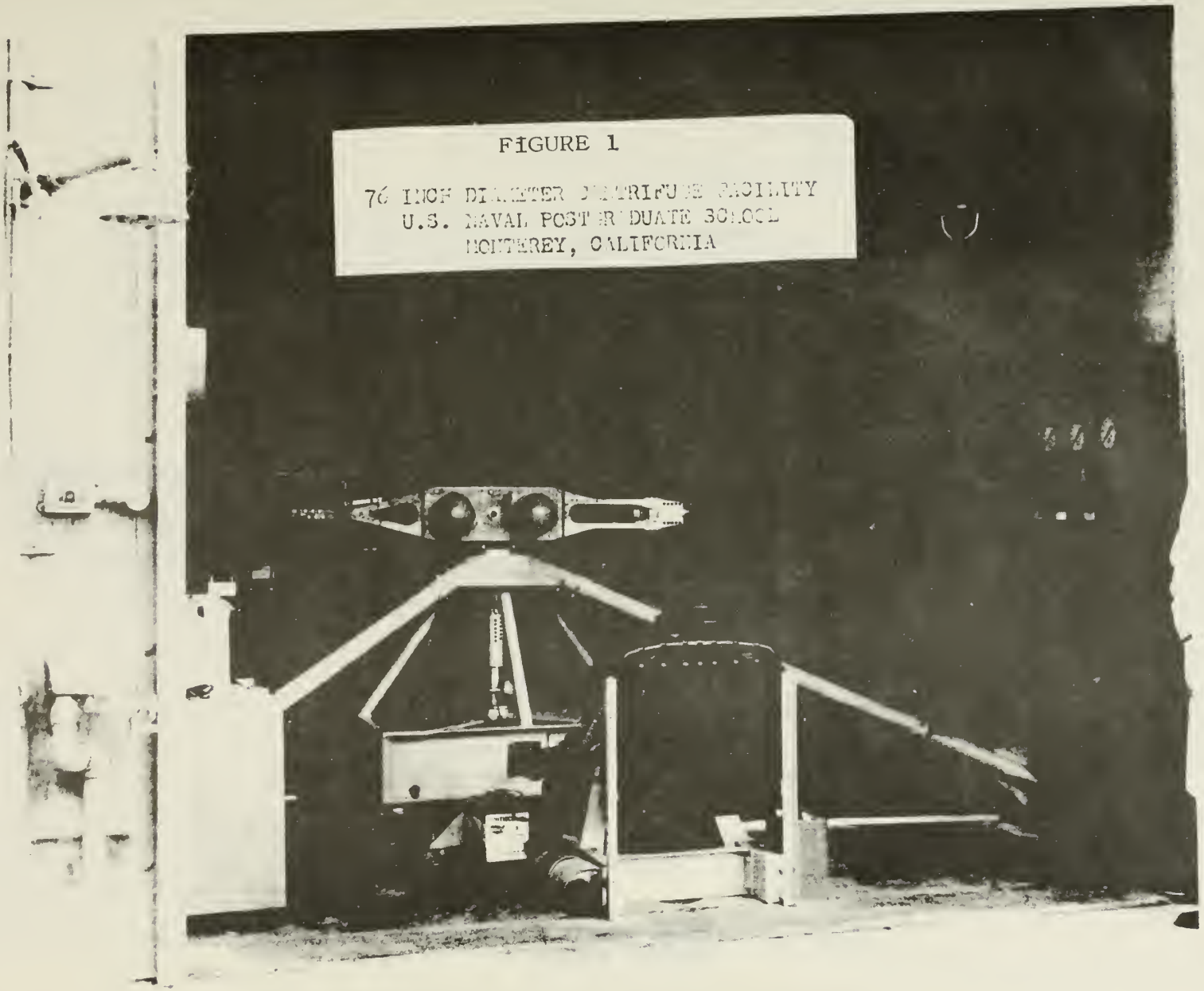

FIGURE 1

76 INCH DIAMETER CENTRIFUGE FACILITY
U.S. NAVAL POSTGRADUATE SCHOOL
MONTEREY, CALIFORNIA

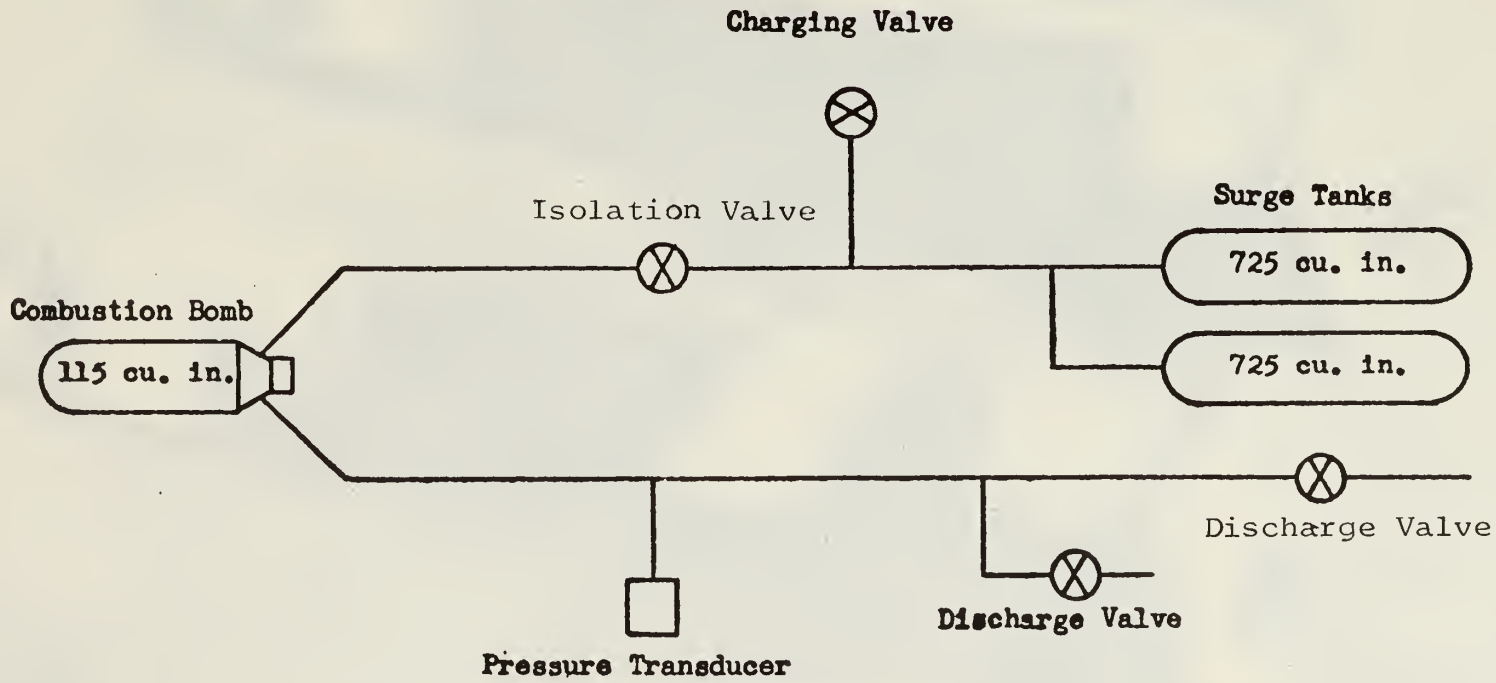

FIGURE 2

COMBUSTION BOMB - SURGE TANK SYSTEM
(ROTOR SYSTEM)

FIGURE 3

STRAND HOLDERS USED WITH PRESSURE INSTRUMENTATION IN BURNING RATE EXPERIMENTS

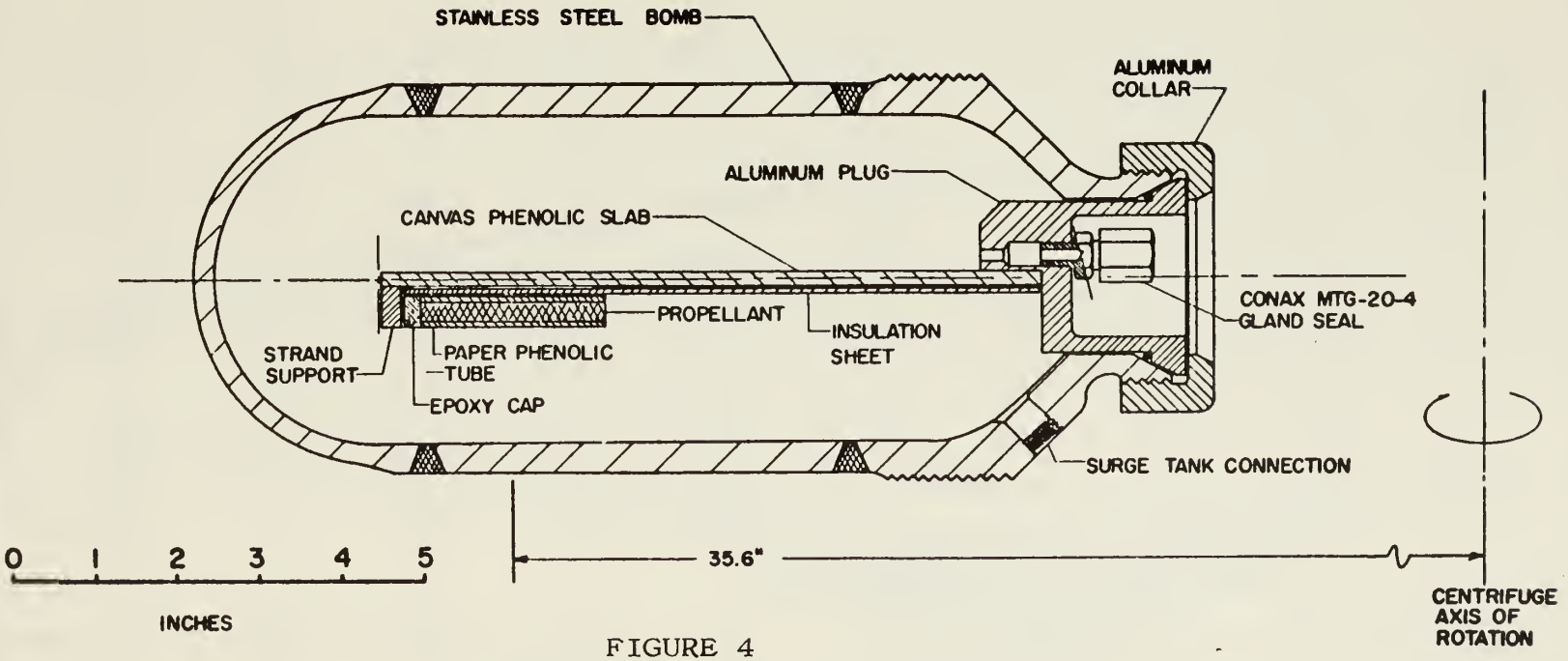

FIGURE 4

STRAND HOLDER AND BOMB ASSEMBLY

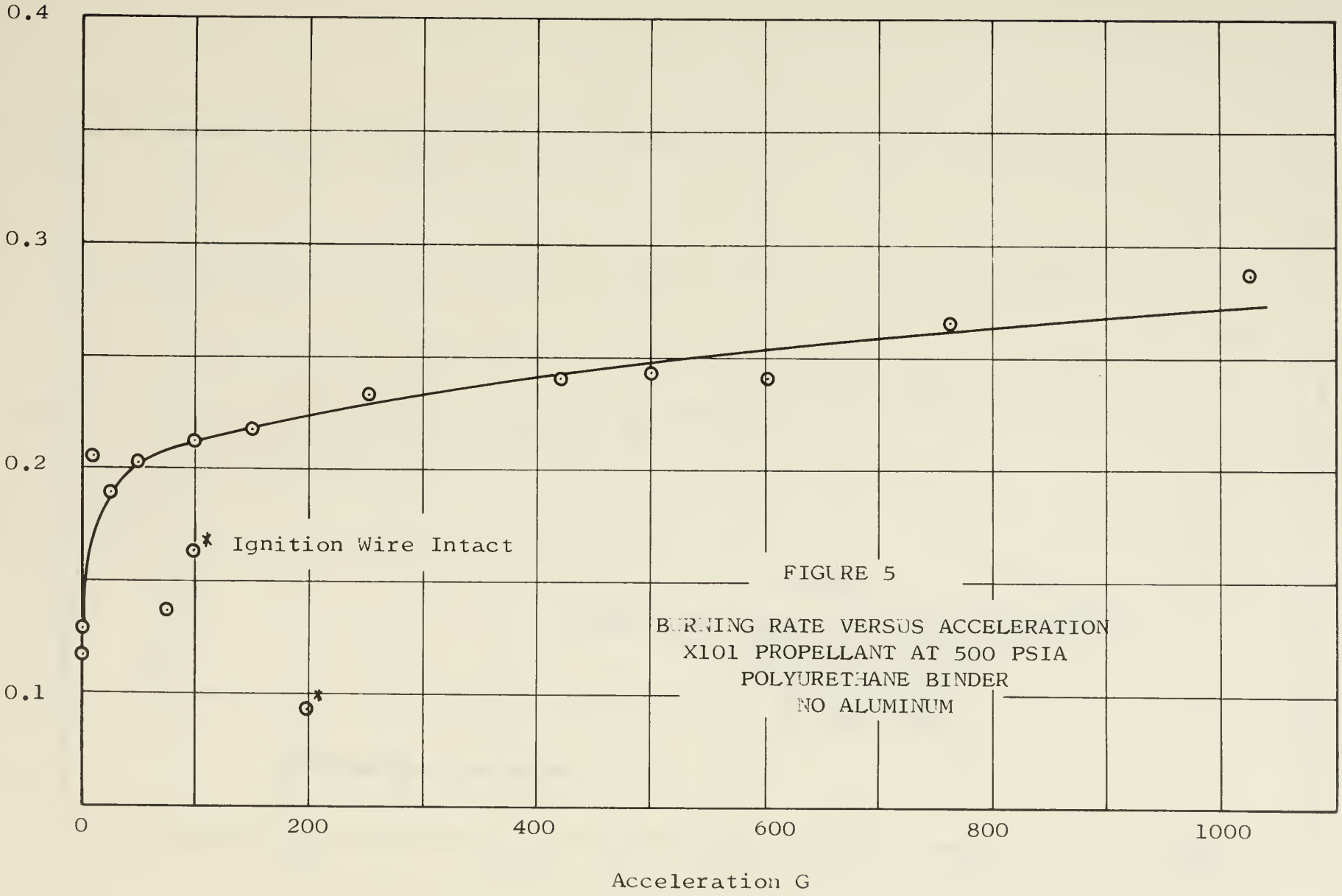

FIGURE 5

BURNING RATE VERSUS ACCELERATION
X101 PROPELLANT AT 500 PSIA
POLYURETHANE BINDER
NO ALUMINUM

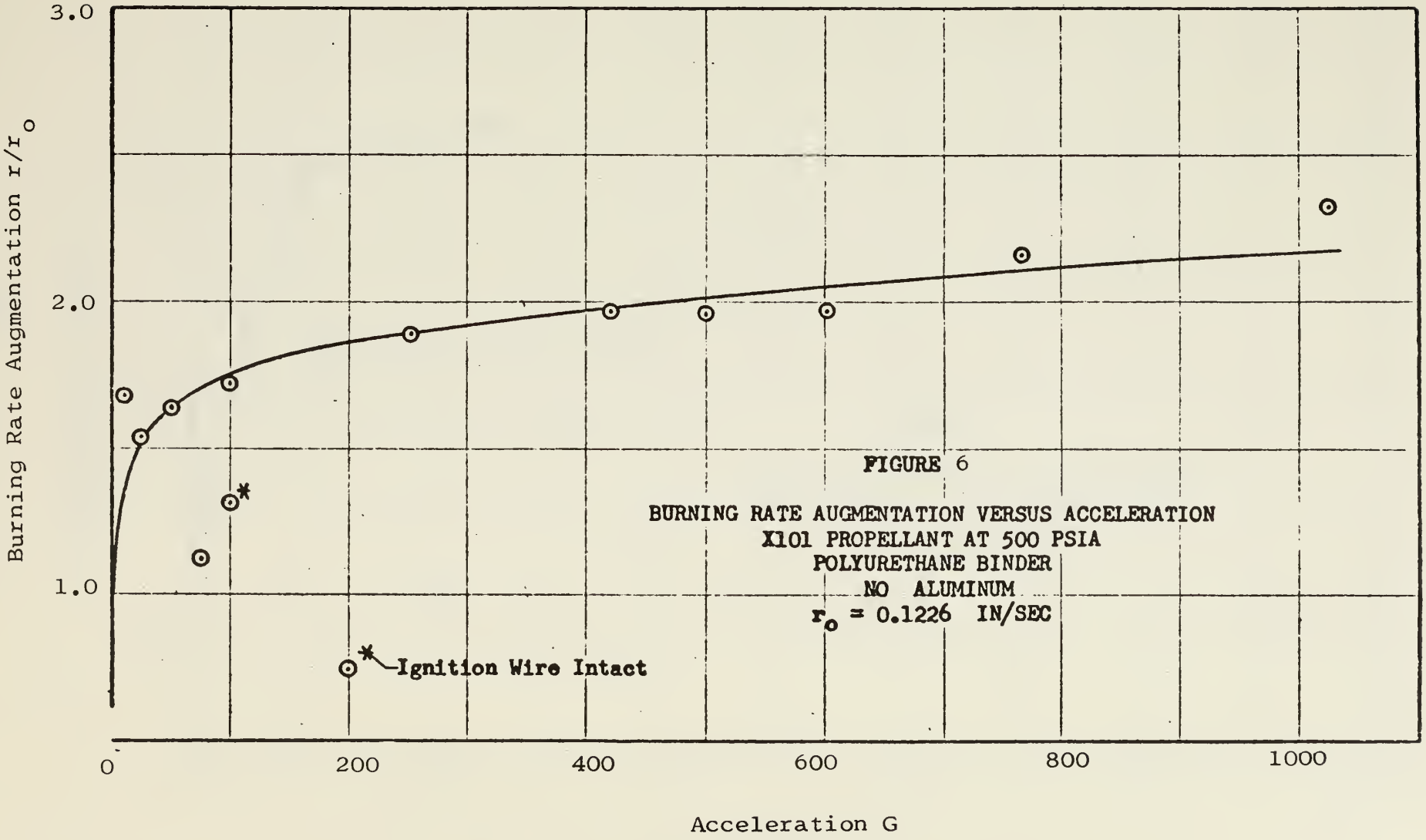

FIGURE 6

BURNING RATE AUGMENTATION VERSUS ACCELERATION
X101 PROPELLANT AT 500 PSIA
POLYURETHANE BINDER
NO ALUMINUM
r_o = 0.1226 IN/SEC

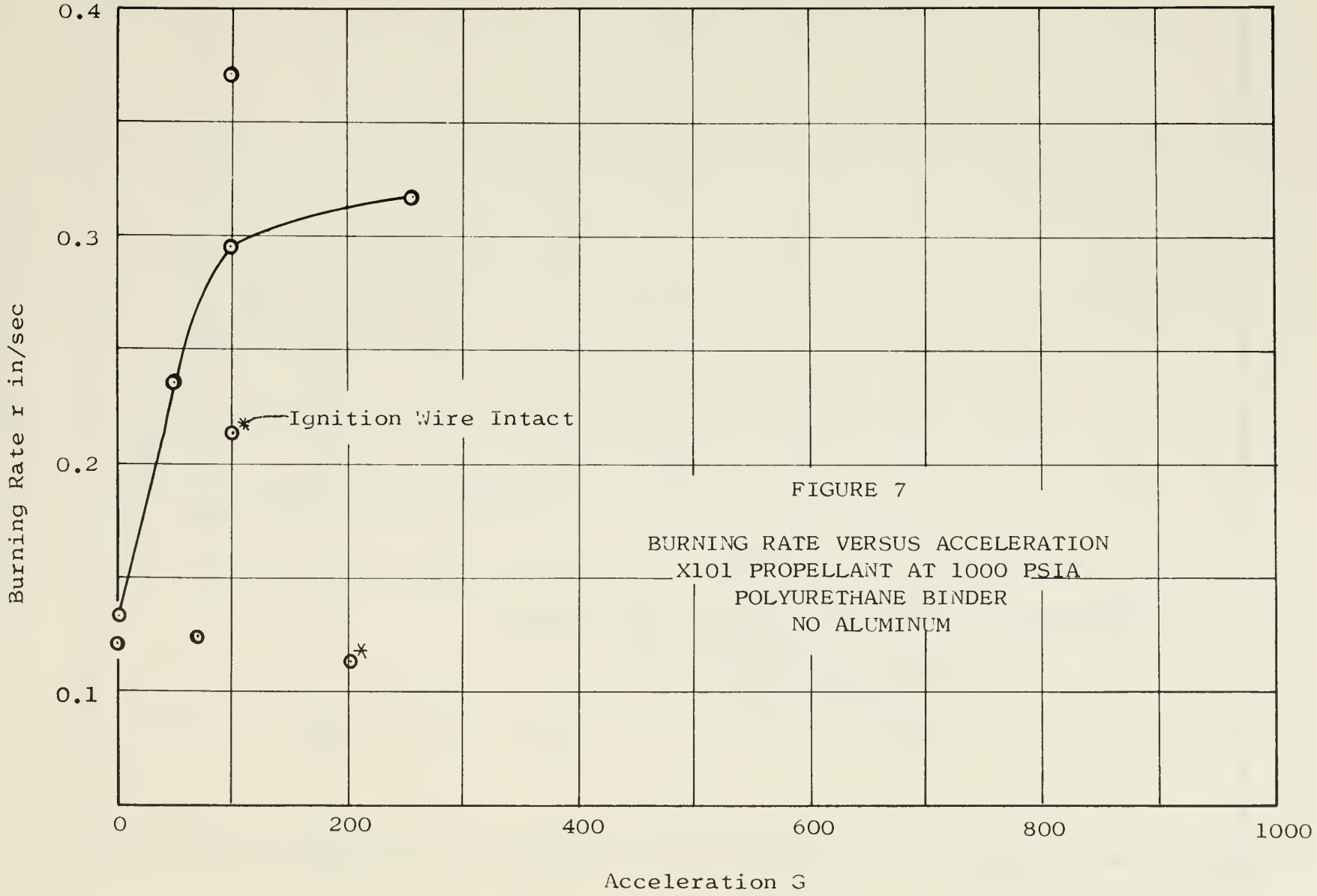

FIGURE 7

BURNING RATE VERSUS ACCELERATION
X101 PROPELLANT AT 1000 PSIA
POLYURETHANE BINDER
NO ALUMINUM

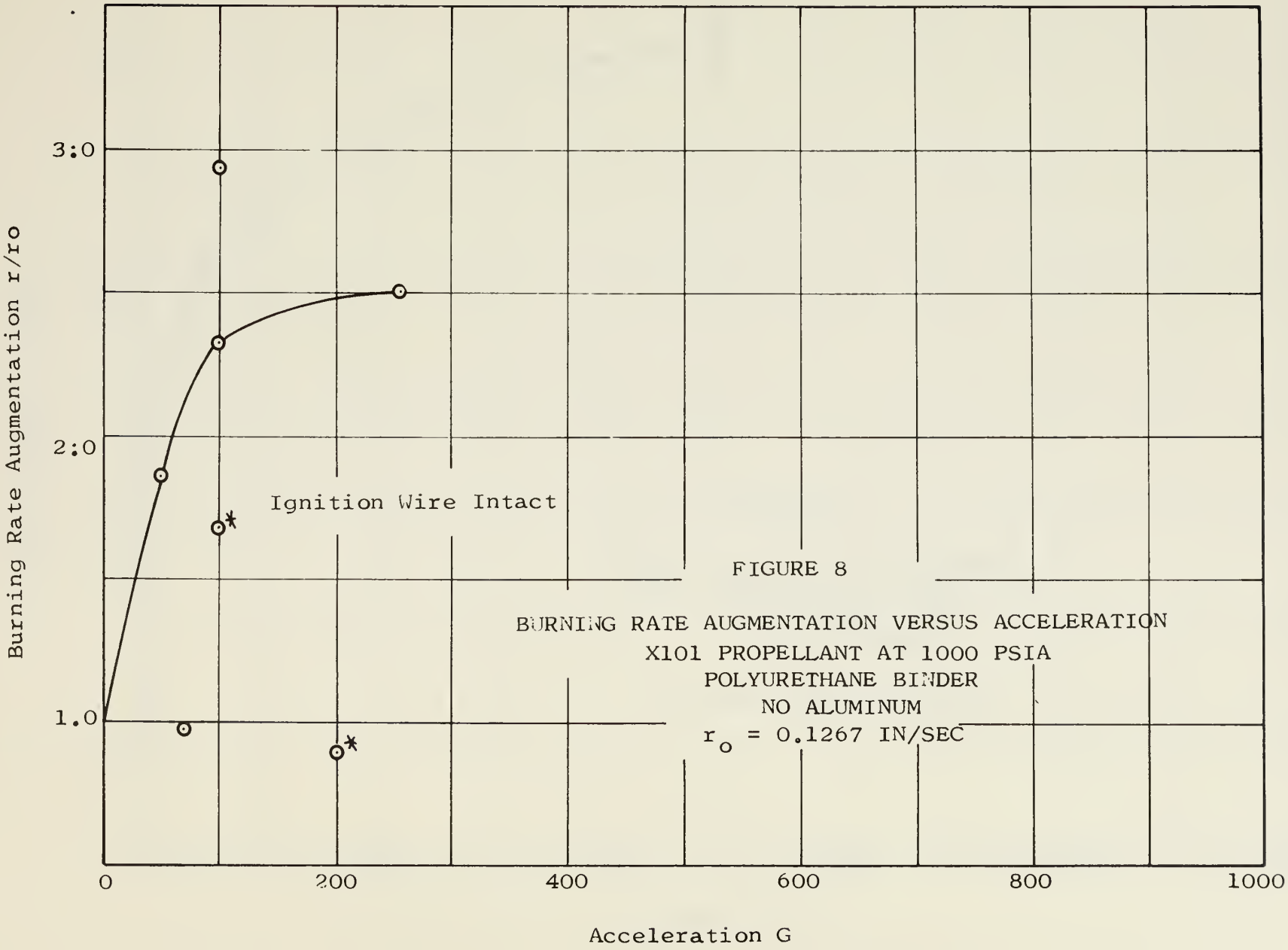

FIGURE 8

BURNING RATE AUGMENTATION VERSUS ACCELERATION
X101 PROPELLANT AT 1000 PSIA
POLYURETHANE BINDER
NO ALUMINUM
r_o = 0.1267 IN/SEC

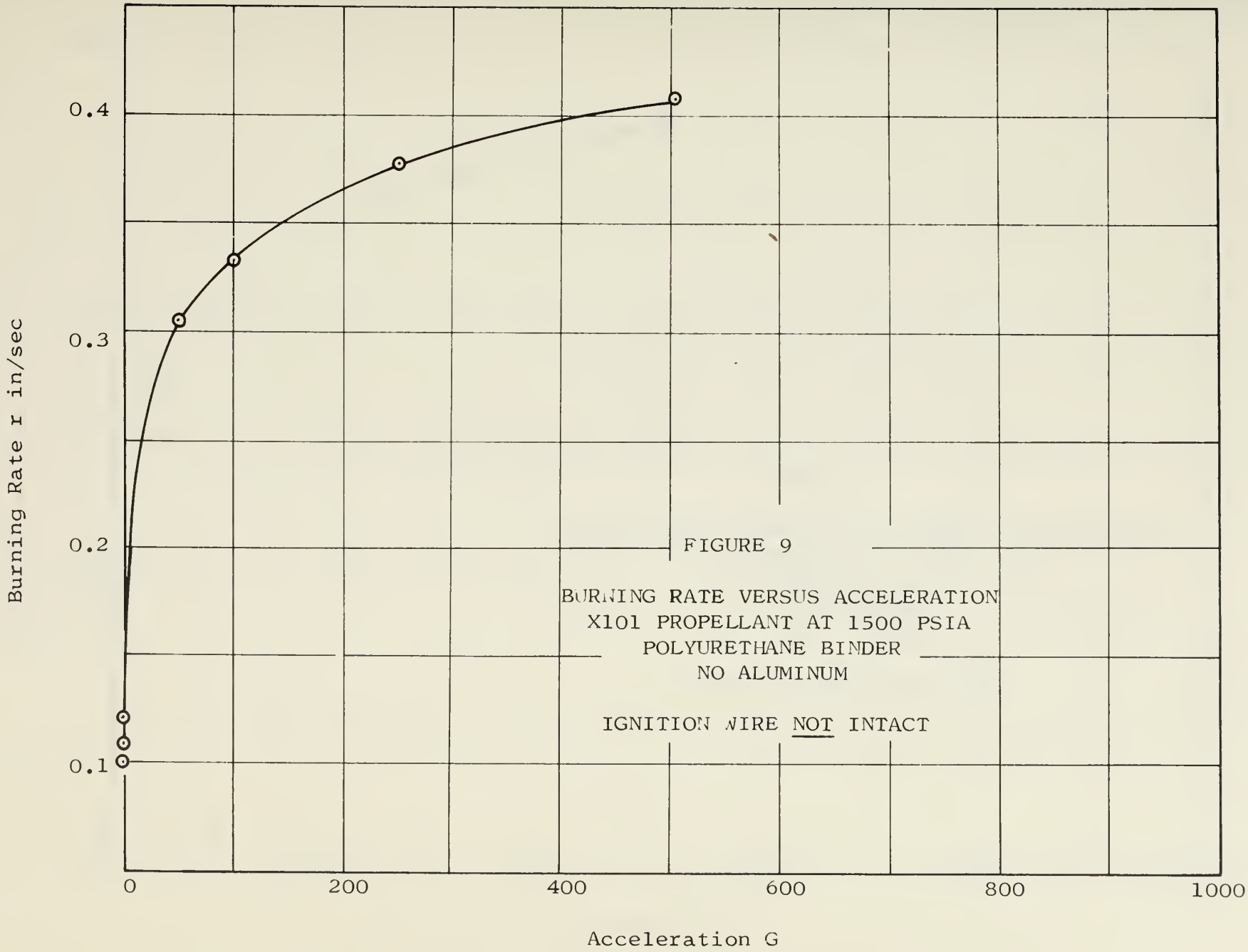

FIGURE 9

BURNING RATE VERSUS ACCELERATION
X101 PROPELLANT AT 1500 PSIA
POLYURETHANE BINDER
NO ALUMINUM

IGNITION WIRE NOT INTACT

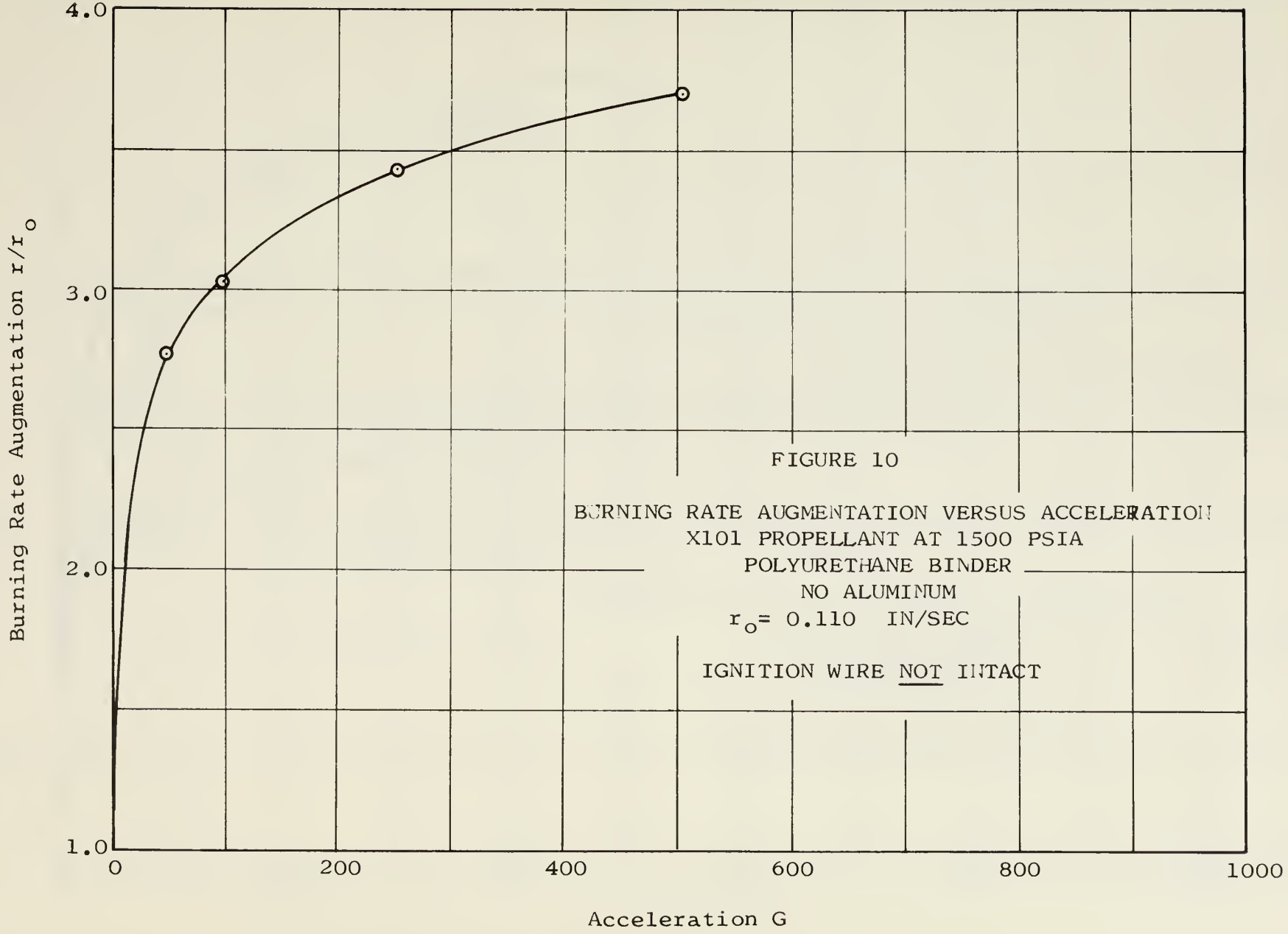

FIGURE 10

BURNING RATE AUGMENTATION VERSUS ACCELERATION
X101 PROPELLANT AT 1500 PSIA
POLYURETHANE BINDER
NO ALUMINUM
r_o= 0.110 IN/SEC

IGNITION WIRE NOT INTACT

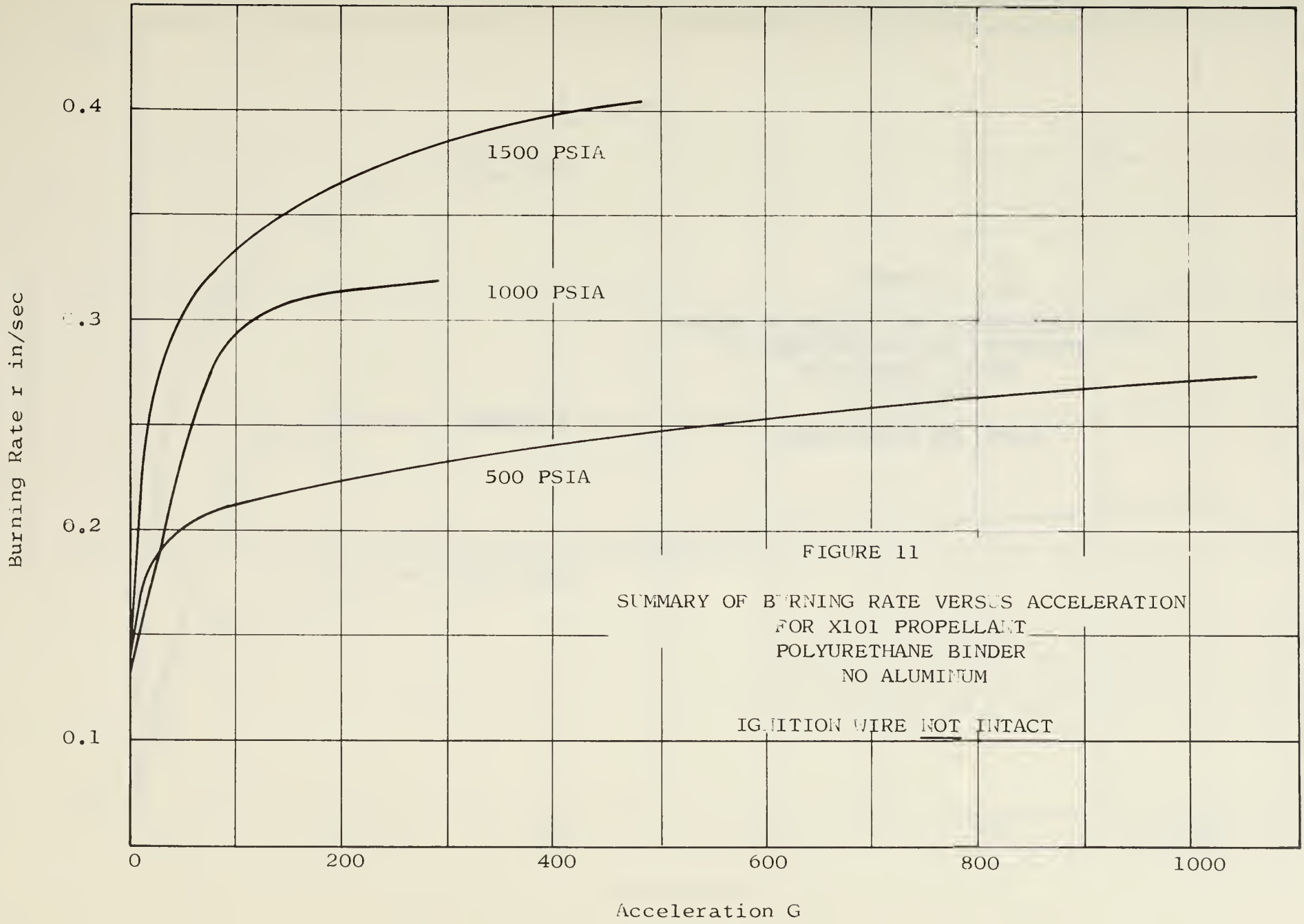

FIGURE 11

SUMMARY OF BURNING RATE VERSUS ACCELERATION
FOR X101 PROPELLANT
POLYURETHANE BINDER
NO ALUMINUM

IGNITION WIRE NOT INTACT

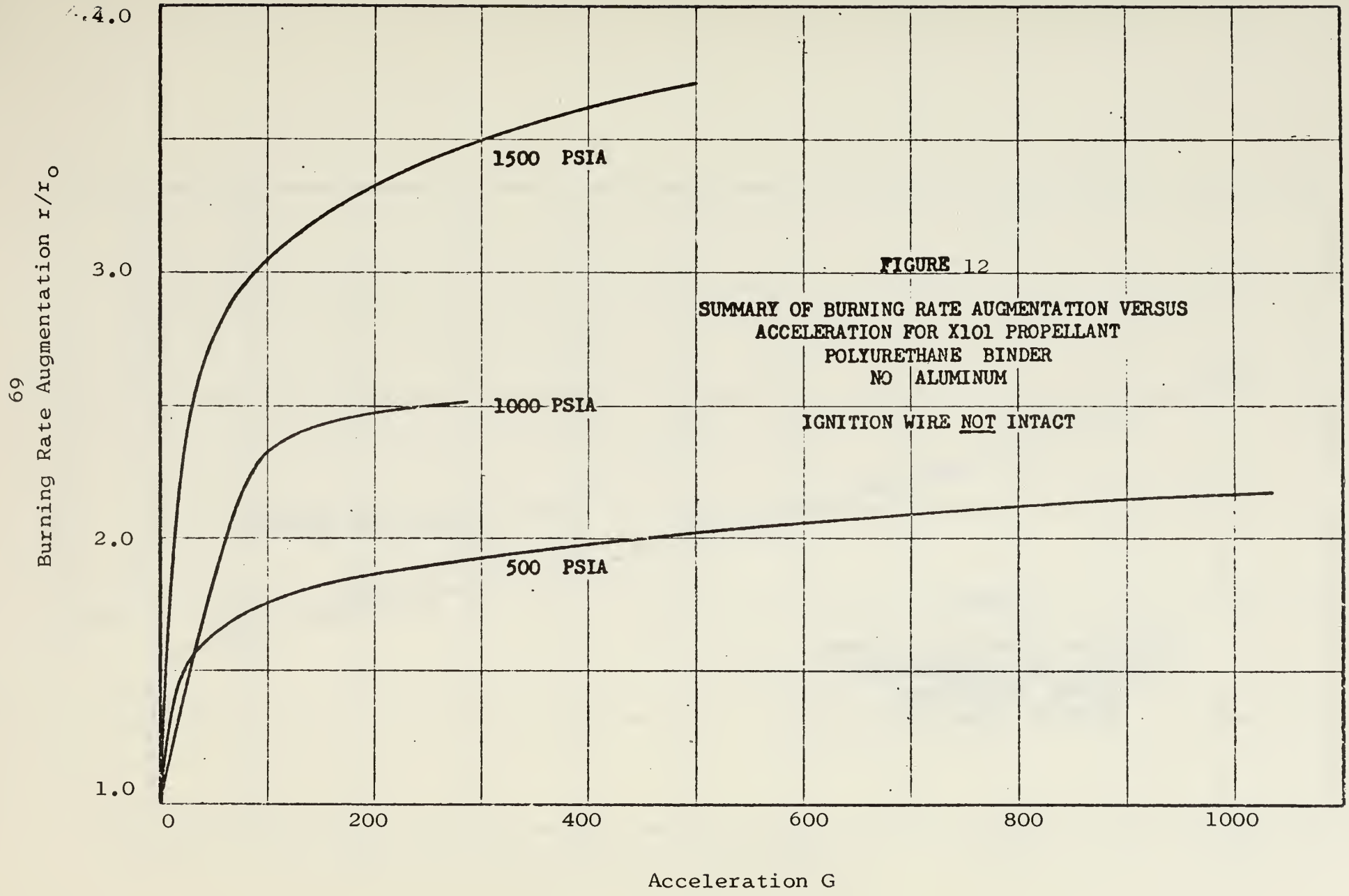

FIGURE 12

SUMMARY OF BURNING RATE AUGMENTATION VERSUS ACCELERATION FOR X101 PROPELLANT
POLYURETHANE BINDER
NO ALUMINUM

IGNITION WIRE NOT INTACT

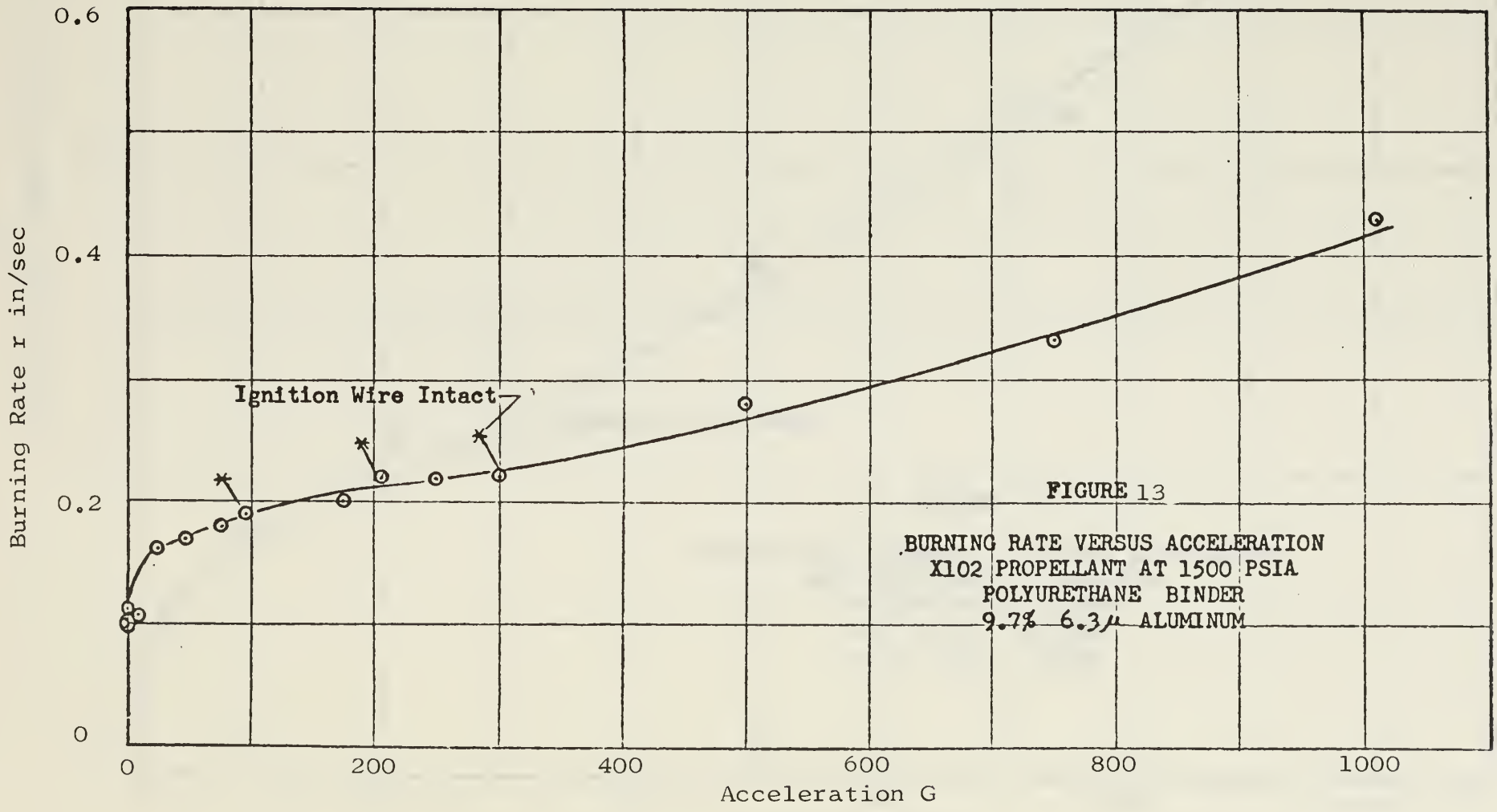

FIGURE 13

BURNING RATE VERSUS ACCELERATION
X102 PROPELLANT AT 1500 PSIA
POLYURETHANE BINDER
9.7% 6.3μ ALUMINUM

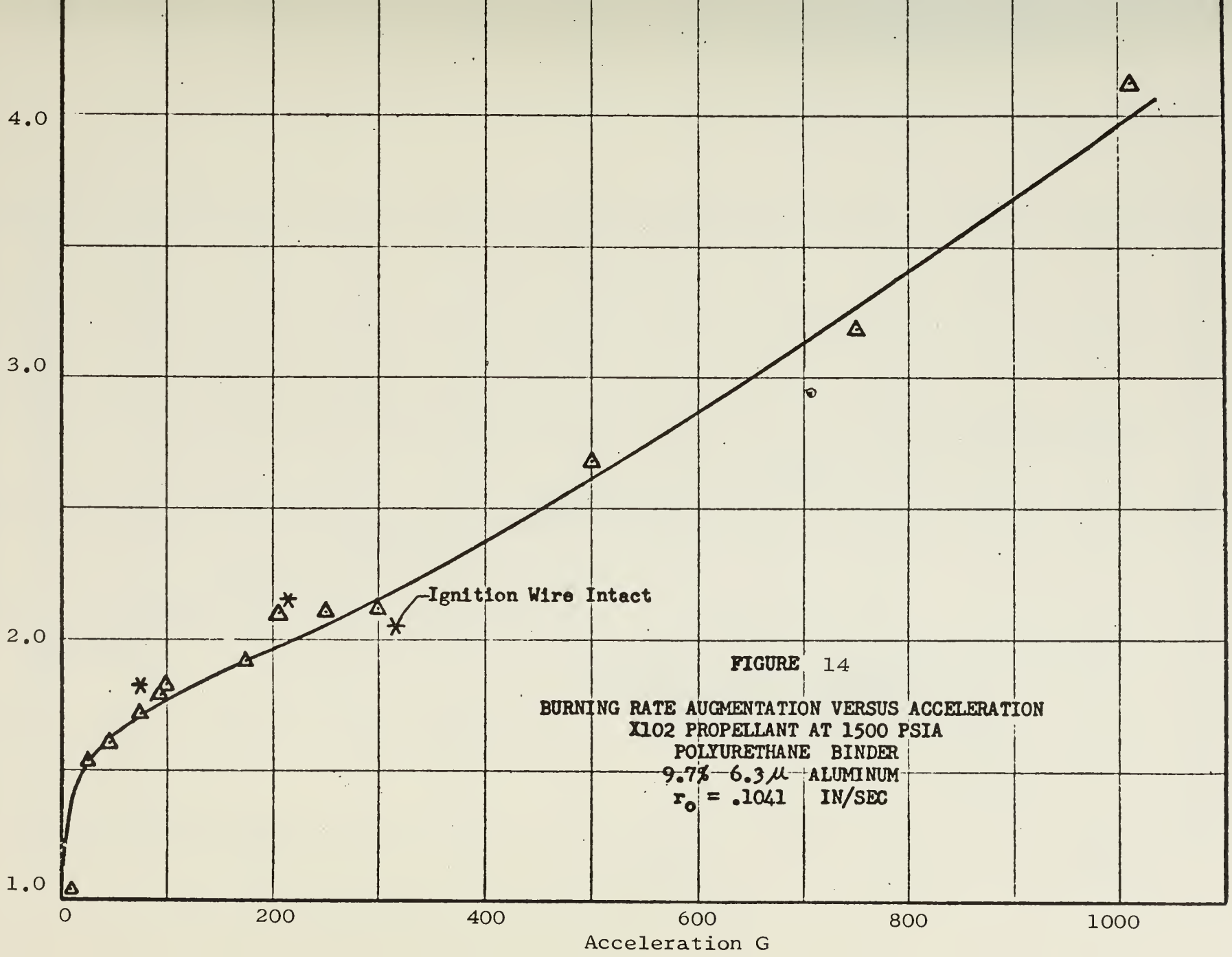

FIGURE 14

BURNING RATE AUGMENTATION VERSUS ACCELERATION
X102 PROPELLANT AT 1500 PSIA
POLYURETHANE BINDER
9.7% 6.3 μ ALUMINUM
r_o = .1041 IN/SEC

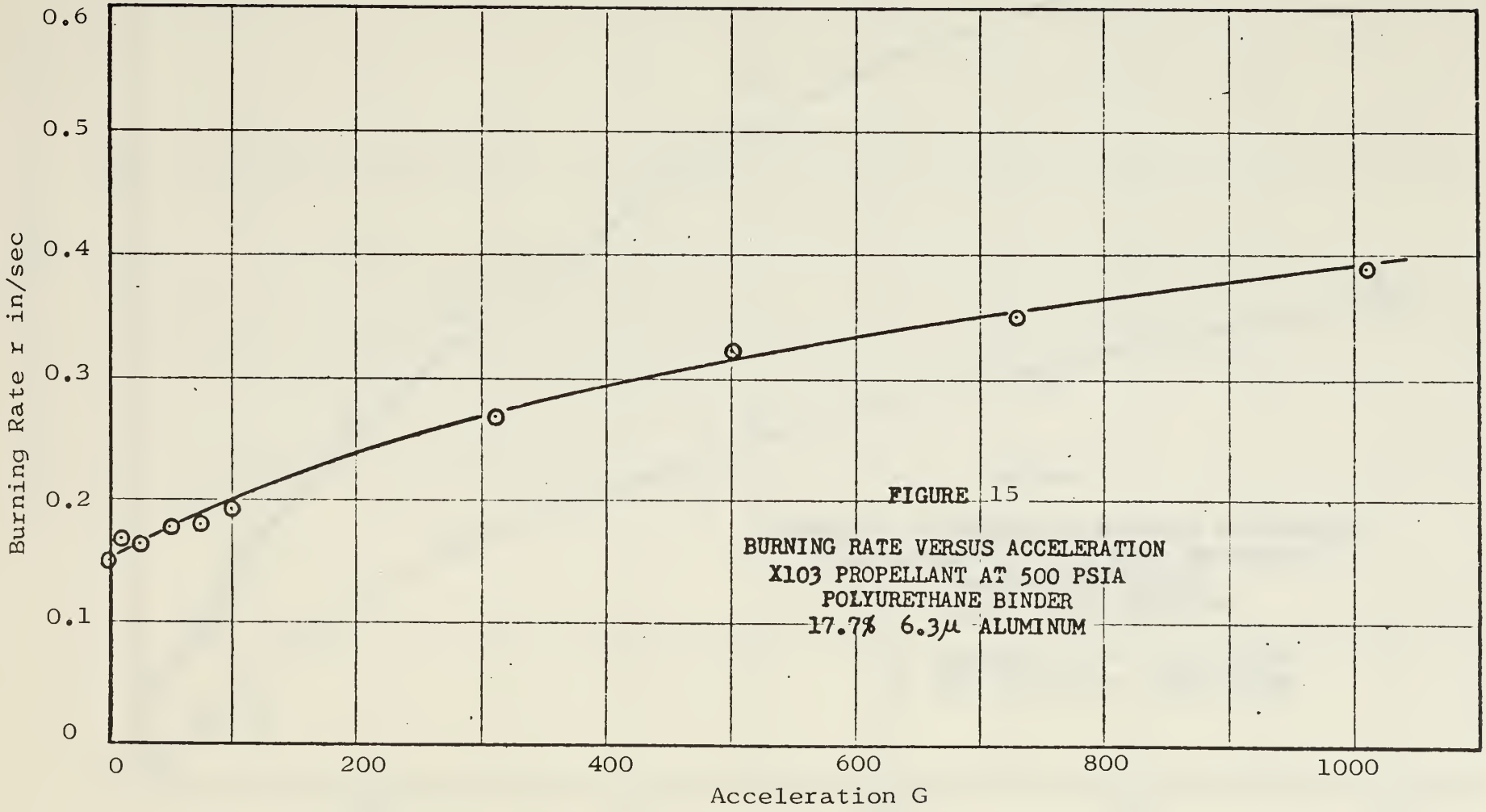

FIGURE 15

BURNING RATE VERSUS ACCELERATION
X103 PROPELLANT AT 500 PSIA
POLYURETHANE BINDER
17.7% 6.3μ ALUMINUM

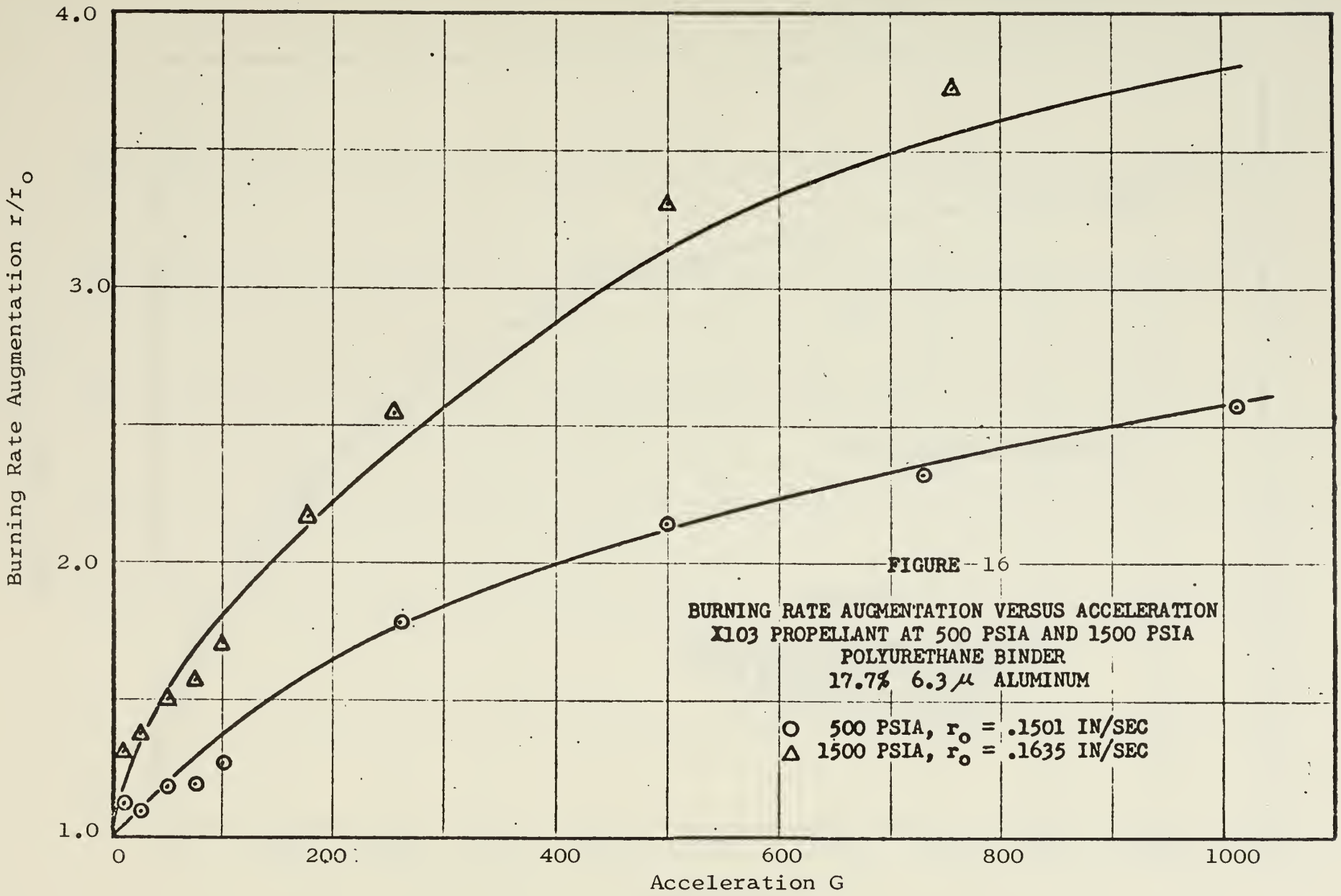

FIGURE 16

BURNING RATE AUGMENTATION VERSUS ACCELERATION
X103 PROPELLANT AT 500 PSIA AND 1500 PSIA
POLYURETHANE BINDER
17.7% 6.3 μ ALUMINUM

○ 500 PSIA, r_o = .1501 IN/SEC
△ 1500 PSIA, r_o = .1635 IN/SEC

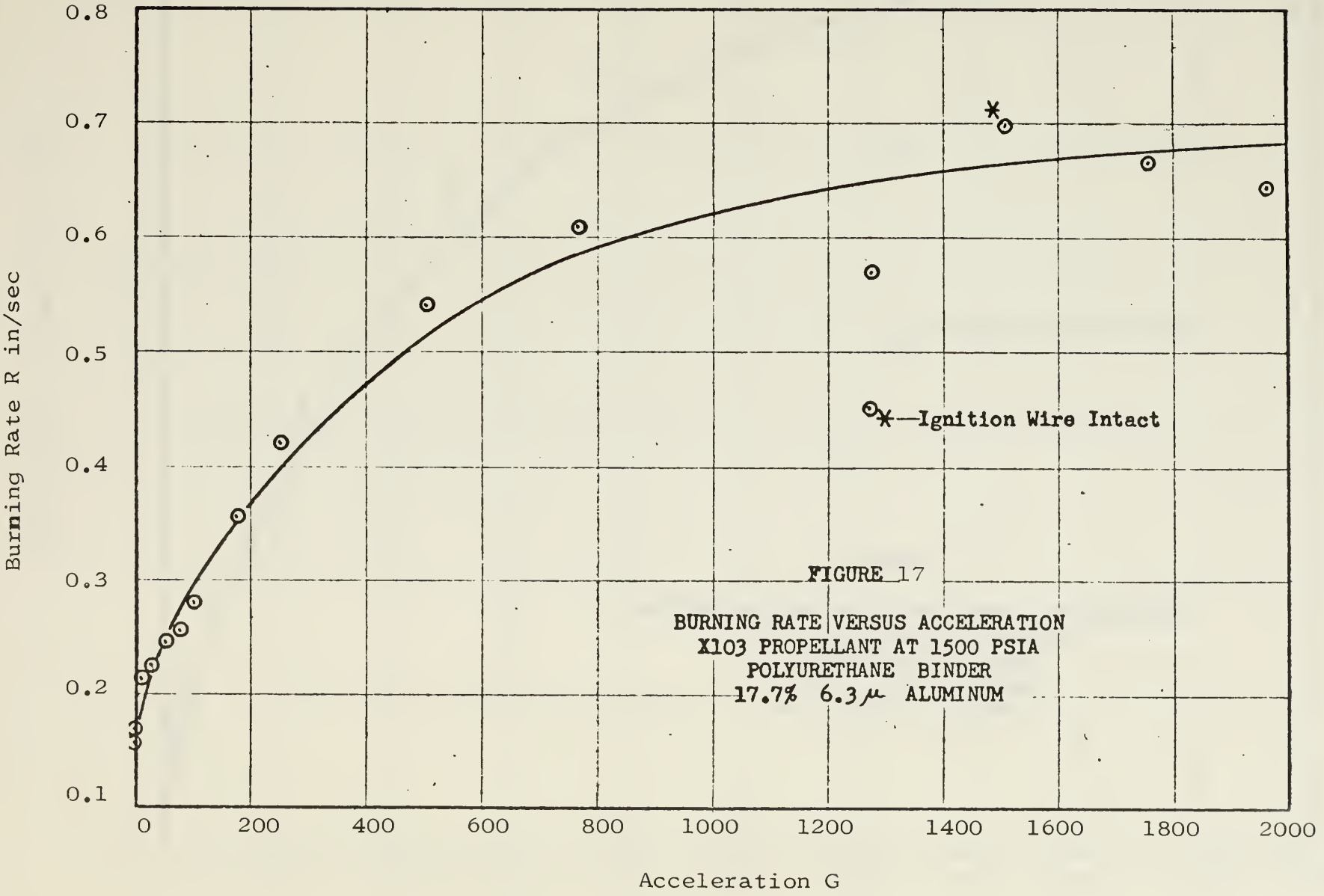

FIGURE 17

BURNING RATE VERSUS ACCELERATION
X103 PROPELLANT AT 1500 PSIA
POLYURETHANE BINDER
17.7% 6.3μ ALUMINUM

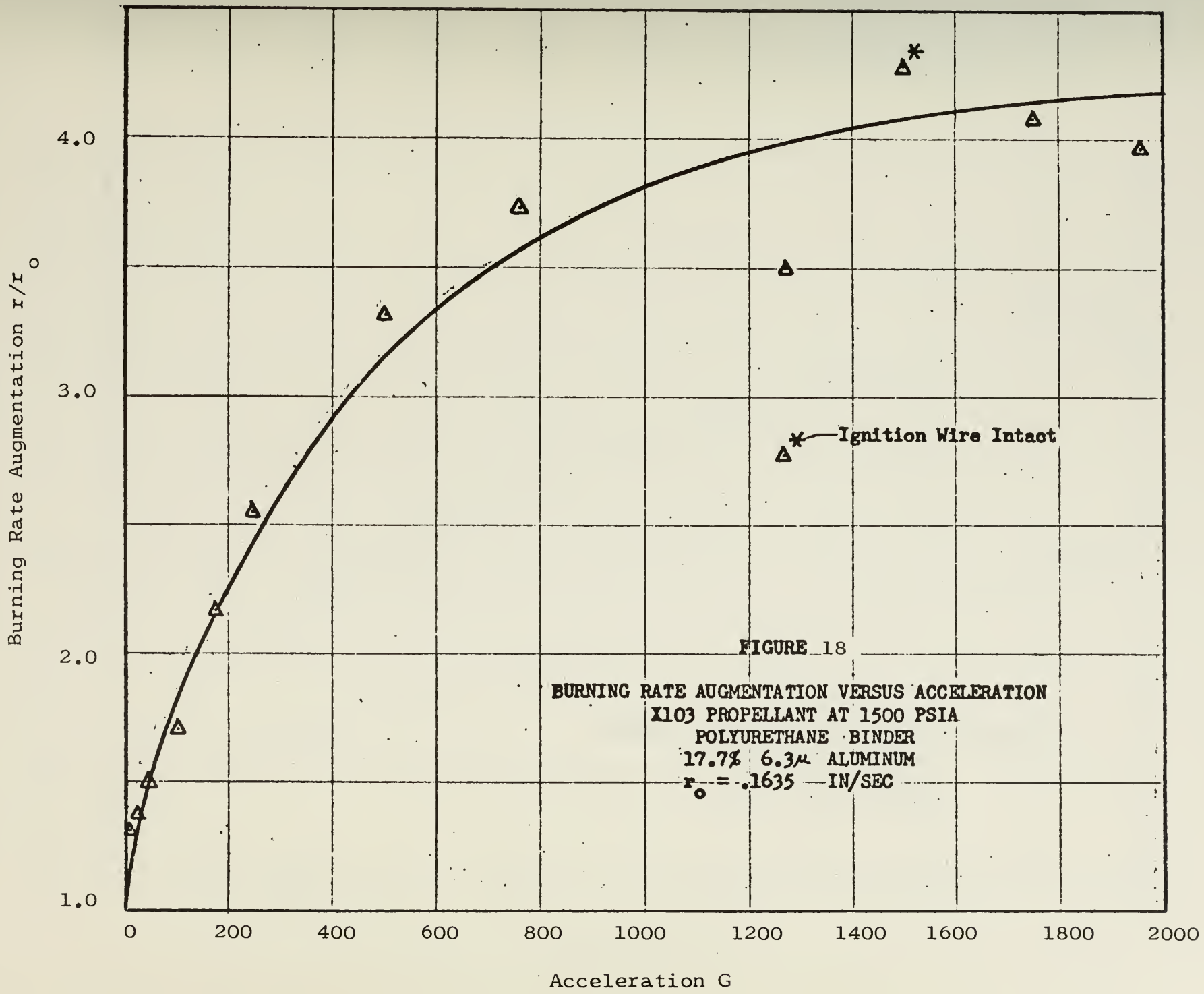

FIGURE 18

BURNING RATE AUGMENTATION VERSUS ACCELERATION
X103 PROPELLANT AT 1500 PSIA
POLYURETHANE BINDER
17.7% 6.3μ ALUMINUM
r_o = .1635 IN/SEC

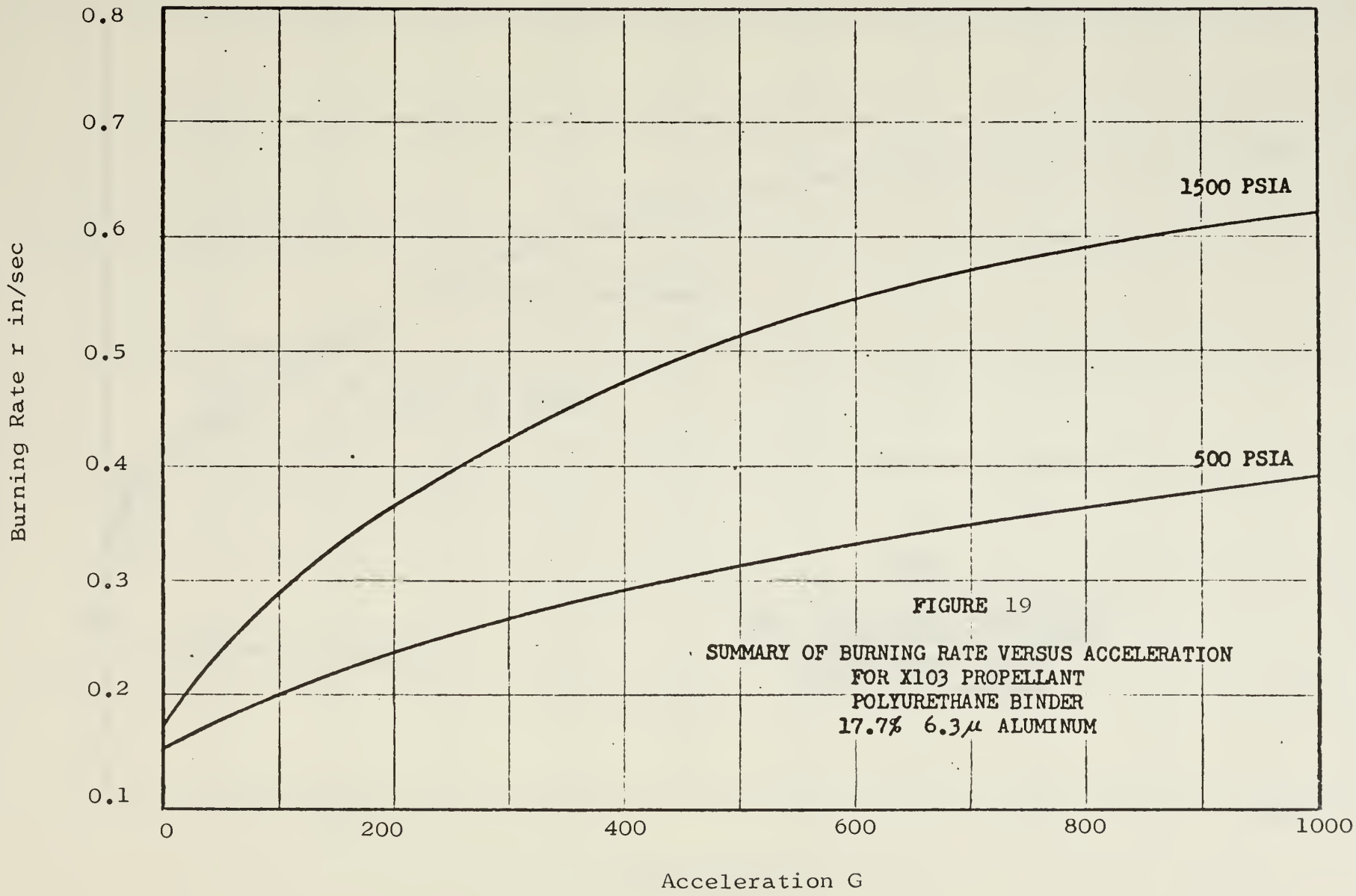

FIGURE 19

SUMMARY OF BURNING RATE VERSUS ACCELERATION
FOR X103 PROPELLANT
POLYURETHANE BINDER
17.7% 6.3μ ALUMINUM

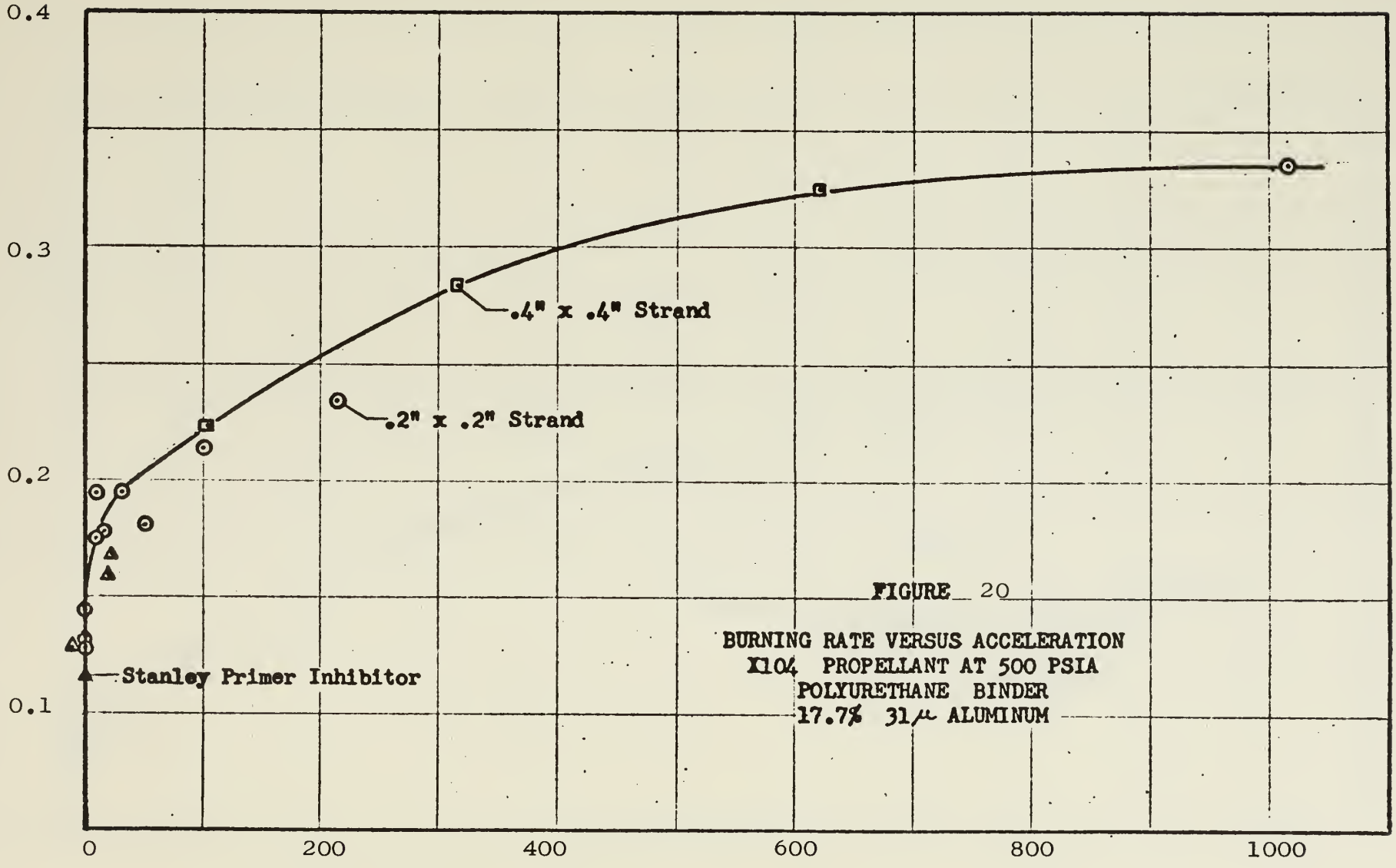

FIGURE 20

BURNING RATE VERSUS ACCELERATION
X104 PROPELLANT AT 500 PSIA
POLYURETHANE BINDER
17.7% 31μ ALUMINUM

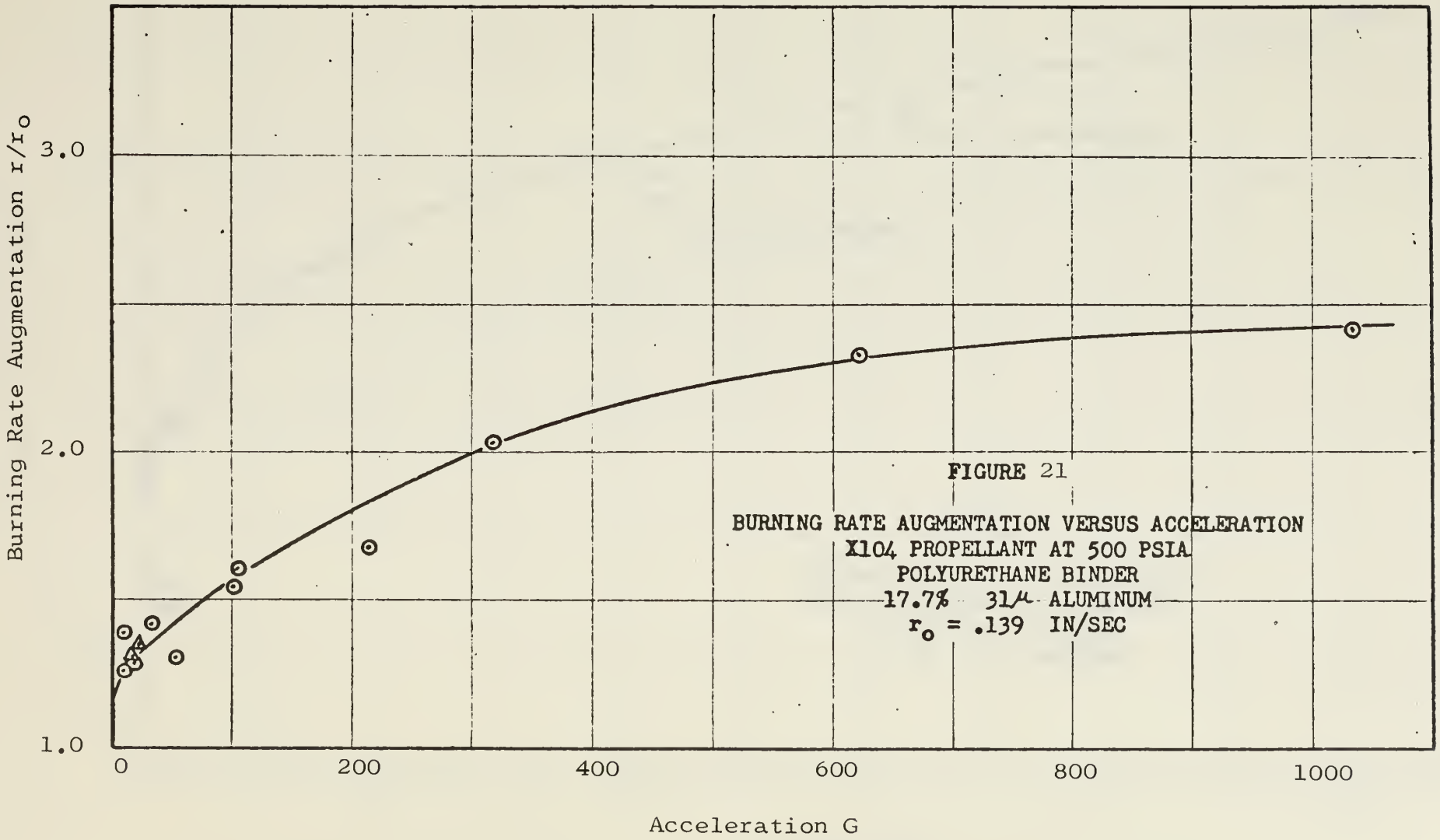

FIGURE 21

BURNING RATE AUGMENTATION VERSUS ACCELERATION
X104 PROPELLANT AT 500 PSIA
POLYURETHANE BINDER
17.7% 31μ ALUMINUM
r_o = .139 IN/SEC

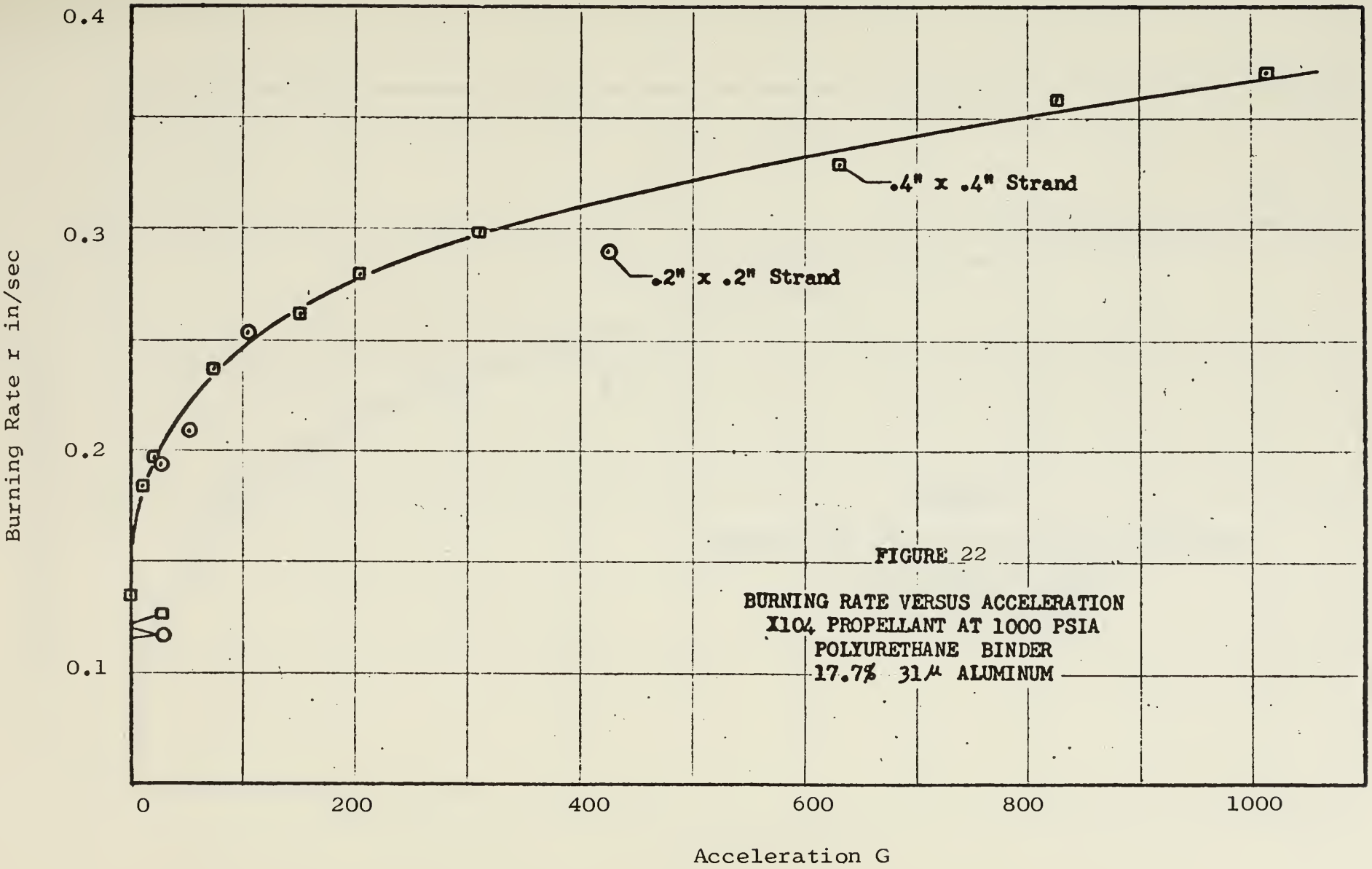

FIGURE 22

BURNING RATE VERSUS ACCELERATION
X104 PROPELLANT AT 1000 PSIA
POLYURETHANE BINDER
17.7% 31μ ALUMINUM

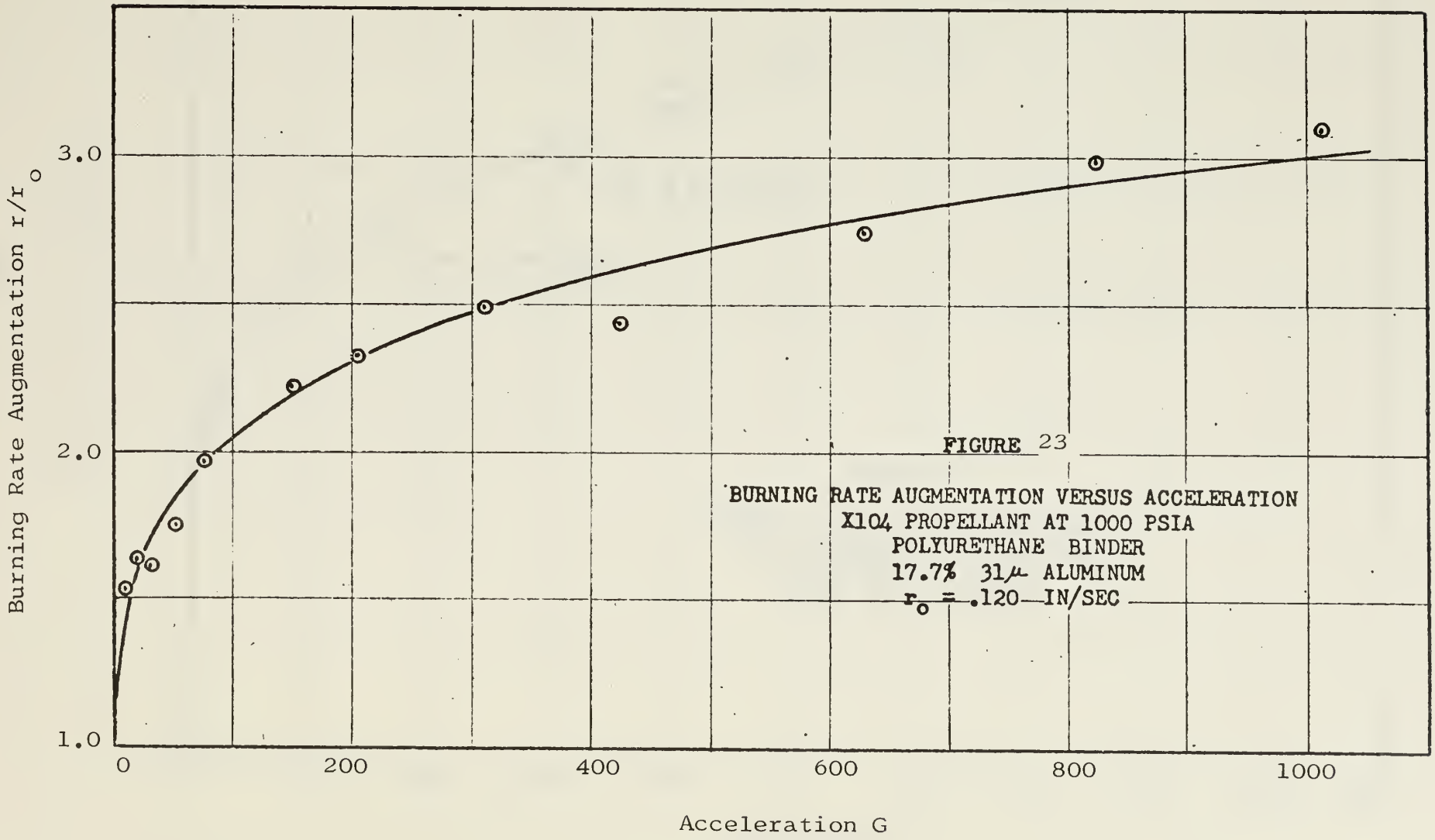

FIGURE 23

BURNING RATE AUGMENTATION VERSUS ACCELERATION
X104 PROPELLANT AT 1000 PSIA
POLYURETHANE BINDER
17.7% 31μ ALUMINUM
r_o = .120 IN/SEC

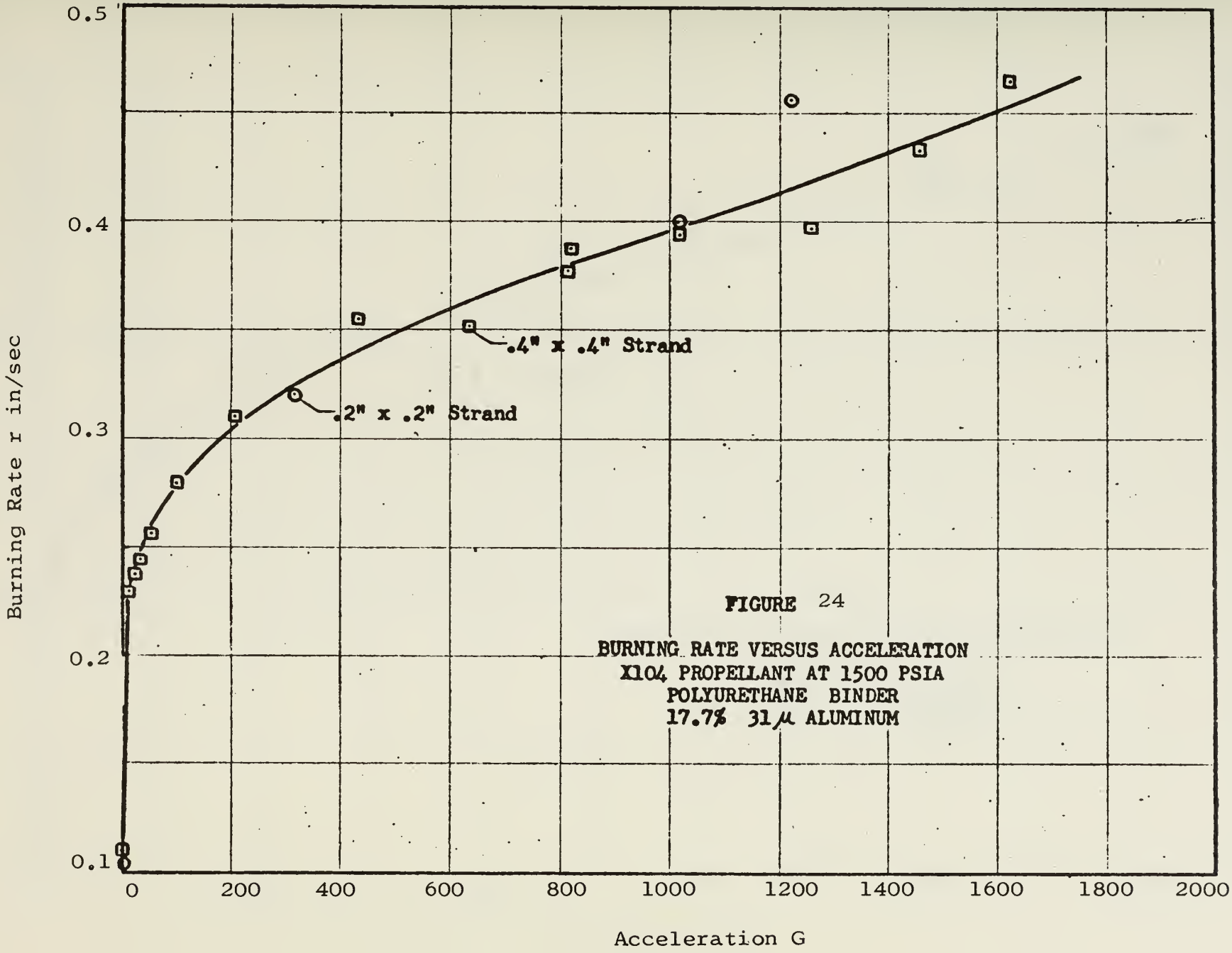

FIGURE 24

BURNING RATE VERSUS ACCELERATION
X104 PROPELLANT AT 1500 PSIA
POLYURETHANE BINDER
17.7% 31 μ ALUMINUM

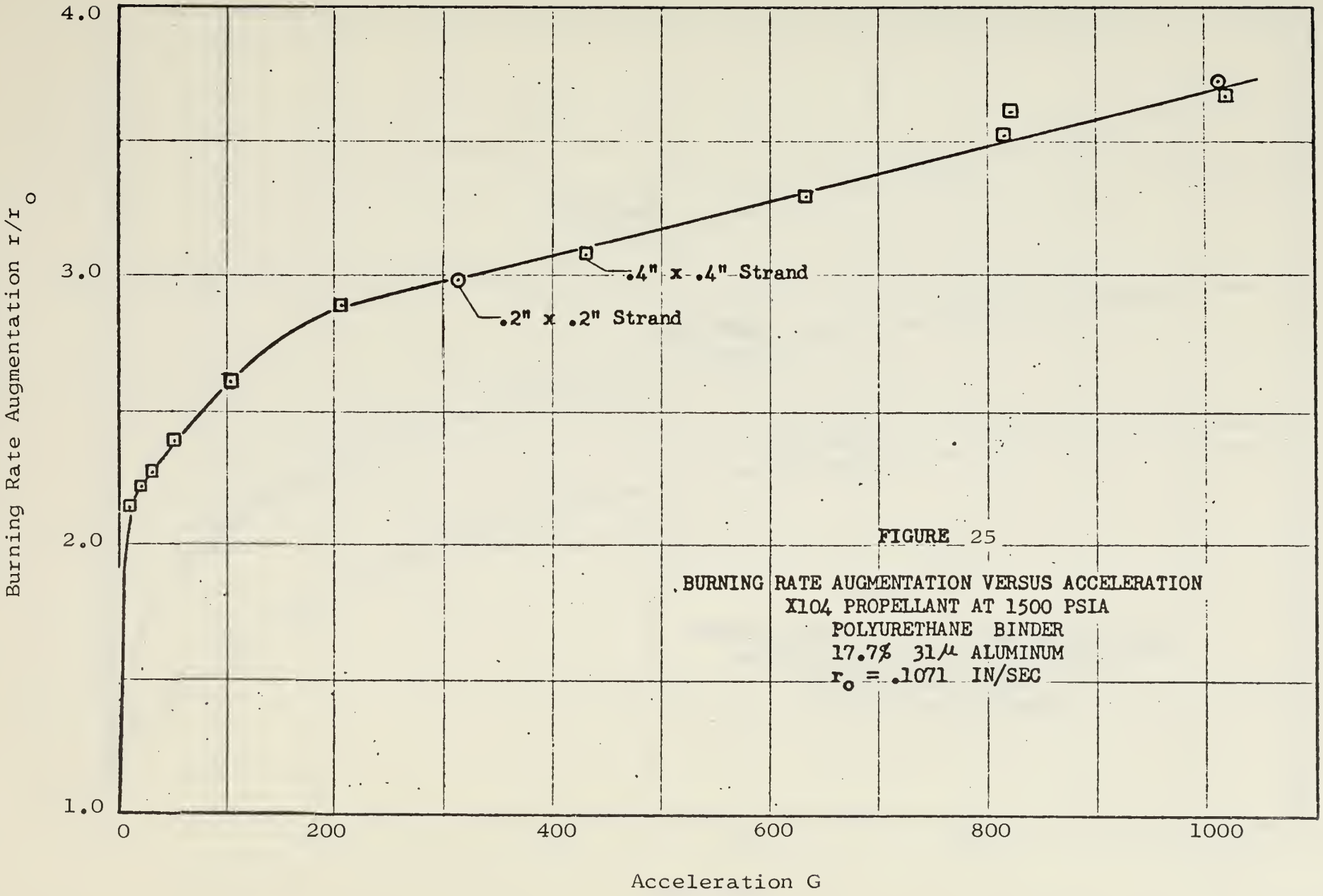

FIGURE 25

BURNING RATE AUGMENTATION VERSUS ACCELERATION
X104 PROPELLANT AT 1500 PSIA
POLYURETHANE BINDER
17.7% 31μ ALUMINUM
r_o = .1071 IN/SEC

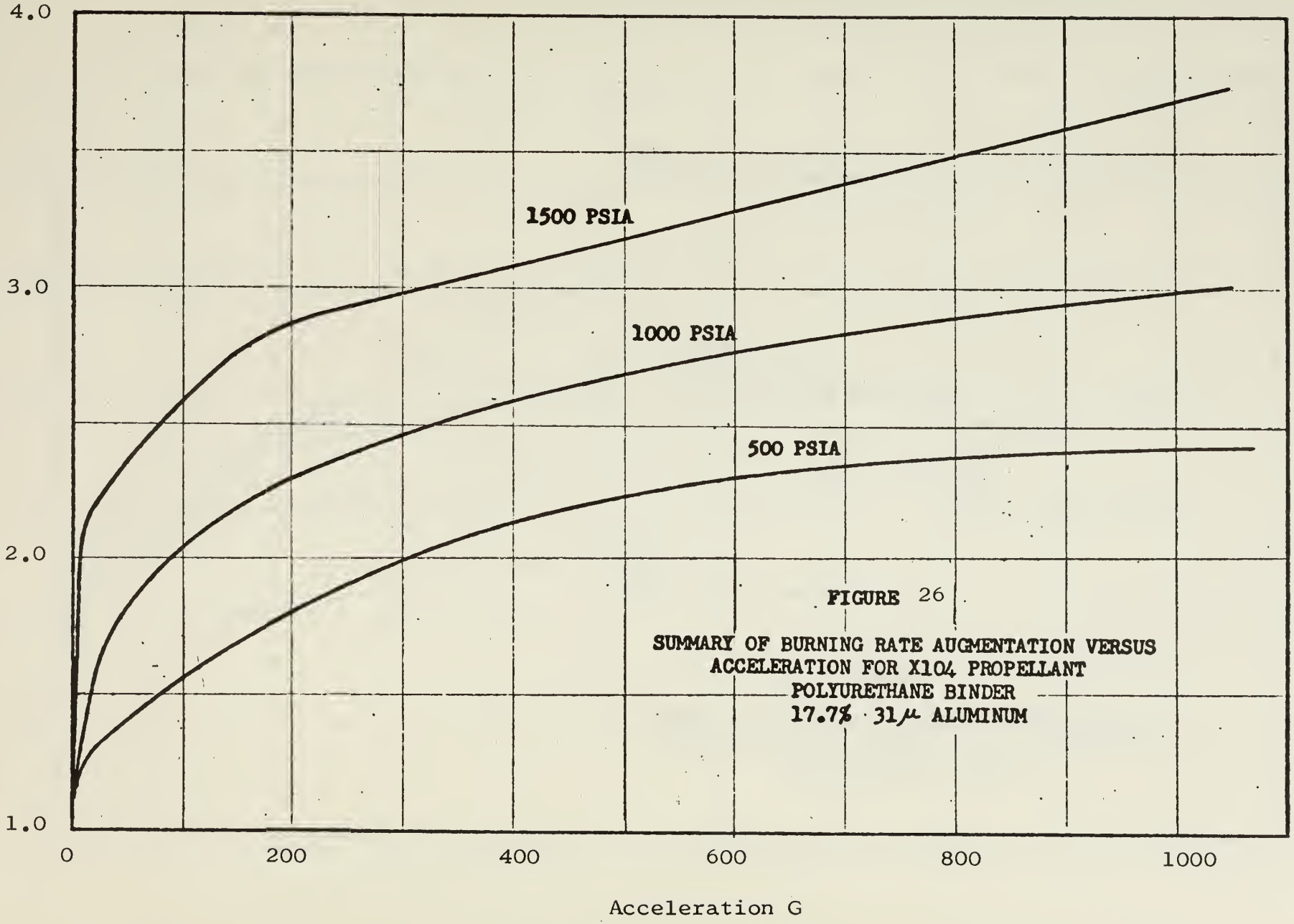

FIGURE 26

SUMMARY OF BURNING RATE AUGMENTATION VERSUS ACCELERATION FOR X104 PROPELLANT POLYURETHANE BINDER 17.7% 31μ ALUMINUM

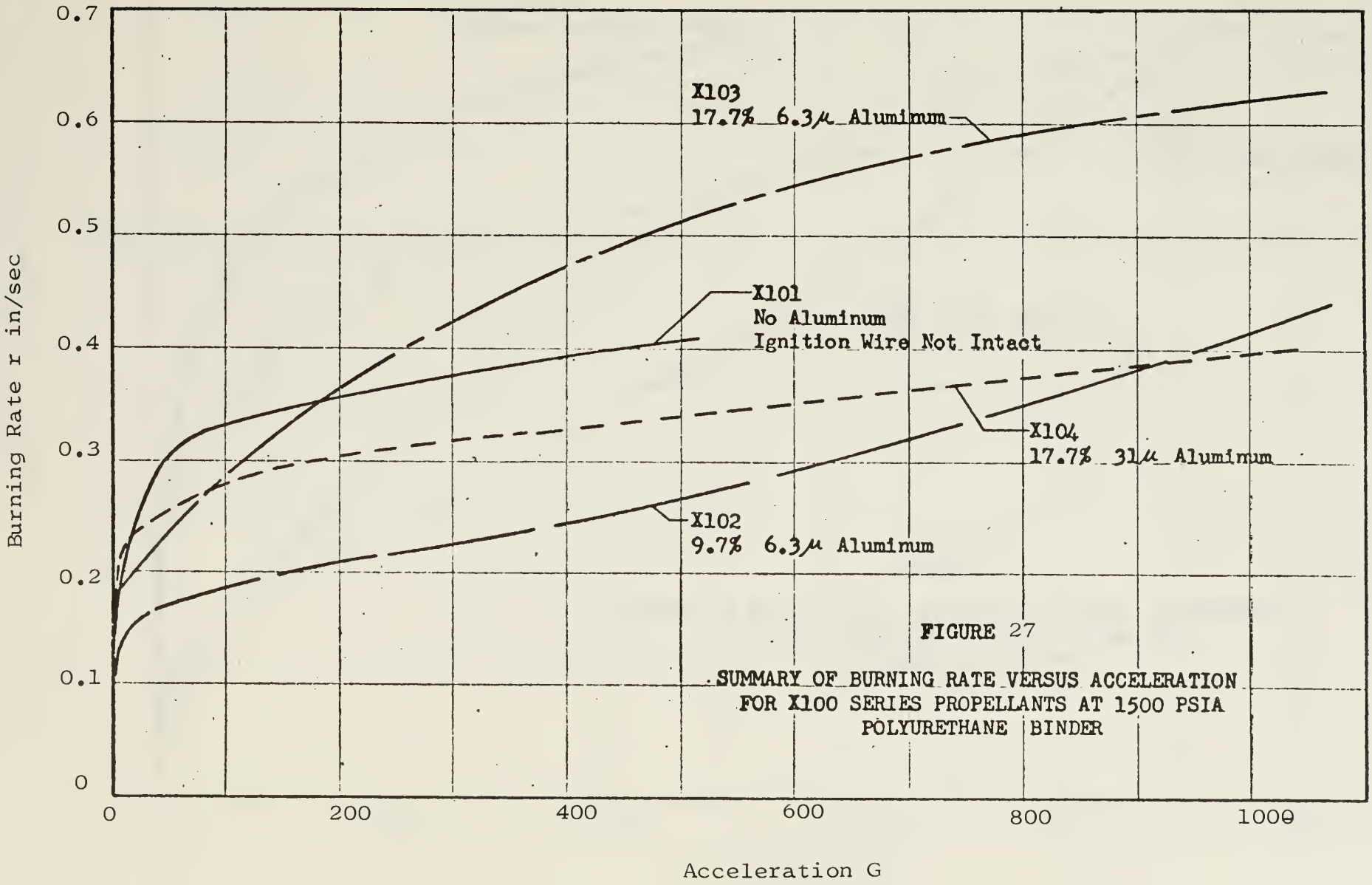

FIGURE 27

SUMMARY OF BURNING RATE VERSUS ACCELERATION
FOR X100 SERIES PROPELLANTS AT 1500 PSIA
POLYURETHANE BINDER

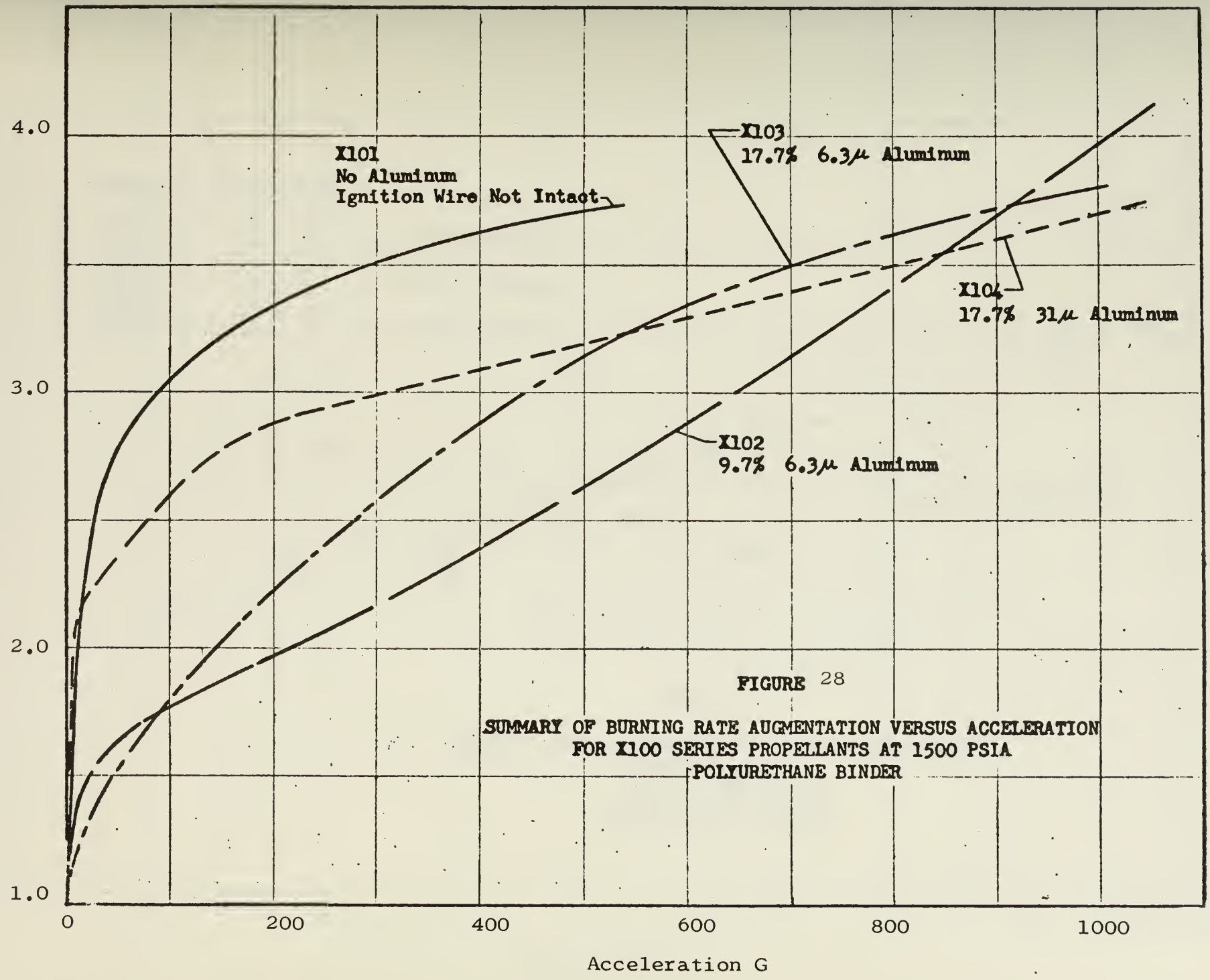

FIGURE 28

SUMMARY OF BURNING RATE AUGMENTATION VERSUS ACCELERATION
FOR X100 SERIES PROPELLANTS AT 1500 PSIA
POLYURETHANE BINDER

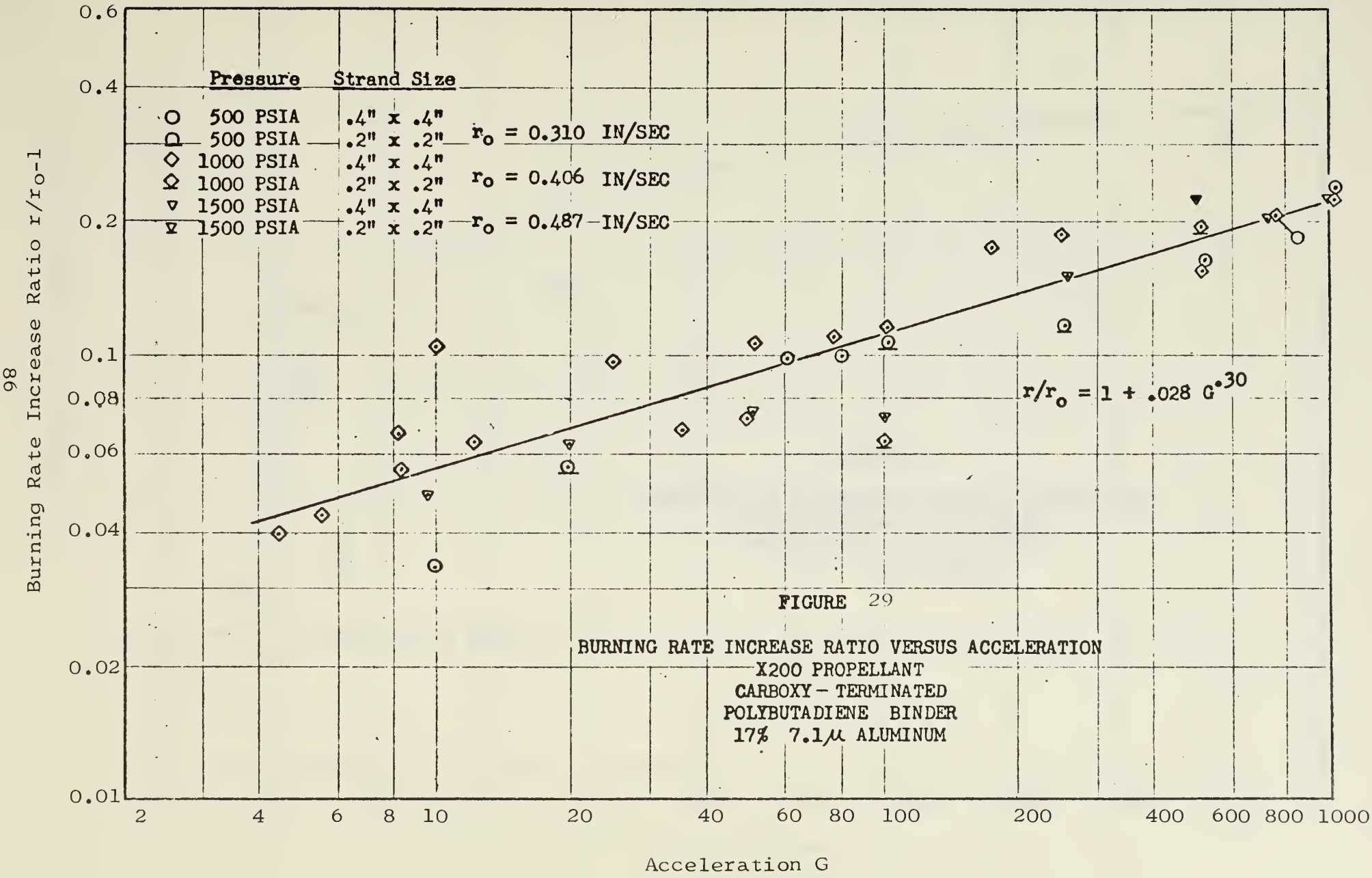

FIGURE 29

BURNING RATE INCREASE RATIO VERSUS ACCELERATION
X200 PROPELLANT
CARBOXY - TERMINATED
POLYBUTADIENE BINDER
17% 7.1μ ALUMINUM

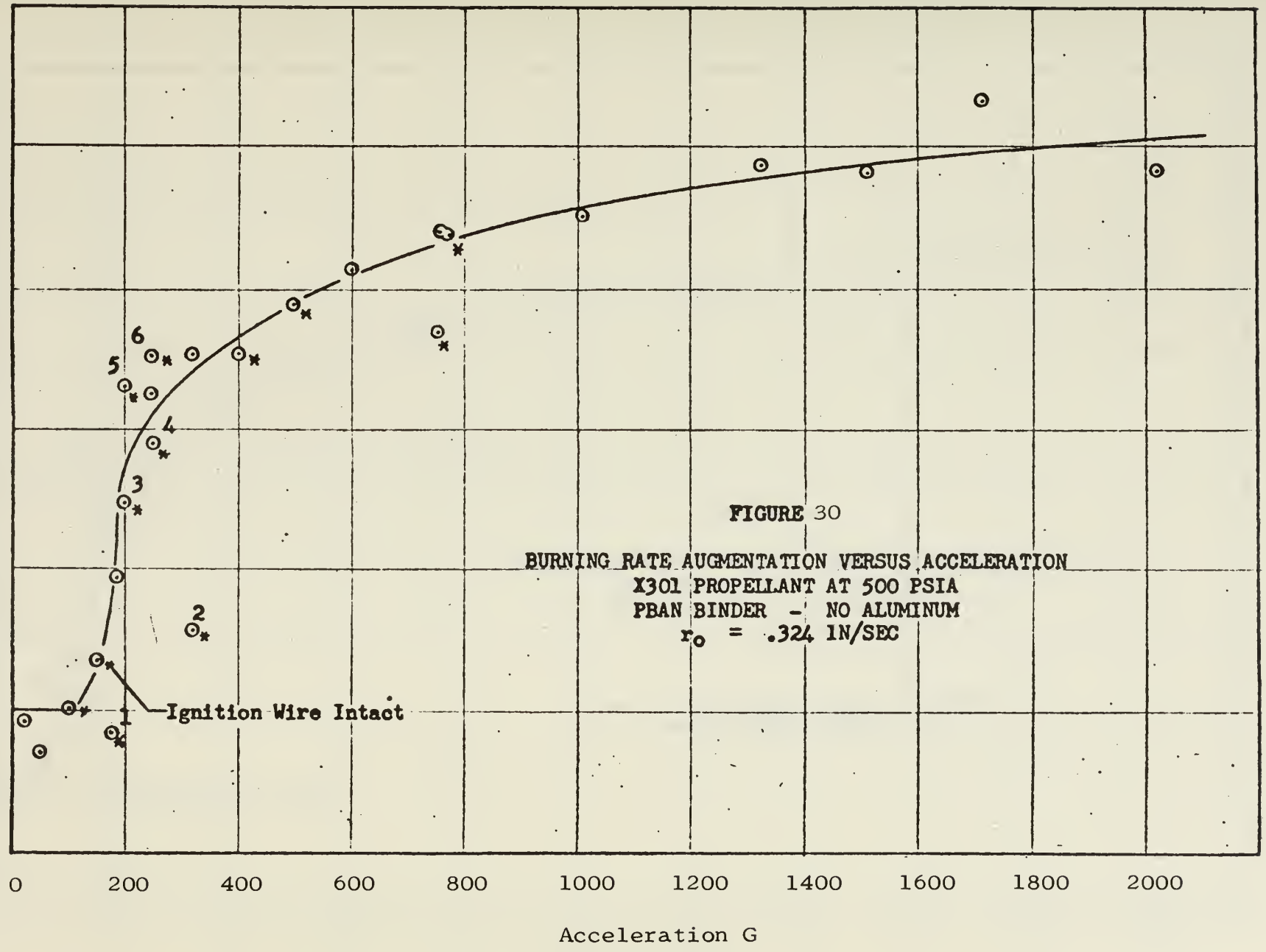

FIGURE 30

BURNING RATE AUGMENTATION VERSUS ACCELERATION
X301 PROPELLANT AT 500 PSIA
PBAN BINDER - NO ALUMINUM
r_o = .324 IN/SEC

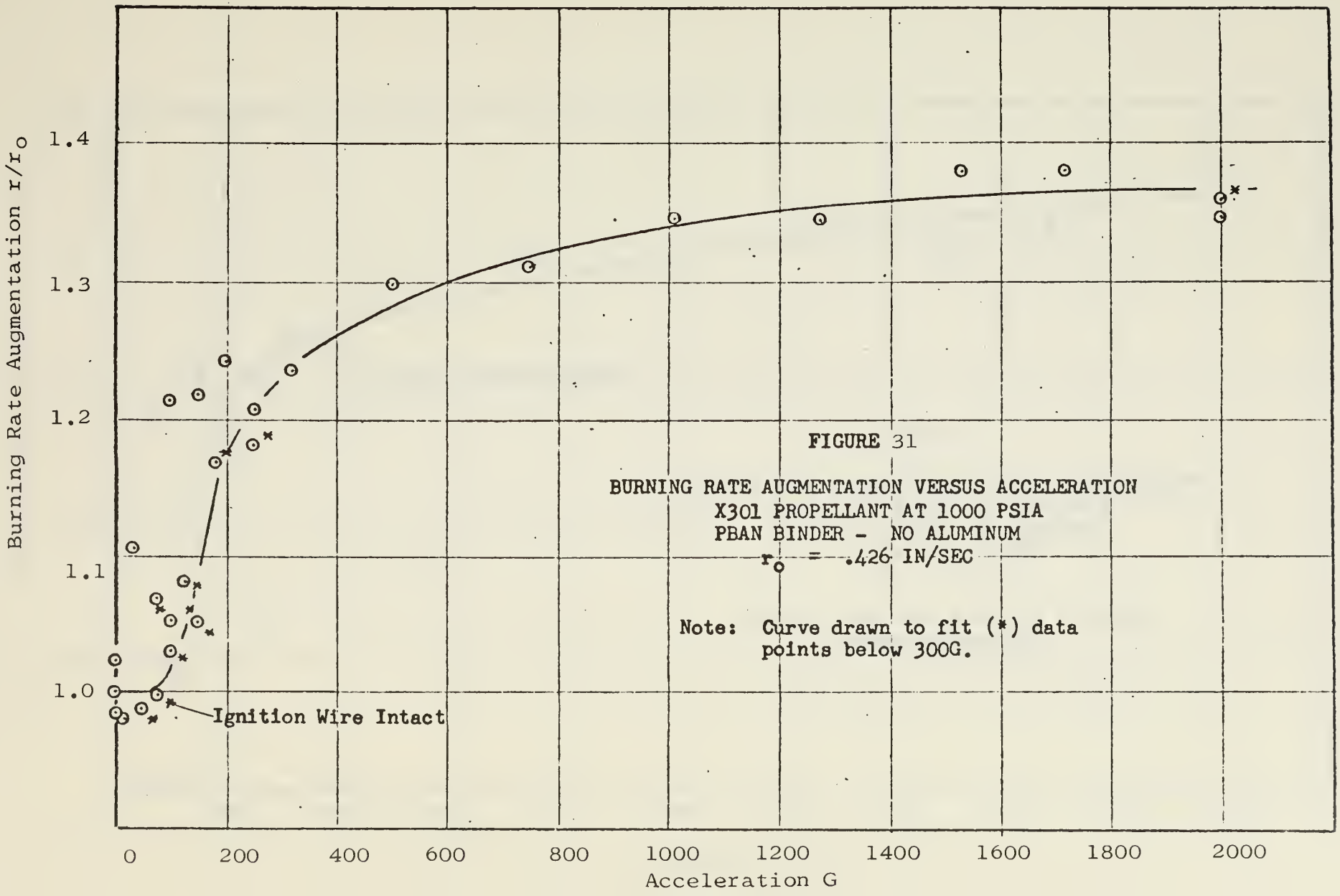

FIGURE 31

BURNING RATE AUGMENTATION VERSUS ACCELERATION
X301 PROPELLANT AT 1000 PSIA
PBAN BINDER - NO ALUMINUM
r_o = .426 IN/SEC

Note: Curve drawn to fit (*) data points below 300G.

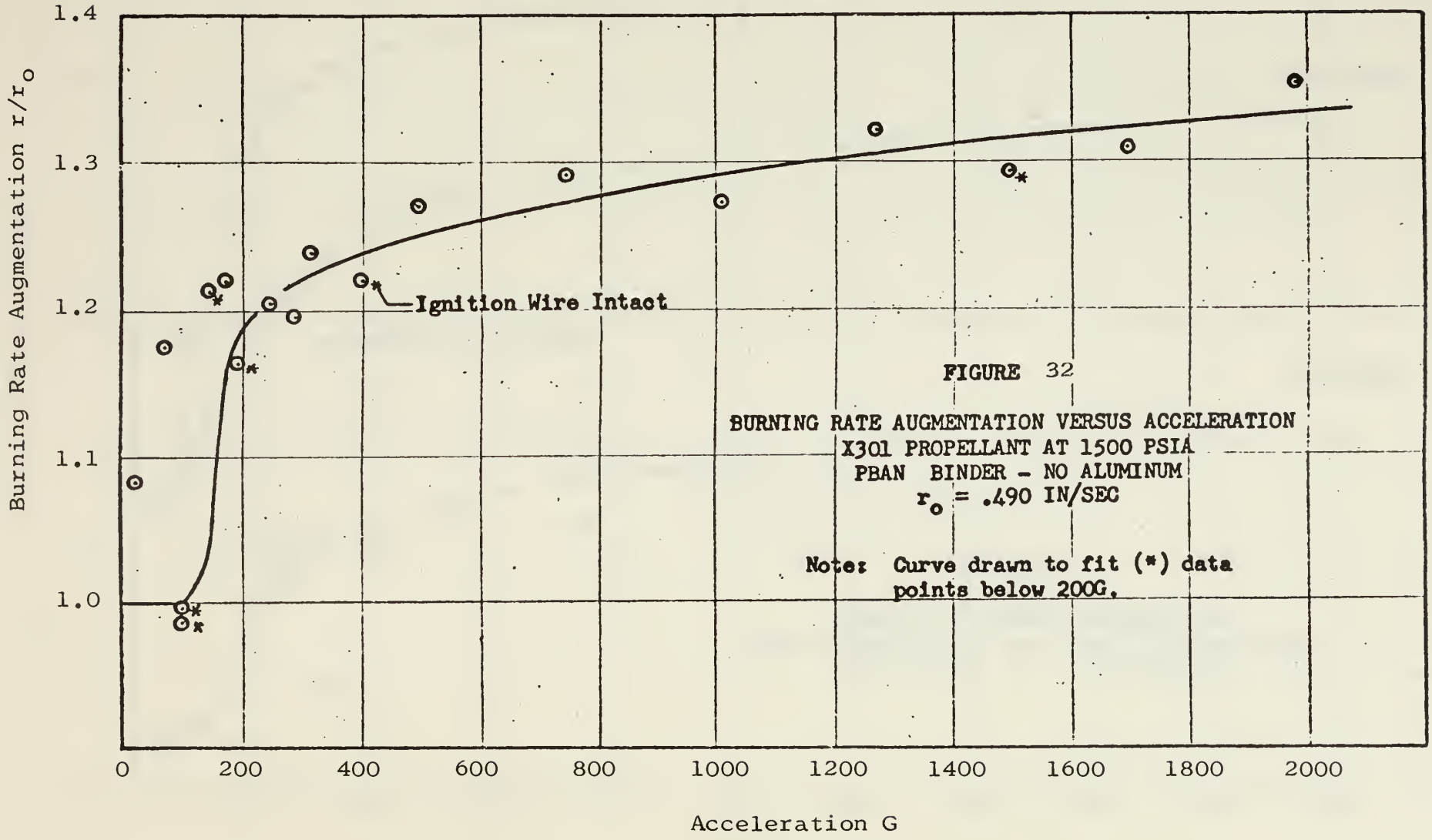

FIGURE 32

BURNING RATE AUGMENTATION VERSUS ACCELERATION
X301 PROPELLANT AT 1500 PSIA
PBAN BINDER - NO ALUMINUM
r_o = .490 IN/SEC

Note: Curve drawn to fit (*) data points below 200G.

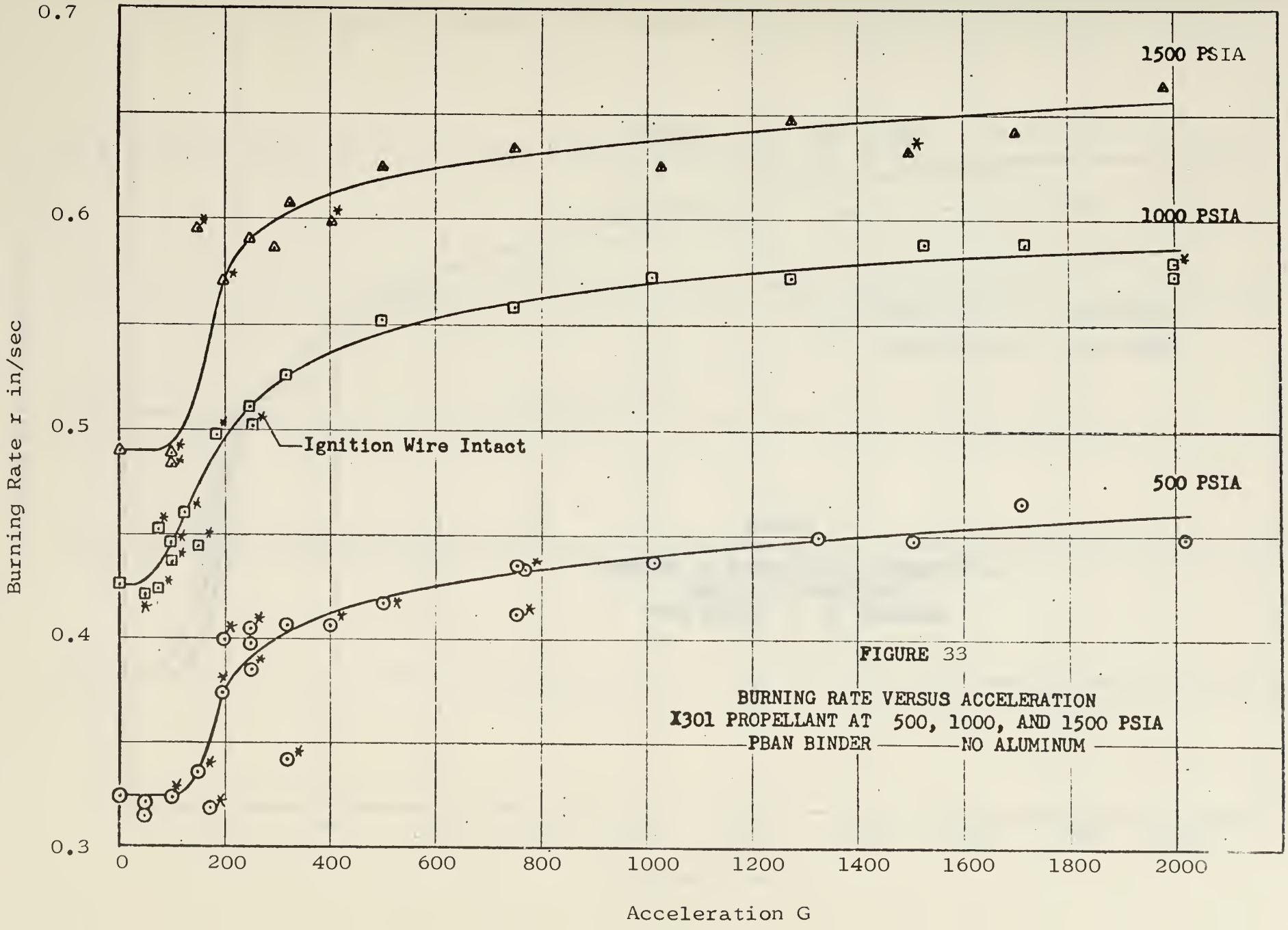

FIGURE 33

BURNING RATE VERSUS ACCELERATION
X301 PROPELLANT AT 500, 1000, AND 1500 PSIA
PBAN BINDER ——— NO ALUMINUM ———

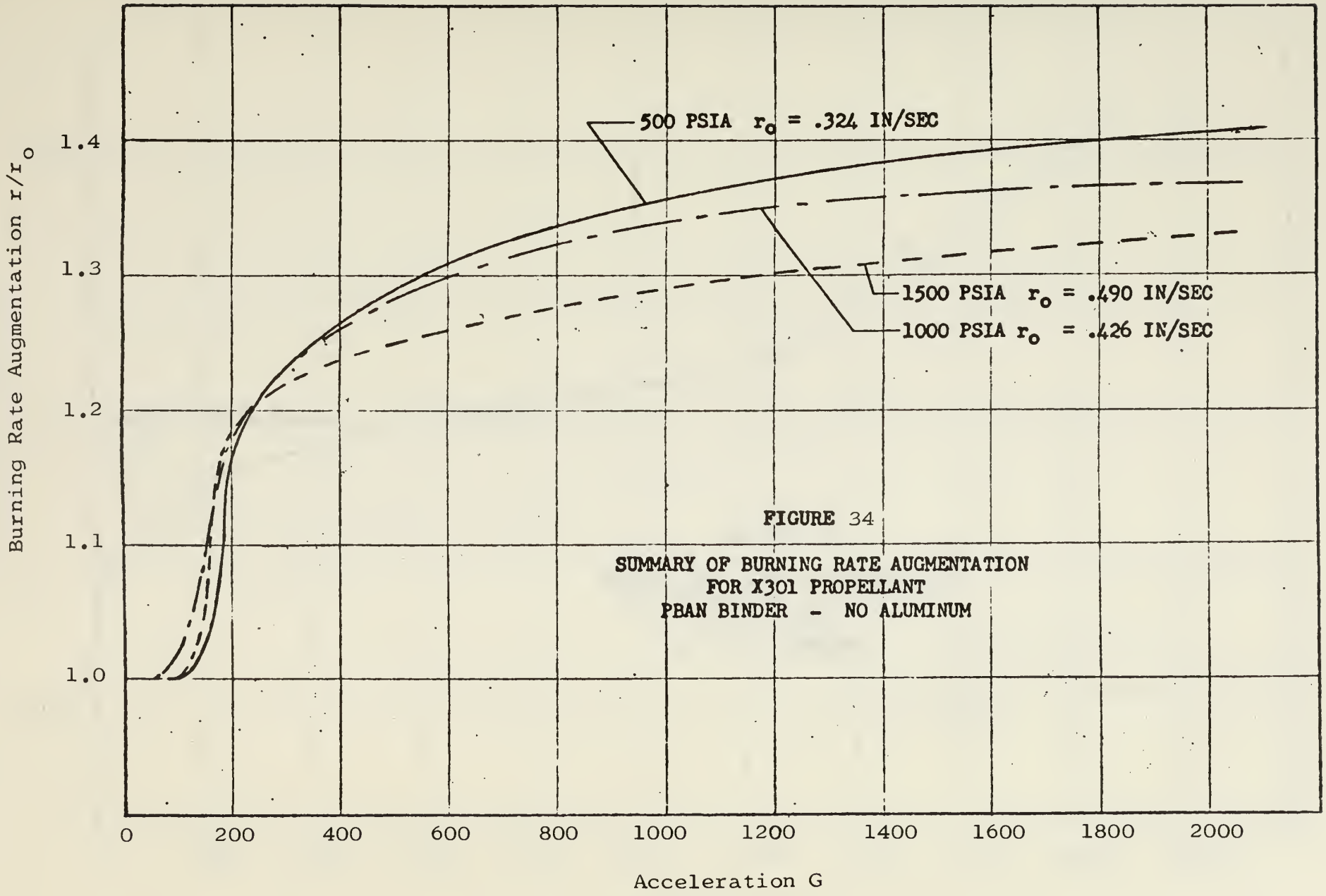

FIGURE 34

SUMMARY OF BURNING RATE AUGMENTATION
FOR X301 PROPELLANT
PBAN BINDER - NO ALUMINUM

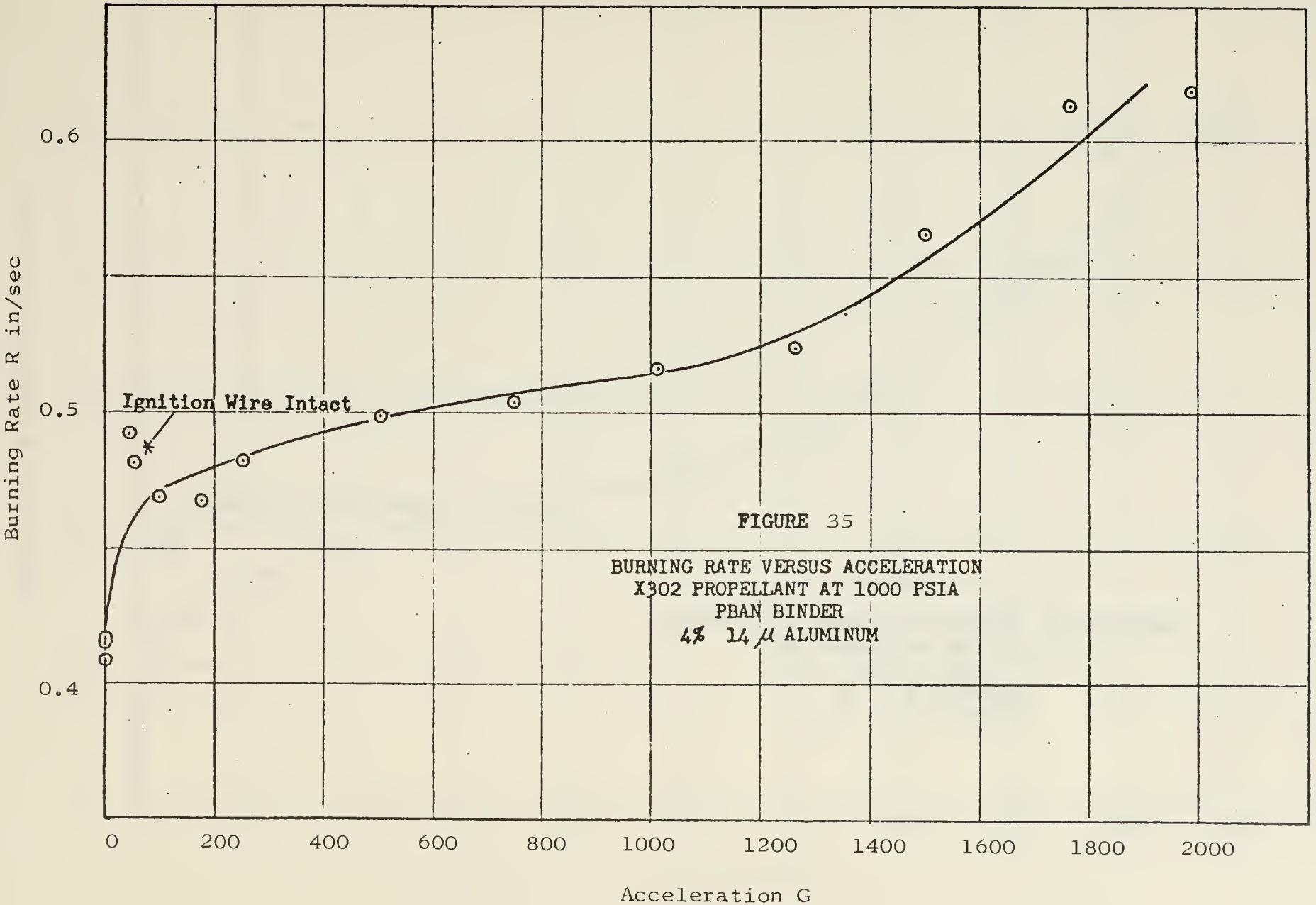

FIGURE 35

BURNING RATE VERSUS ACCELERATION
X302 PROPELLANT AT 1000 PSIA
PBAN BINDER
4% 14 μ ALUMINUM

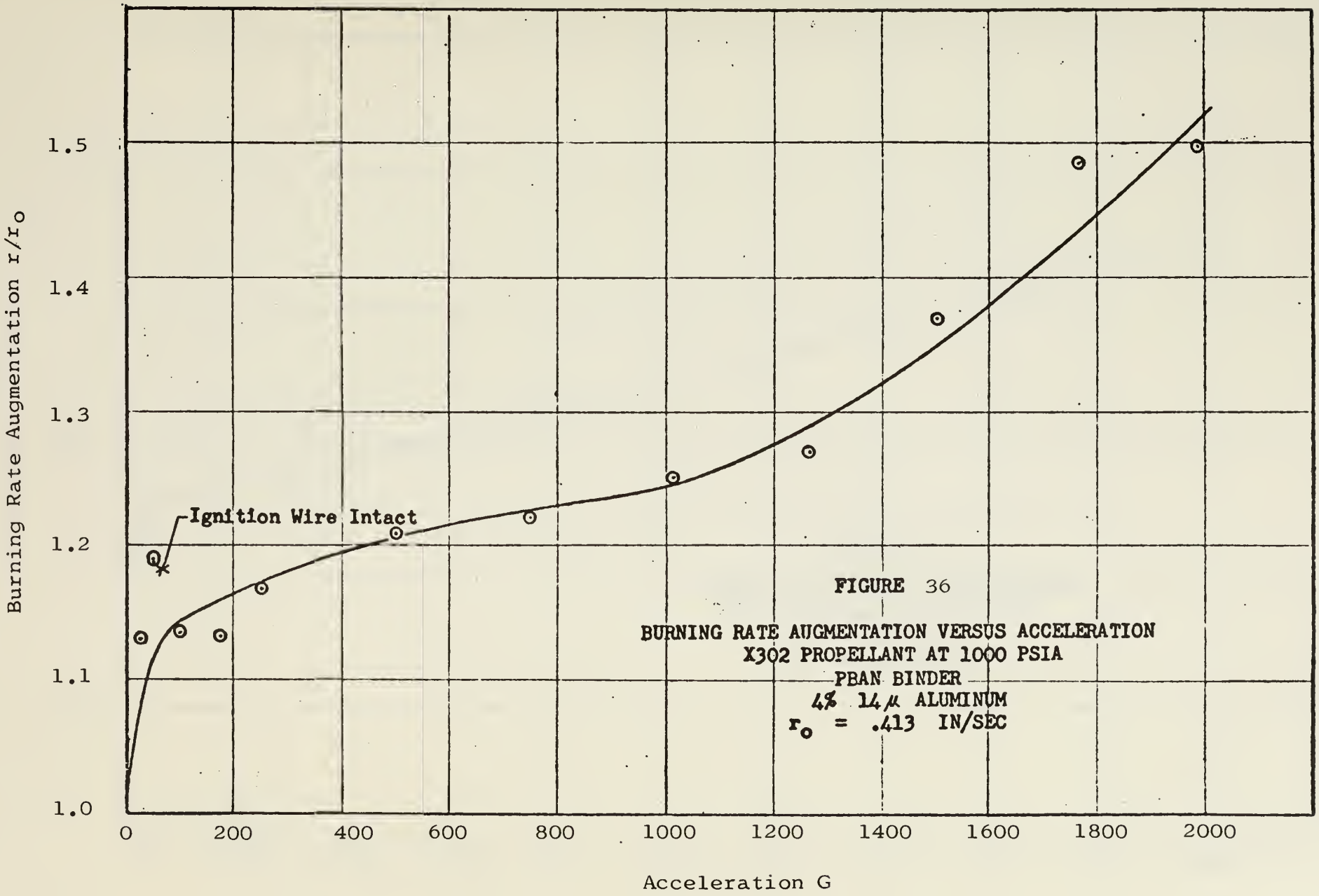

FIGURE 36

BURNING RATE AUGMENTATION VERSUS ACCELERATION
X302 PROPELLANT AT 1000 PSIA
PBAN BINDER
4% 14 μ ALUMINUM
r_o = .413 IN/SEC

500
0
1.0
1.1
1.2
1.3
1.4
1.2

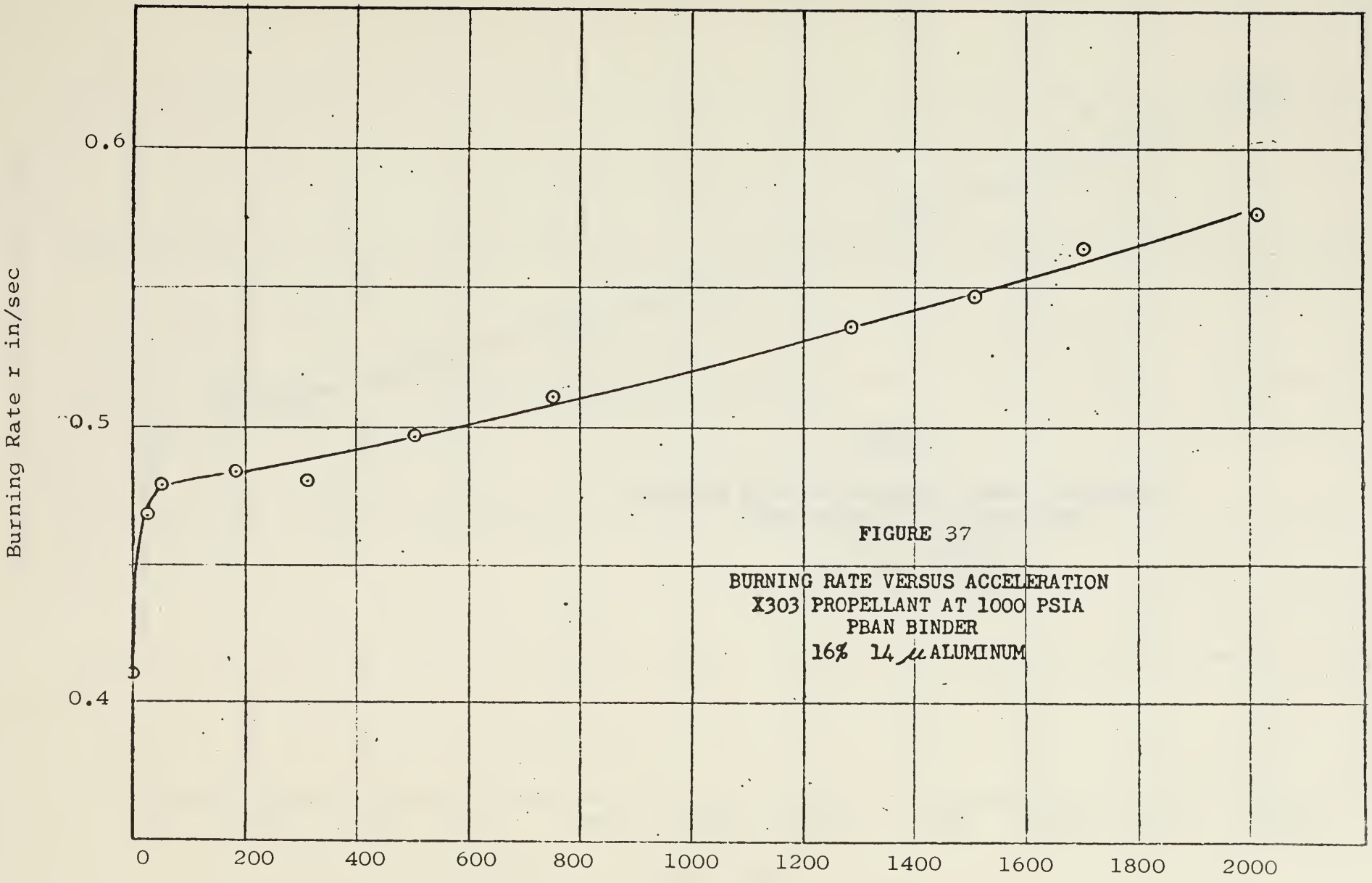

FIGURE 37

BURNING RATE VERSUS ACCELERATION
X303 PROPELLANT AT 1000 PSIA
PBAN BINDER
16% 14 μ ALUMINUM

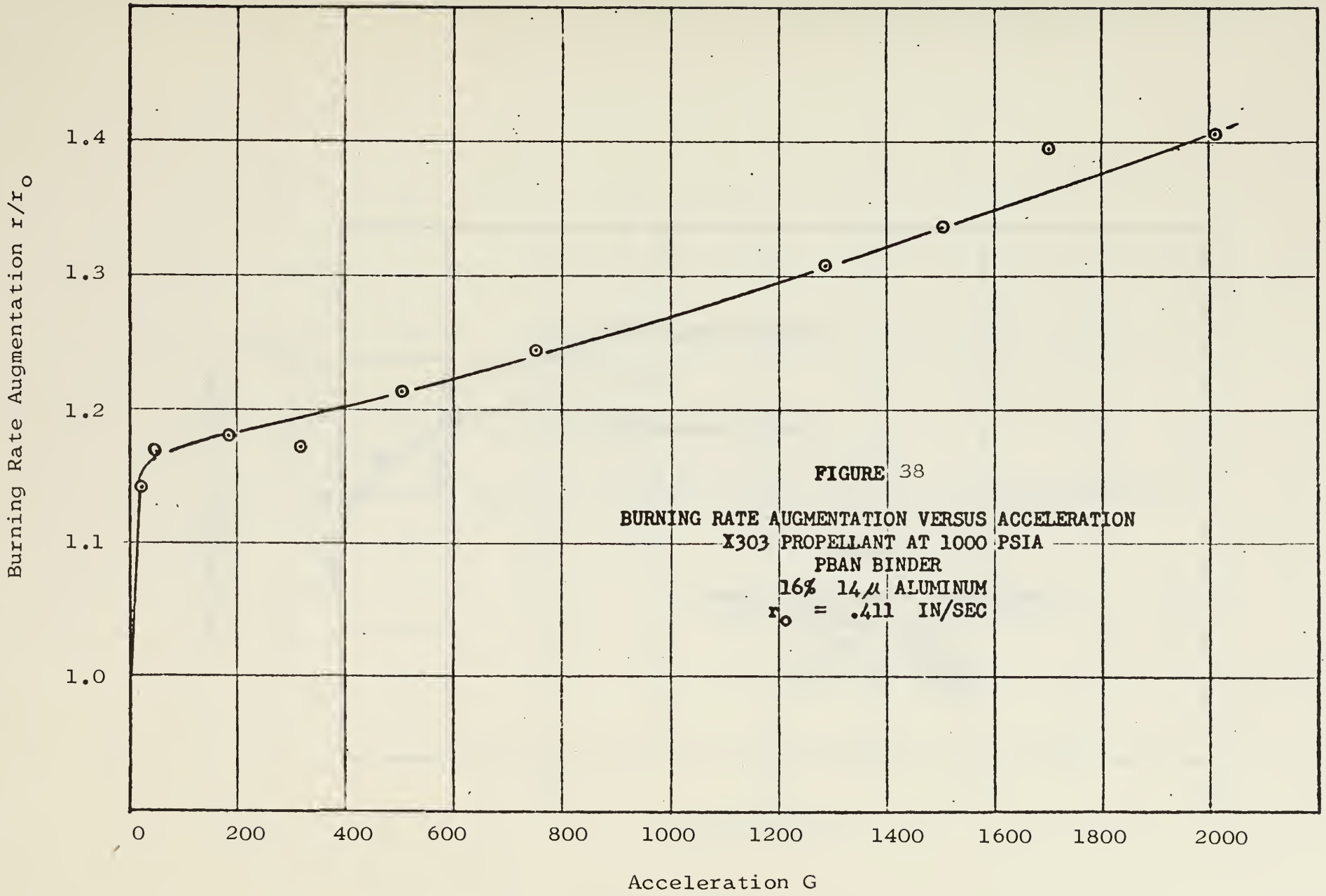

FIGURE 38

BURNING RATE AUGMENTATION VERSUS ACCELERATION
X303 PROPELLANT AT 1000 PSIA
PBAN BINDER
16% 14μ ALUMINUM
r_o = .411 IN/SEC

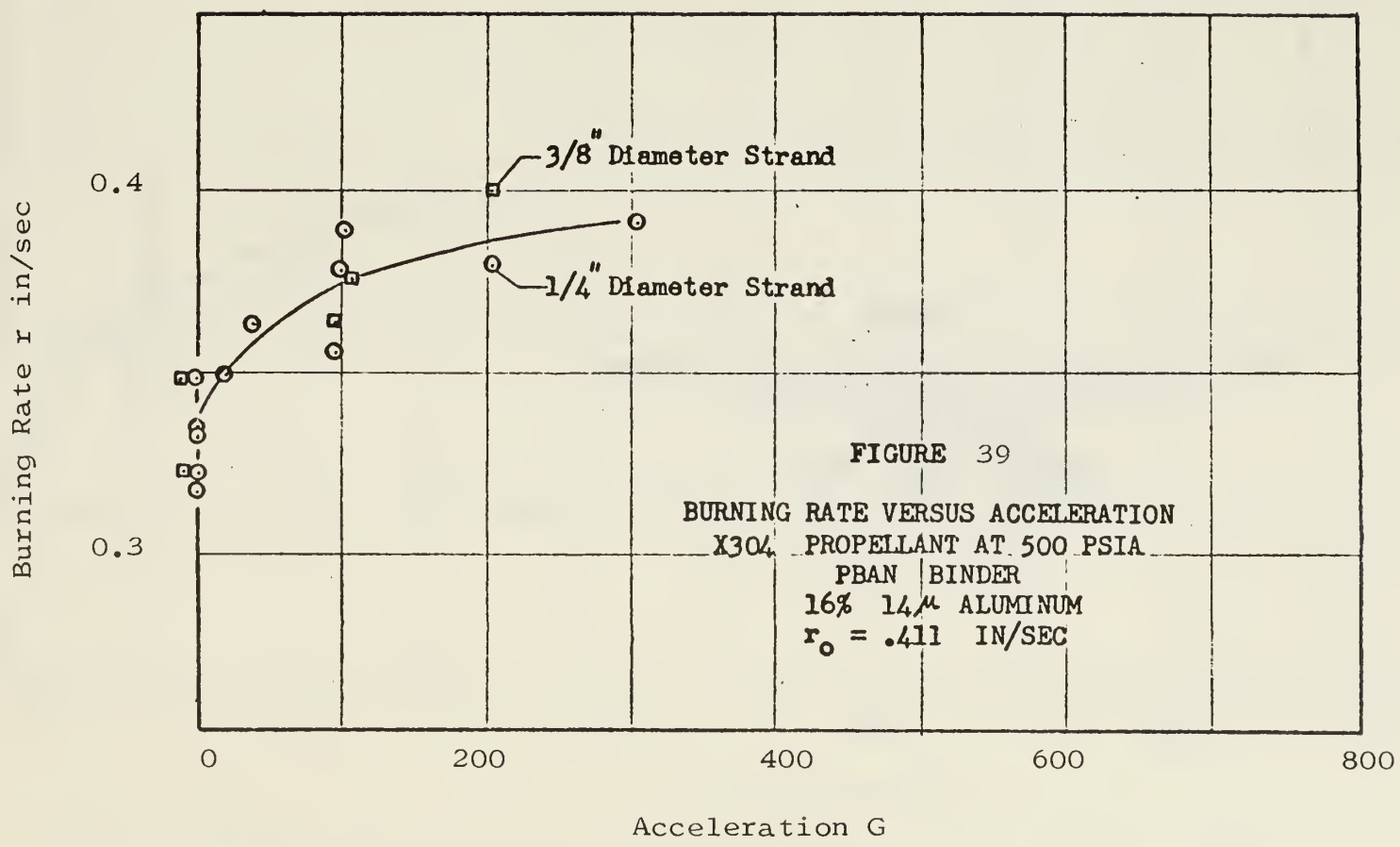

FIGURE 39

BURNING RATE VERSUS ACCELERATION
X304 PROPELLANT AT 500 PSIA
PBAN BINDER
16% 14μ ALUMINUM
r_o = .411 IN/SEC

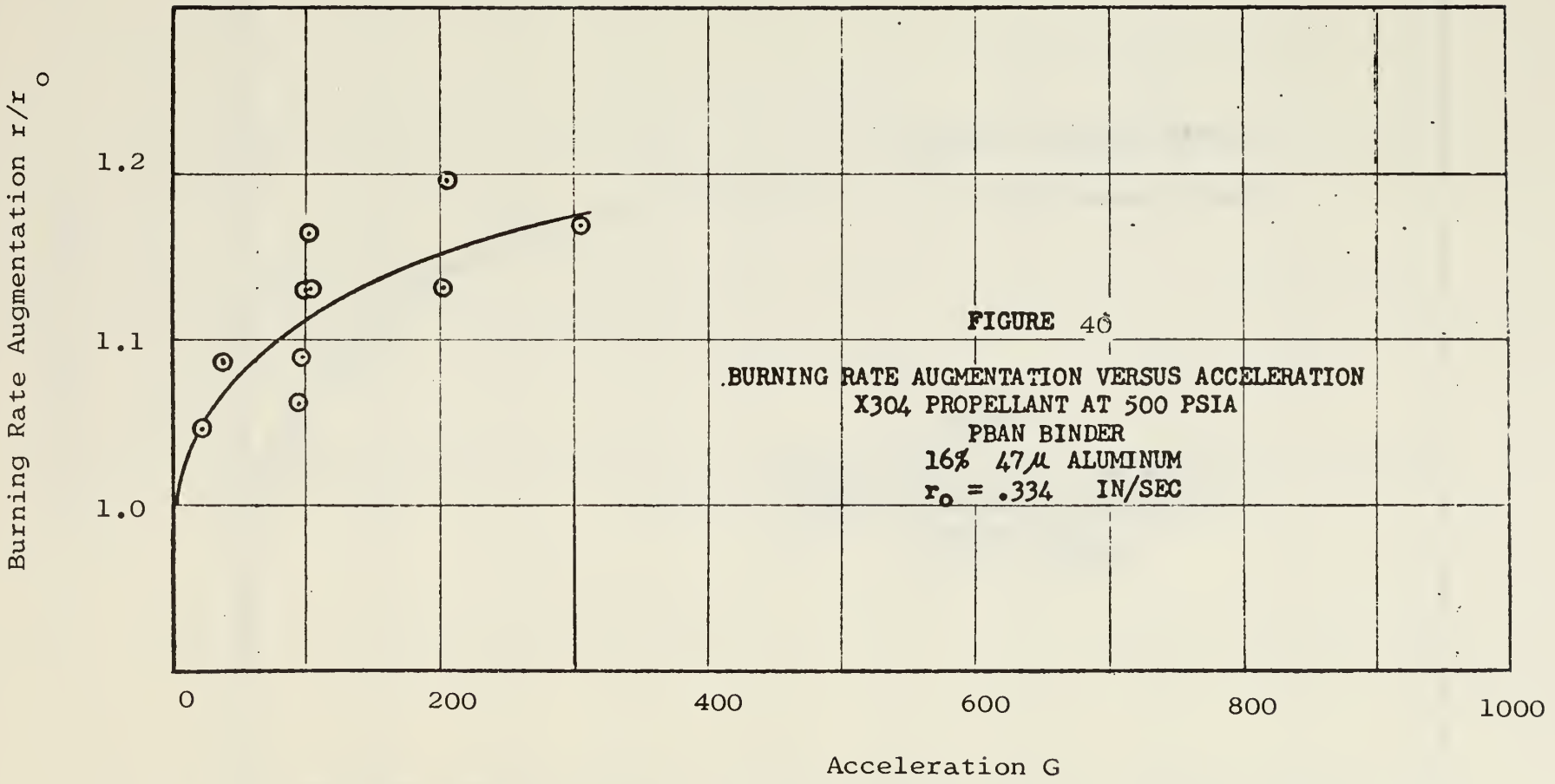

FIGURE 46

BURNING RATE AUGMENTATION VERSUS ACCELERATION
X304 PROPELLANT AT 500 PSIA
PBAN BINDER
16% 47μ ALUMINUM
r_o = .334 IN/SEC

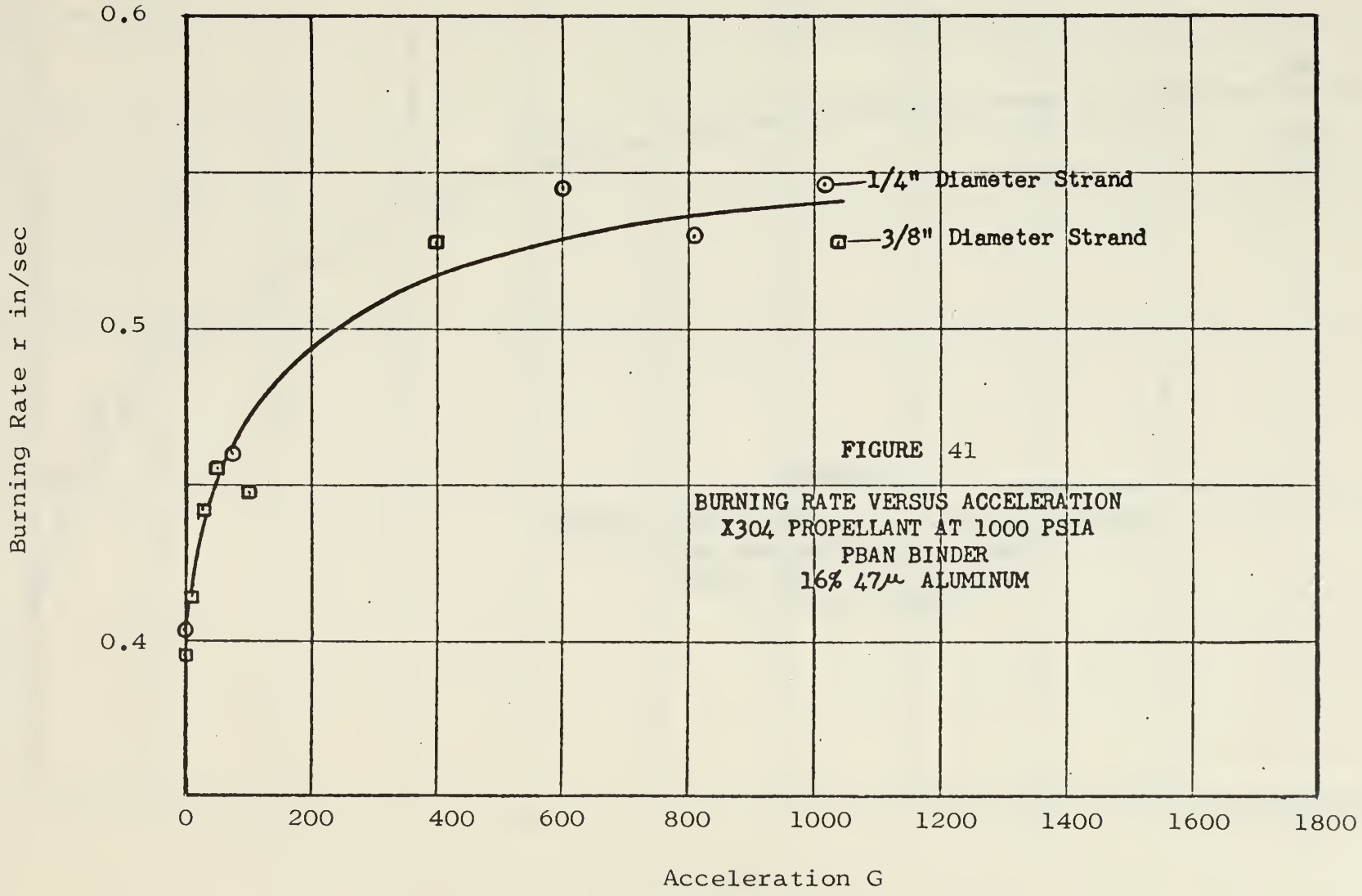

FIGURE 41

BURNING RATE VERSUS ACCELERATION
X304 PROPELLANT AT 1000 PSIA
PBAN BINDER
16% 47μ ALUMINUM

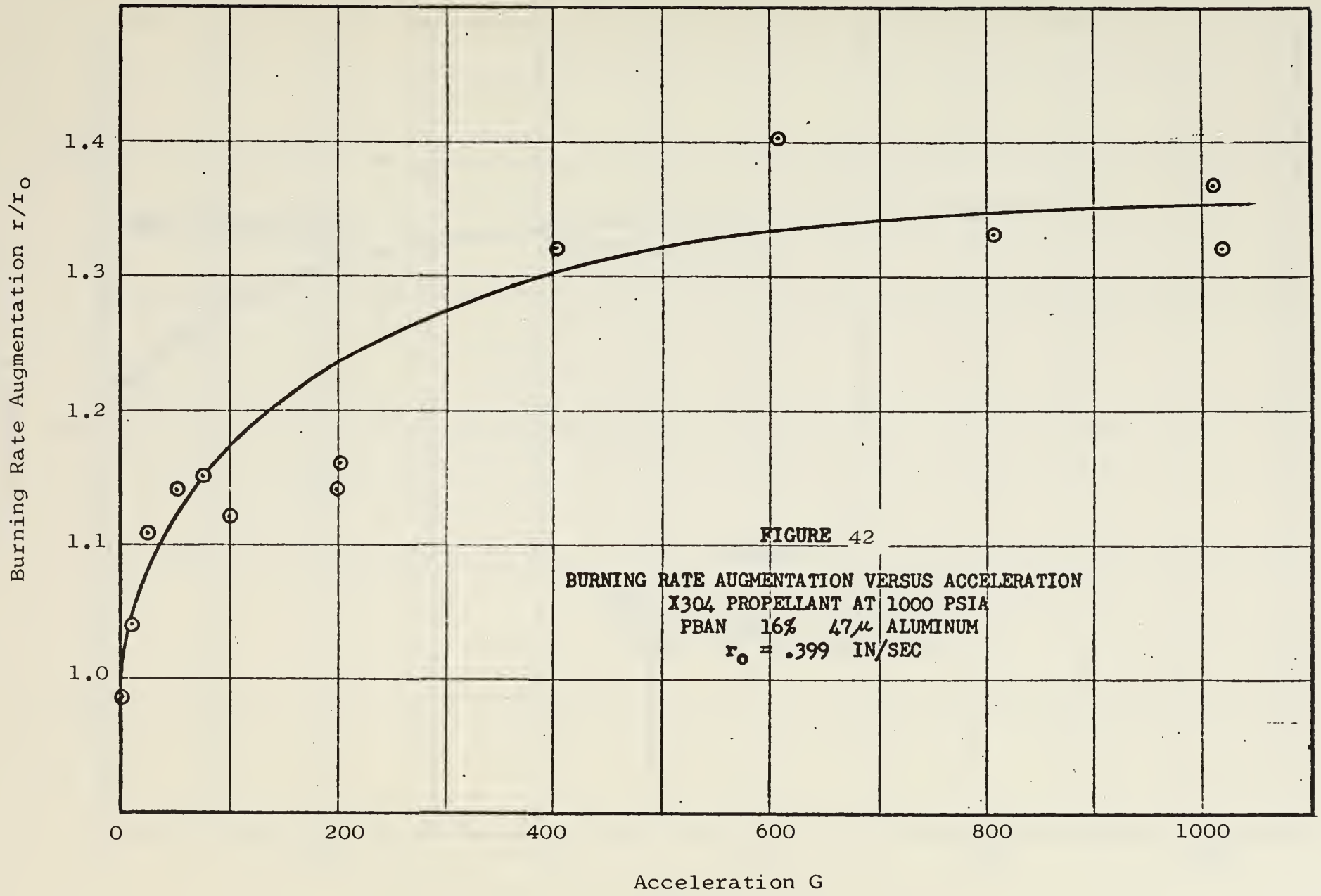

FIGURE 42

BURNING RATE AUGMENTATION VERSUS ACCELERATION
X304 PROPELLANT AT 1000 PSIA
PBAN 16% 47μ ALUMINUM
r_o = .399 IN/SEC

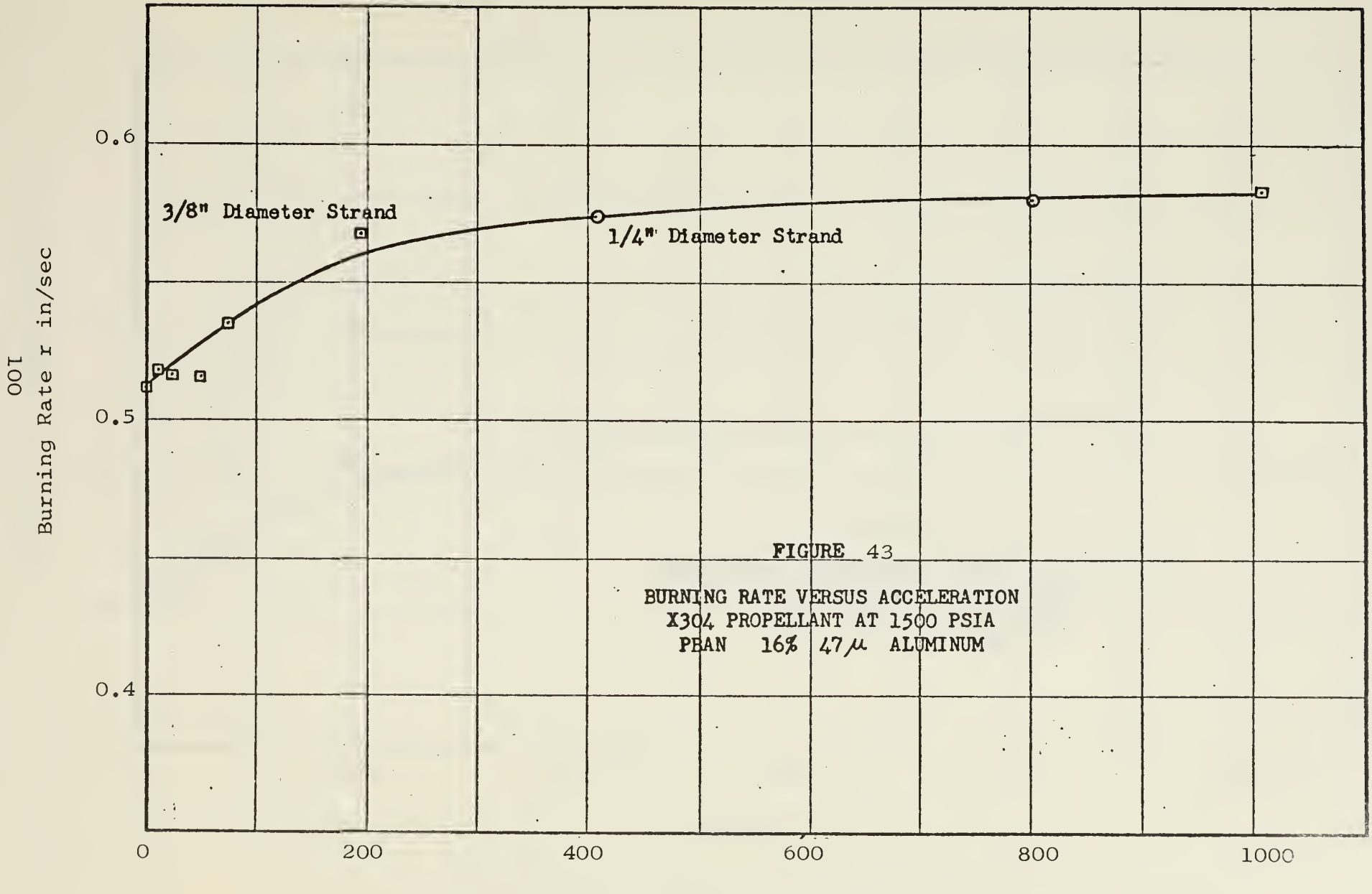

FIGURE 43

BURNING RATE VERSUS ACCELERATION
X304 PROPELLANT AT 1500 PSIA
PBAN 16% 47μ ALUMINUM

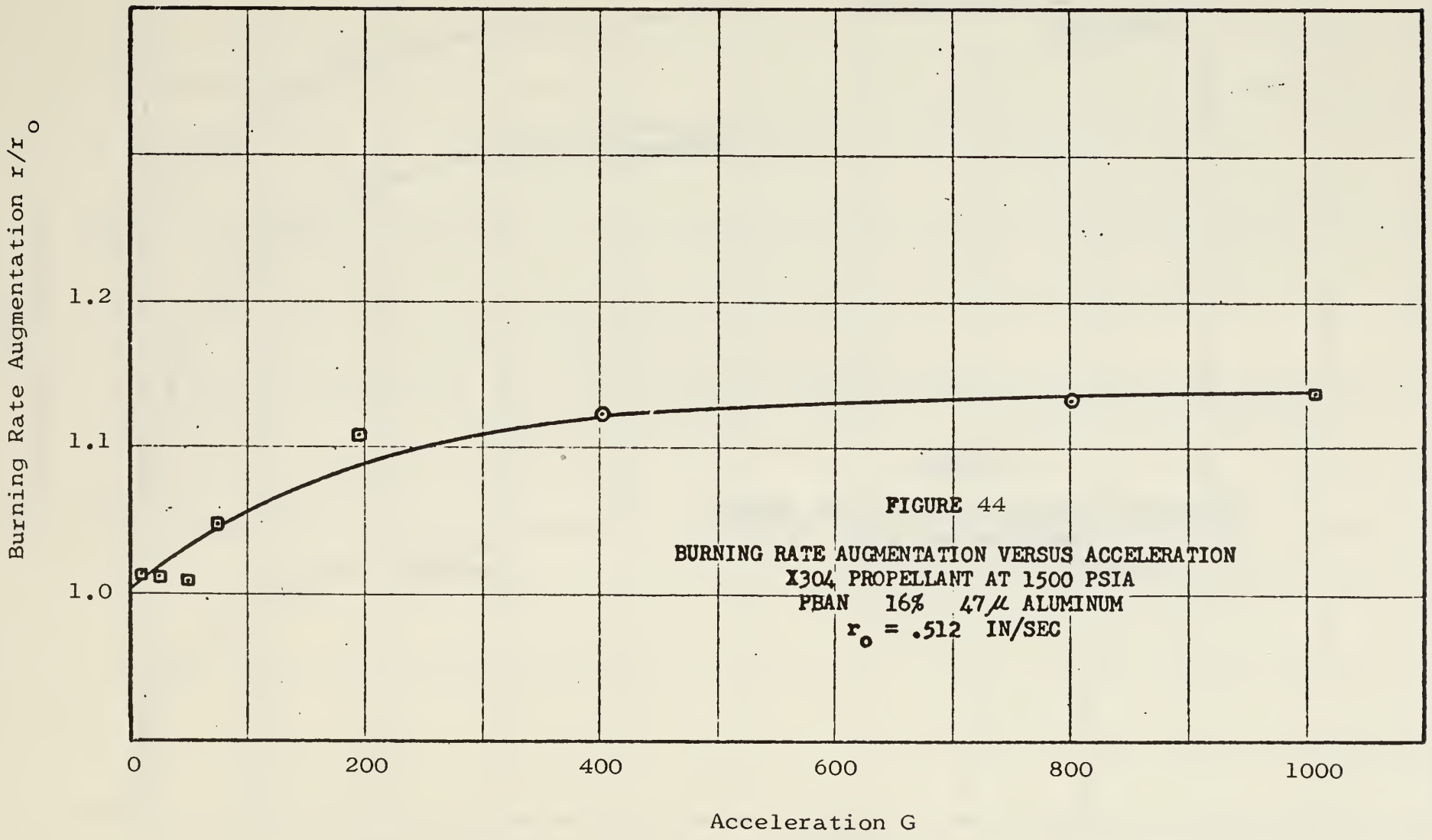

FIGURE 44

BURNING RATE AUGMENTATION VERSUS ACCELERATION
X304 PROPELLANT AT 1500 PSIA
PBAN 16% 47μ ALUMINUM
r_o = .512 IN/SEC

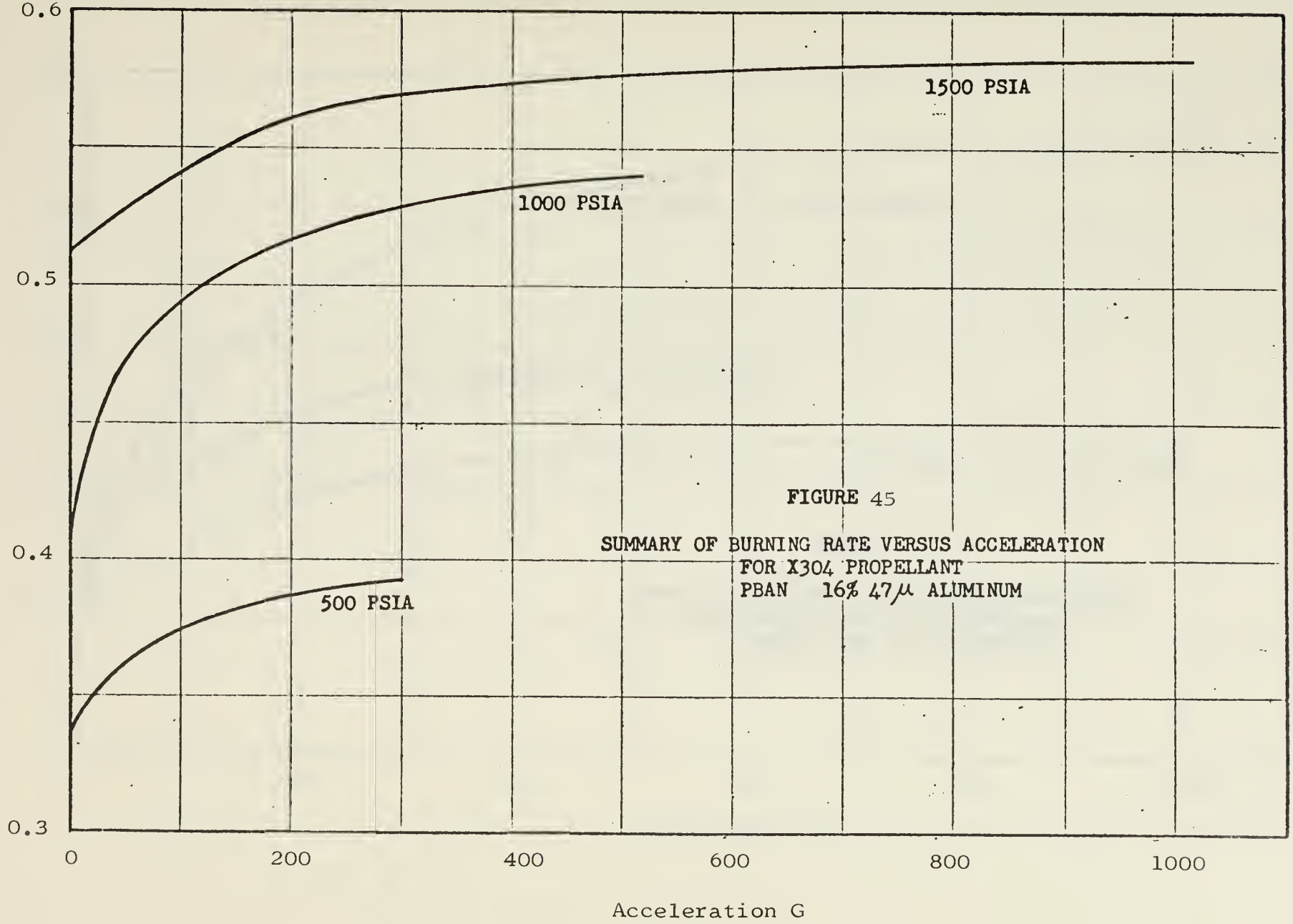

FIGURE 45

SUMMARY OF BURNING RATE VERSUS ACCELERATION
FOR X304 PROPELLANT
PBAN 16% 47μ ALUMINUM

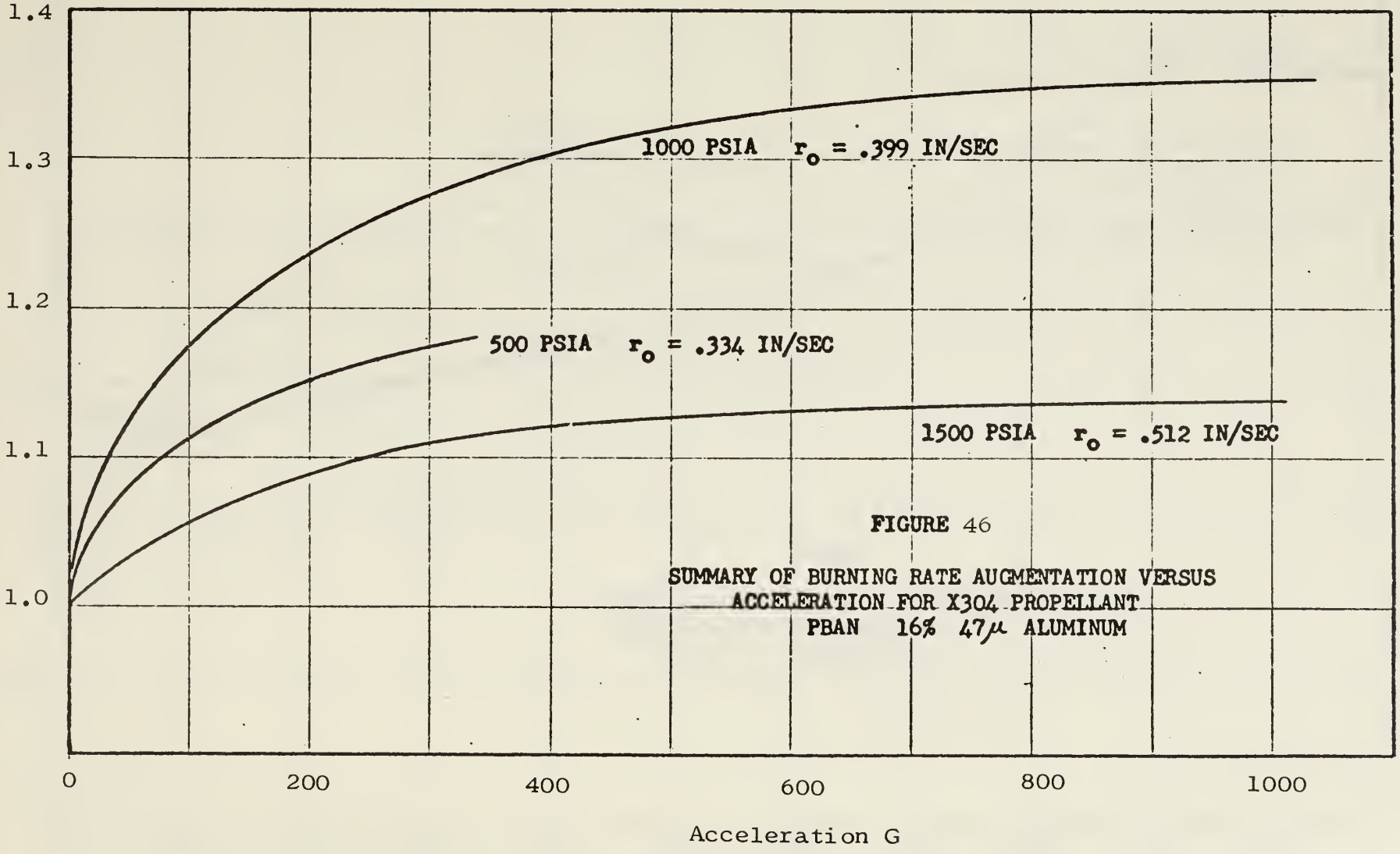

FIGURE 46

SUMMARY OF BURNING RATE AUGMENTATION VERSUS ACCELERATION FOR X304 PROPELLANT PBAN 16% 47μ ALUMINUM

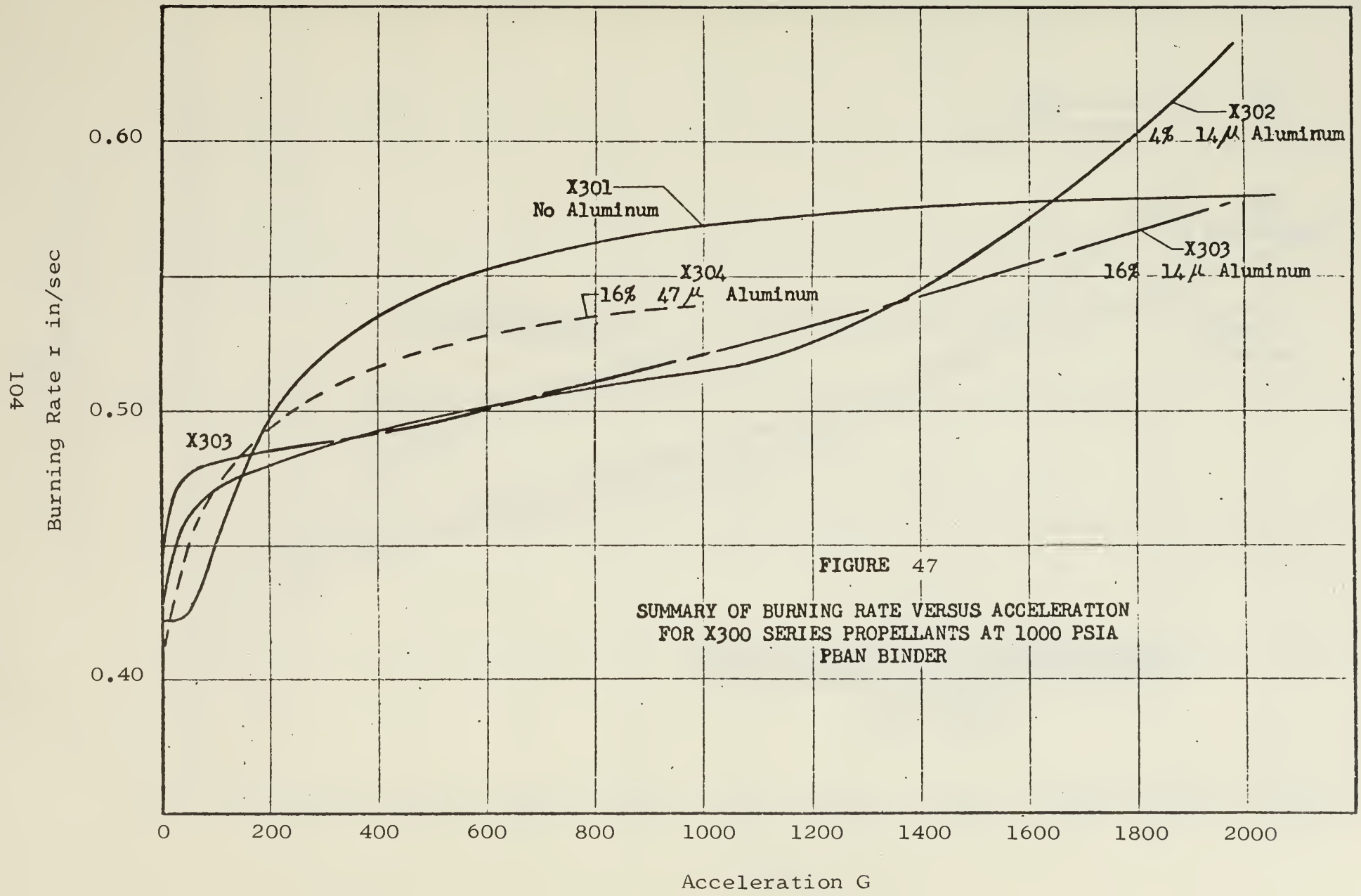

FIGURE 47

SUMMARY OF BURNING RATE VERSUS ACCELERATION
FOR X300 SERIES PROPELLANTS AT 1000 PSIA
PBAN BINDER

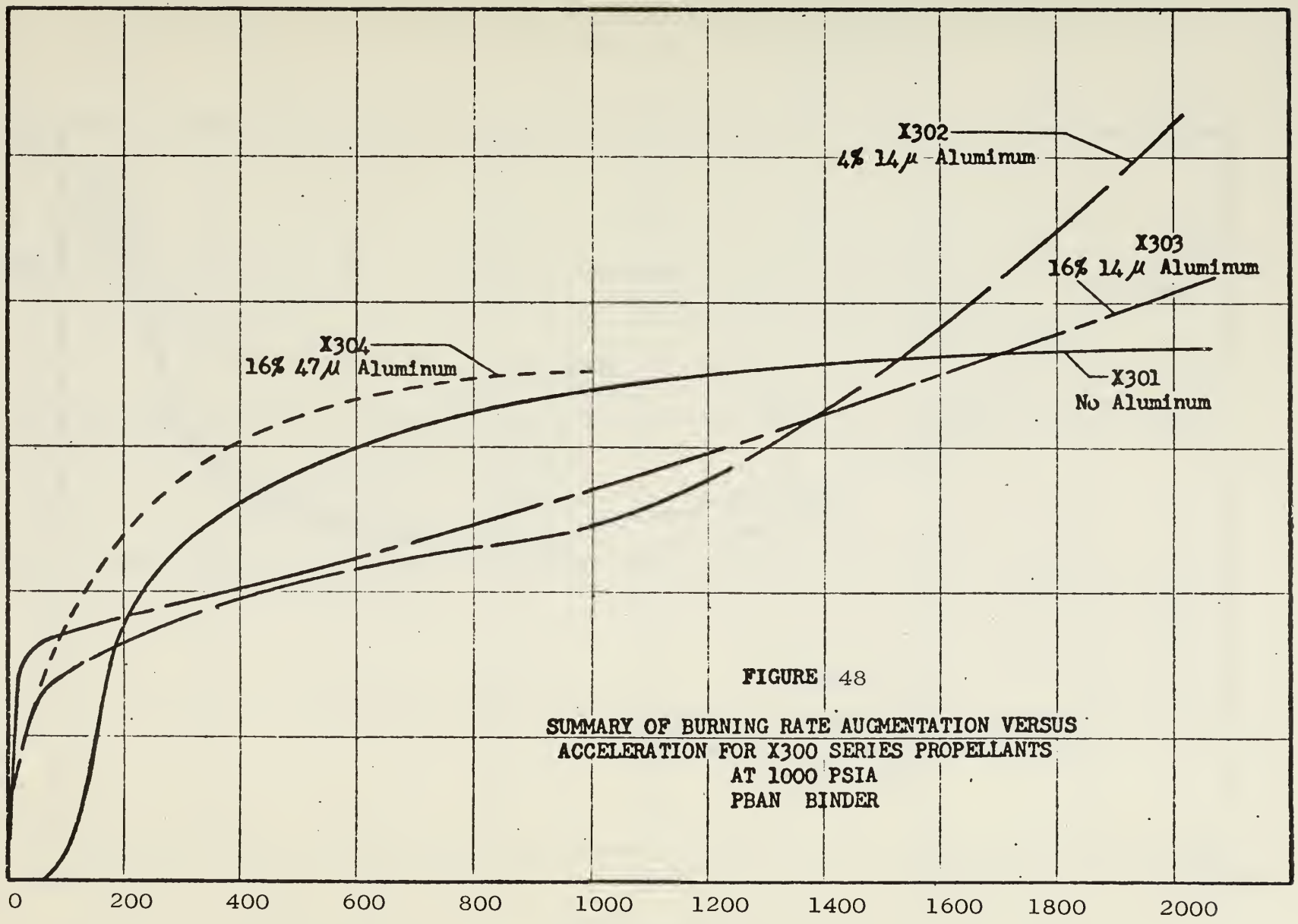

FIGURE 48

SUMMARY OF BURNING RATE AUGMENTATION VERSUS ACCELERATION FOR X300 SERIES PROPELLANTS AT 1000 PSIA PBAN BINDER

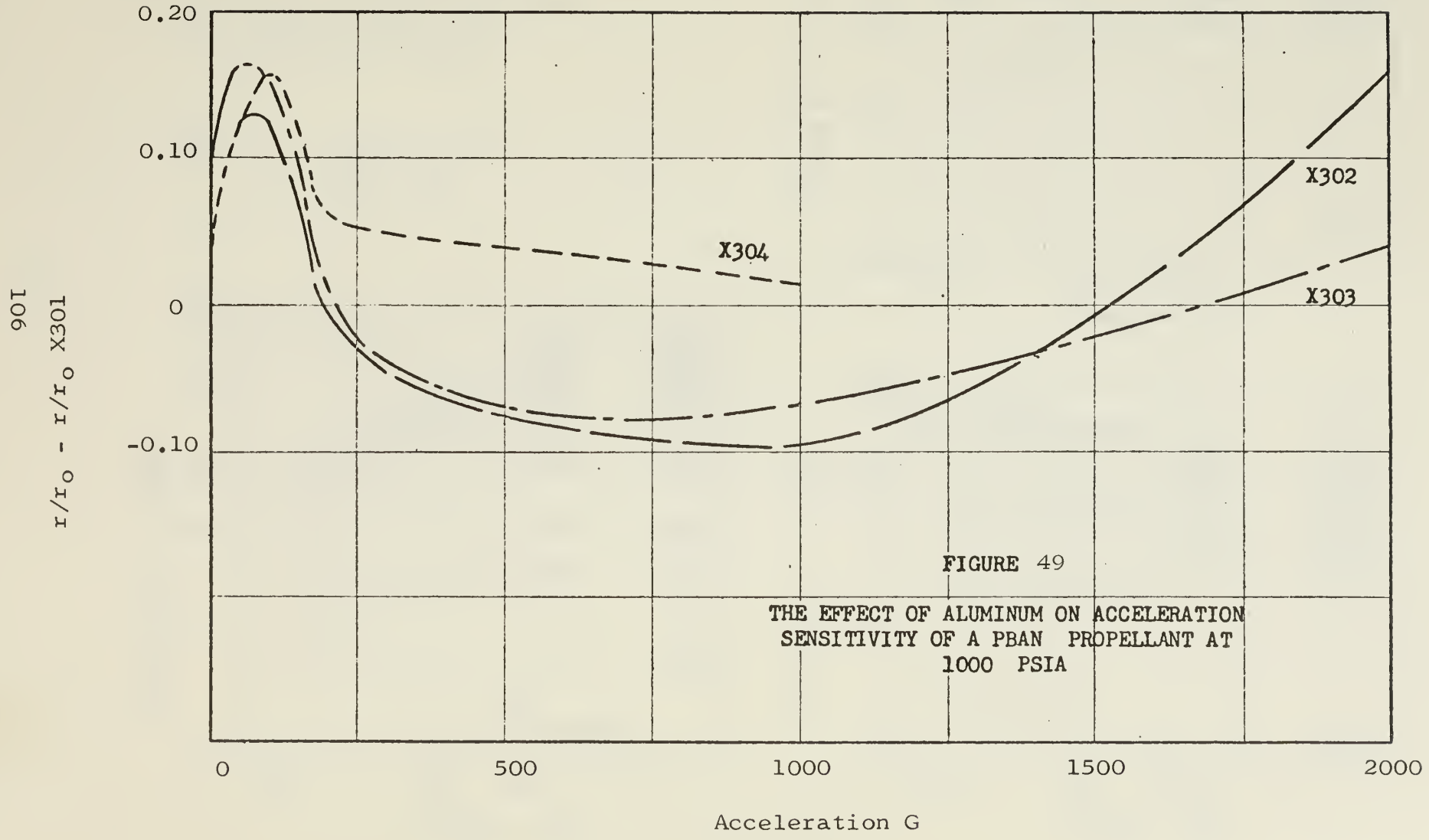

FIGURE 49

THE EFFECT OF ALUMINUM ON ACCELERATION SENSITIVITY OF A PBAN PROPELLANT AT 1000 PSIA

FIGURE 50

THE EFFECT OF ACCELERATION
ON BURNING RATE PRESSURE EXPONENT
X100 SERIES PROPELLANTS
POLYURETHANE BINDER

NOte: G = Acceleration
n = Exponent
($r = aP^n$)

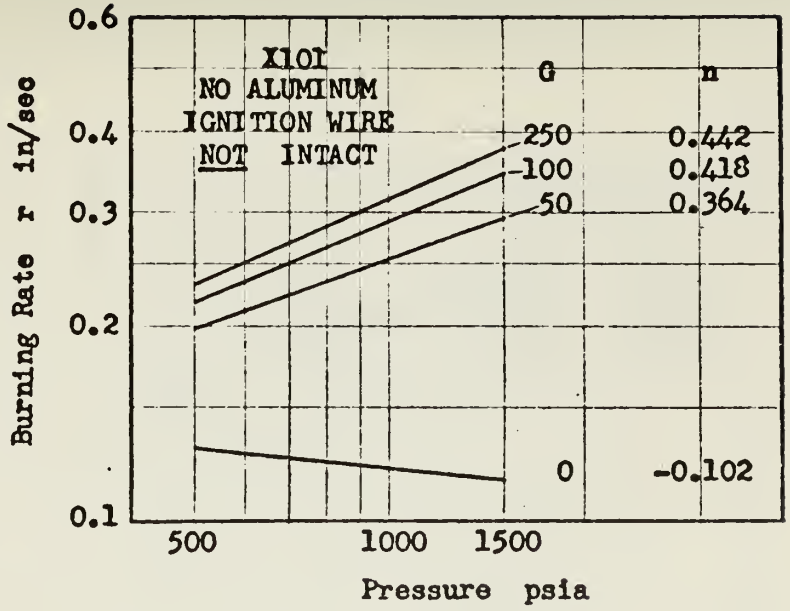

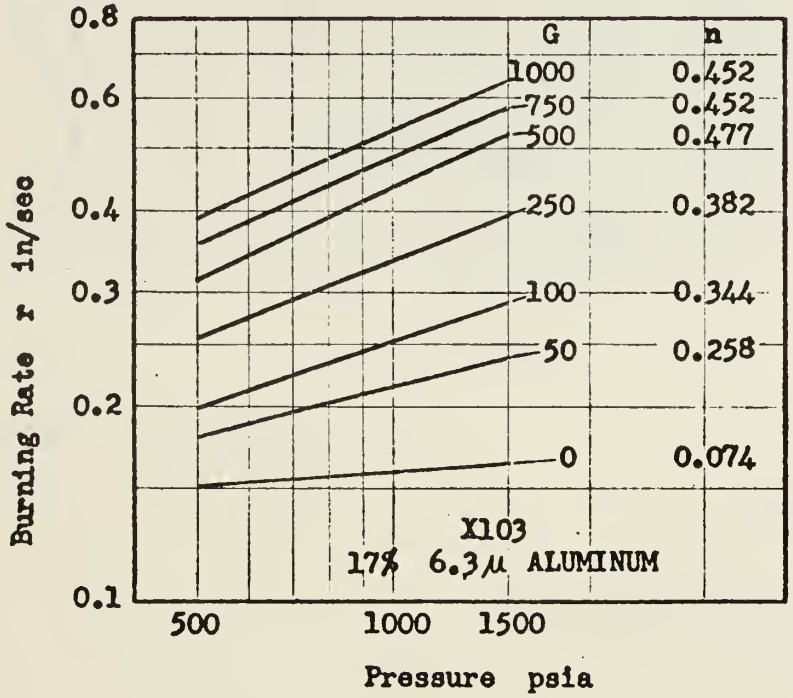

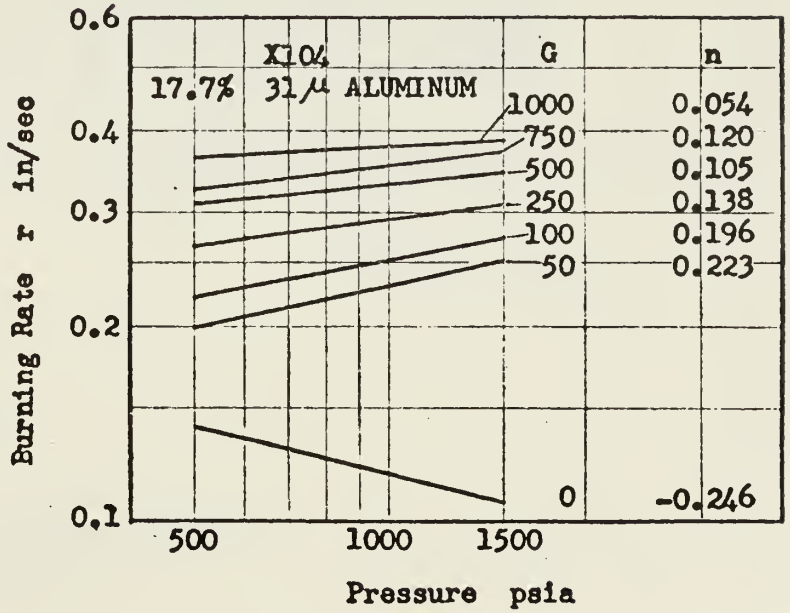

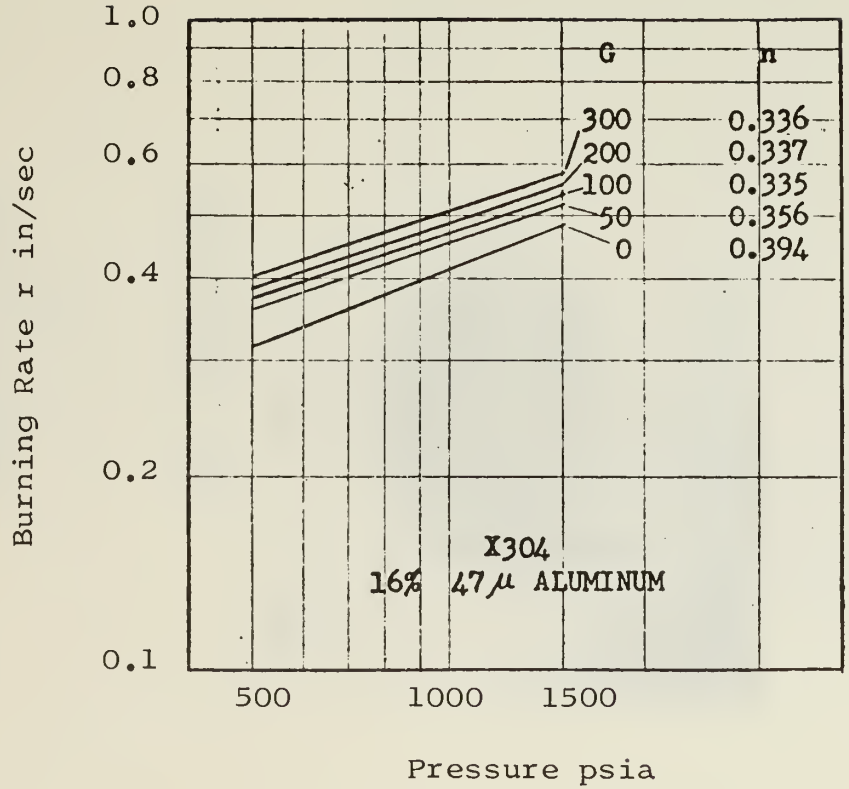

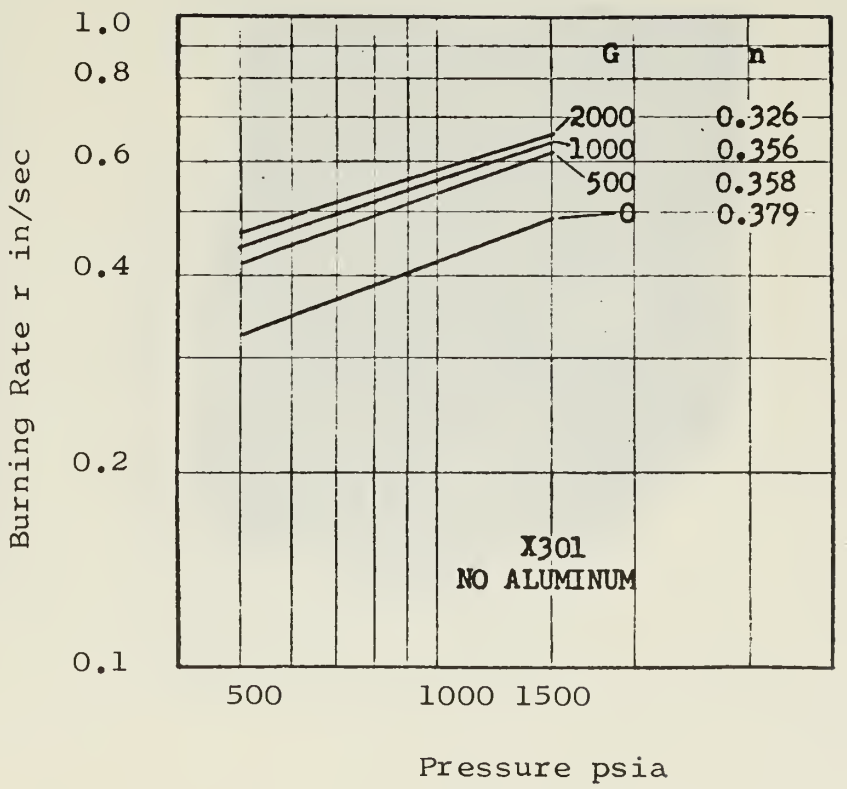

Note: G = Acceleration
n = Exponent
($r = aP^n$)

FIGURE 51

THE EFFECT OF ACCELERATION
ON BURNING RATE PRESSURE EXPONENT
X300 SERIES PROPELLANTS
PBAN BINDER

X10% Propellant 1014G
Magnification: 15X

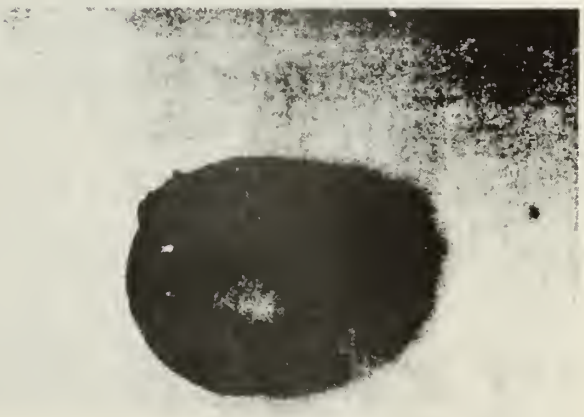

X200 Propellant 8.3G
Magnification: 10X

FIGURE 52

PROPELLANT RESIDUES

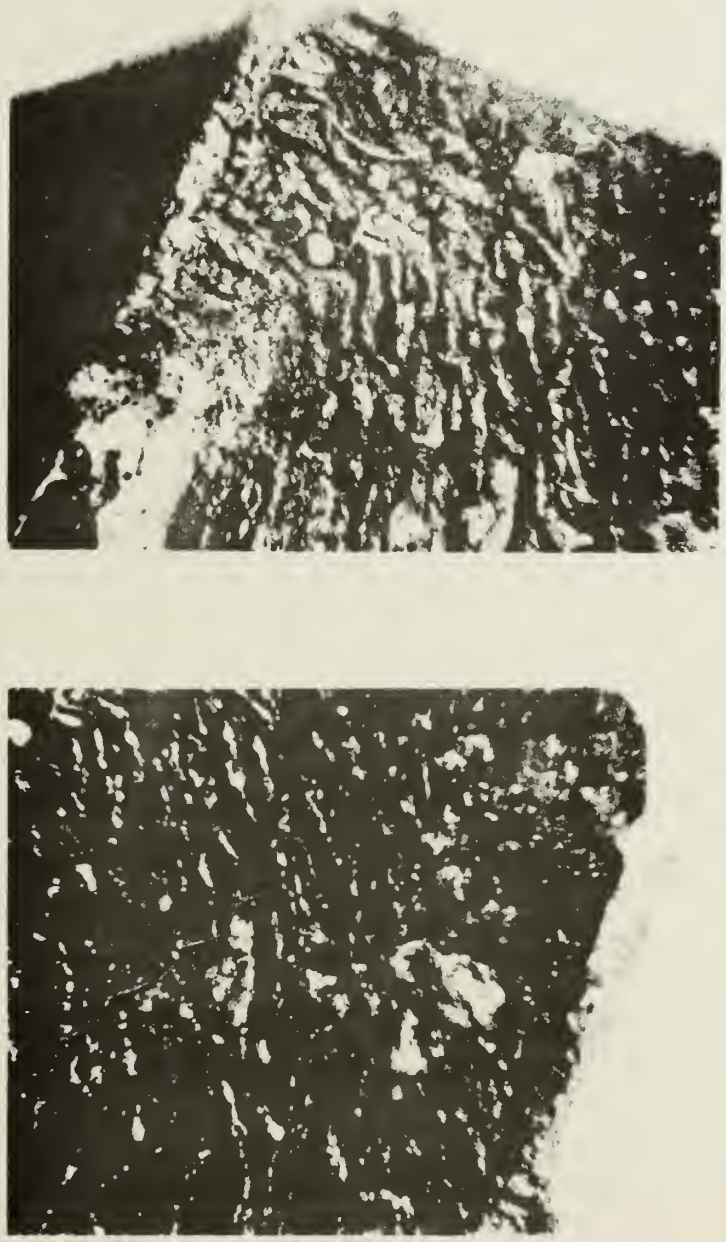

FIGURE 53

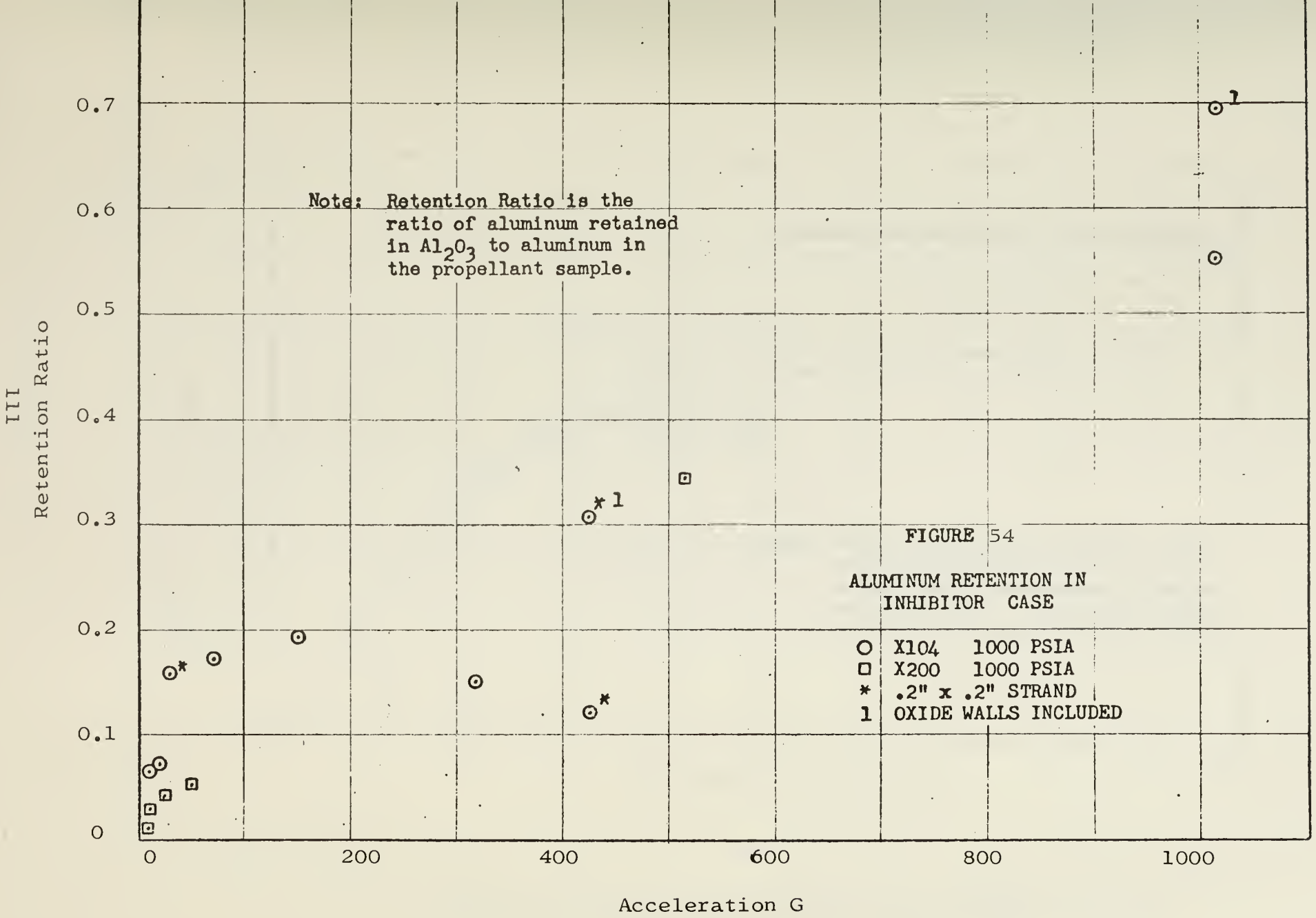

FIGURE 54

ALUMINUM RETENTION IN INHIBITOR CASE

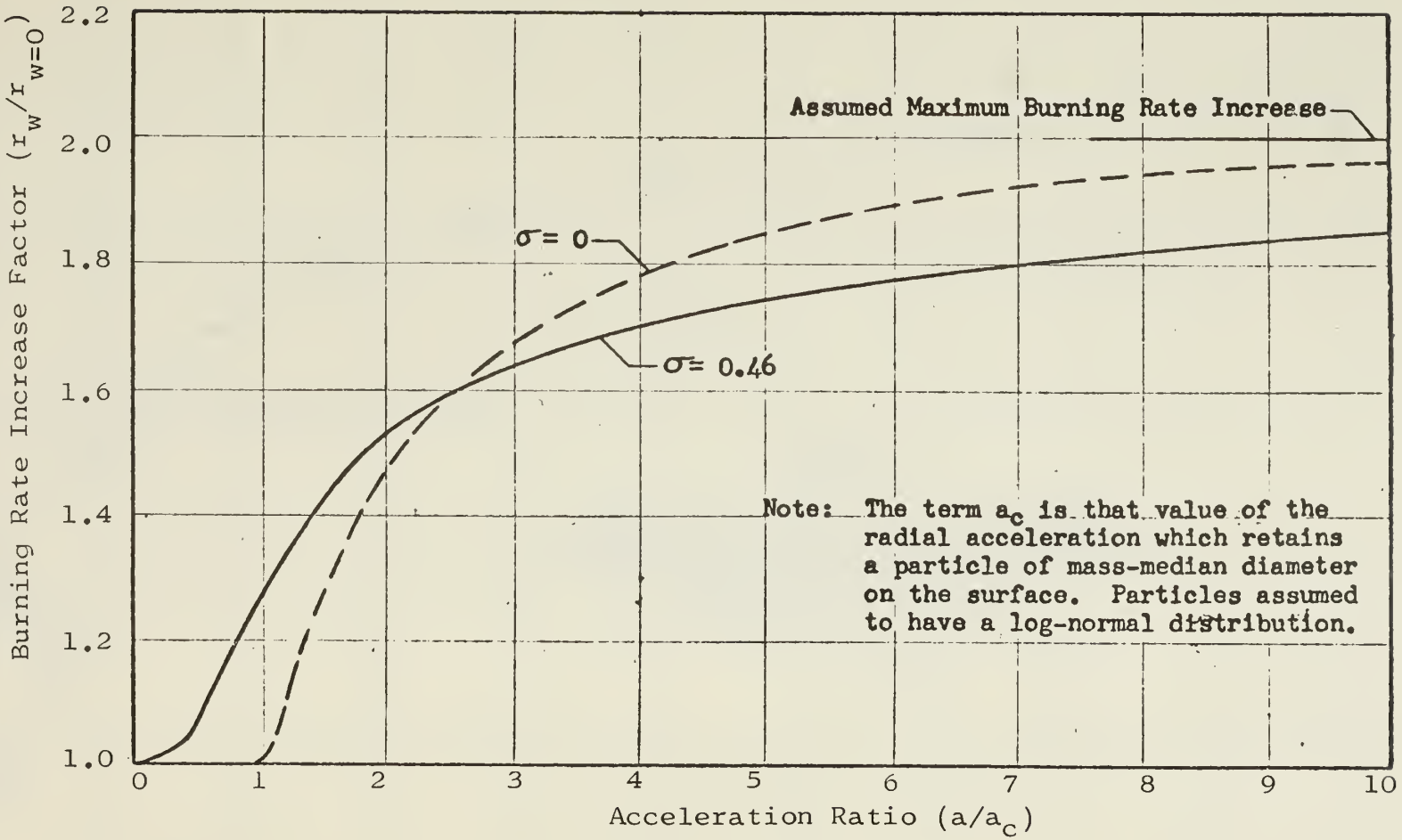

FIGURE 55

PREDICTED BURNING RATE INCREASE WITH ACCELERATION LEVEL
FOR TWO PARTICLE SIZE DISTRIBUTIONS
(CROWE, et al., [6])

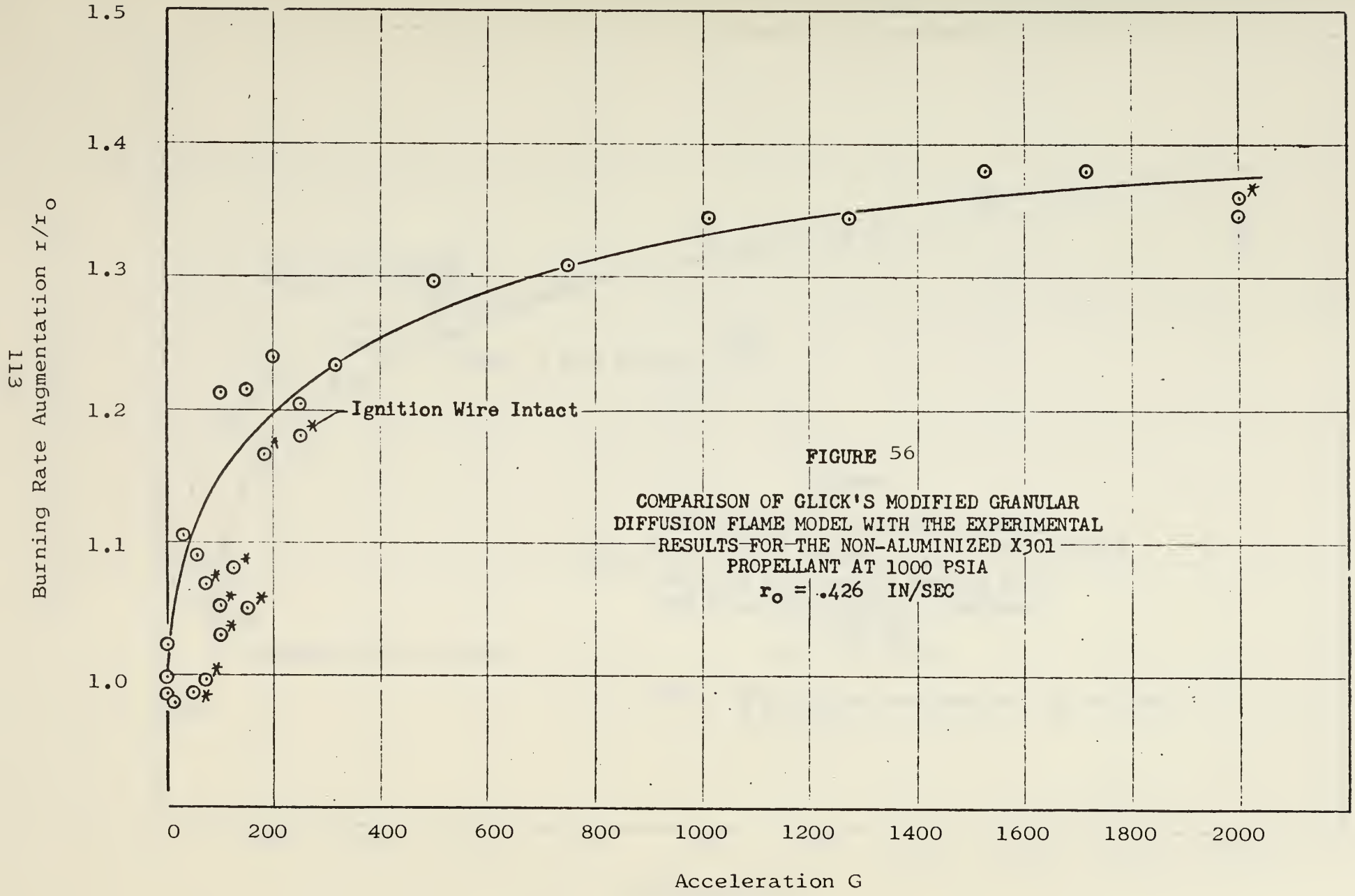

FIGURE 56

COMPARISON OF GLICK'S MODIFIED GRANULAR DIFFUSION FLAME MODEL WITH THE EXPERIMENTAL RESULTS FOR THE NON-ALUMINIZED X301 PROPELLANT AT 1000 PSIA

r_o = .426 IN/SEC

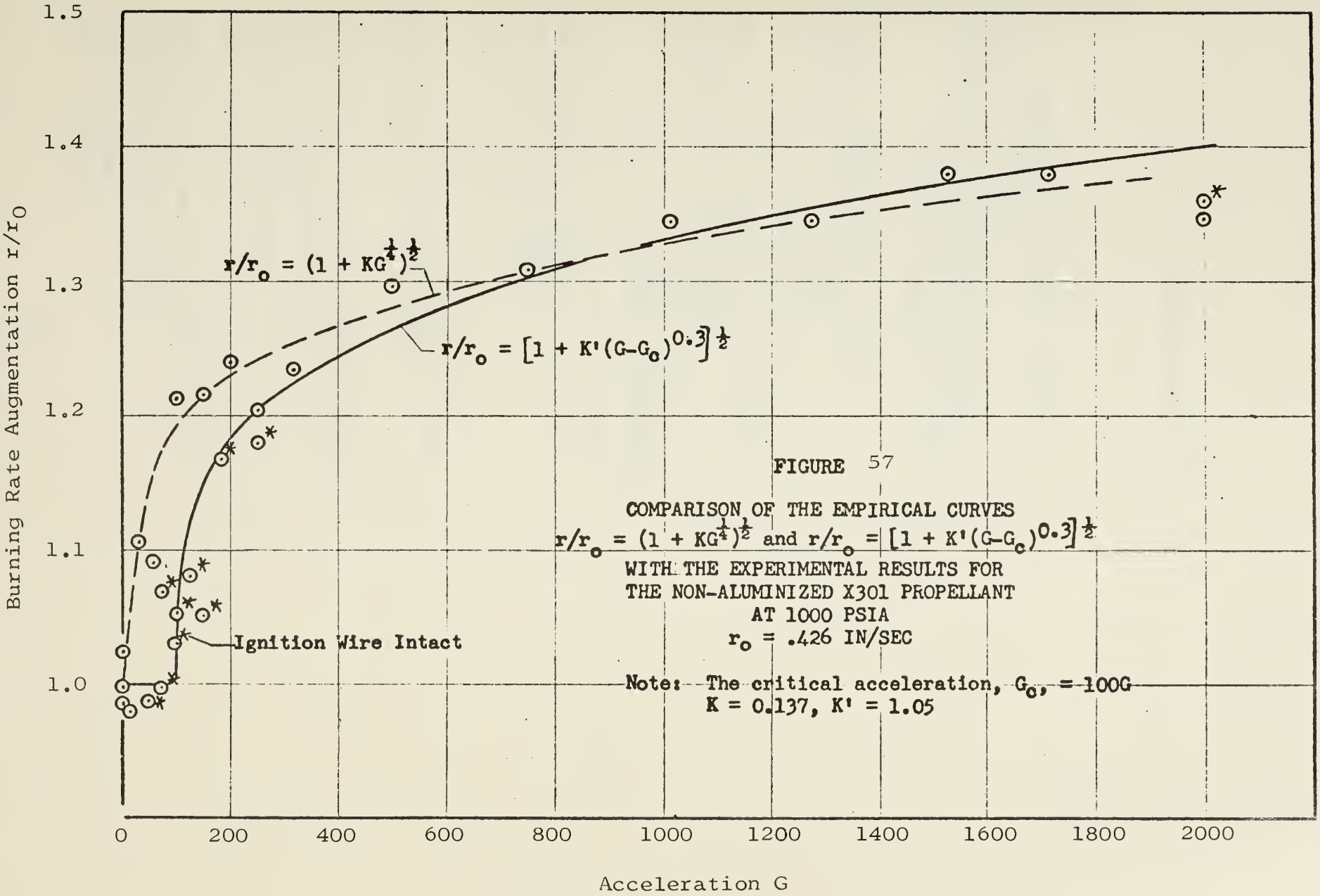

FIGURE 57

COMPARISON OF THE EMPIRICAL CURVES
$r/r_o = (1 + KG^{\frac{1}{4}})^{\frac{1}{2}}$ and $r/r_o = [1 + K'(G-G_c)^{0.3}]^{\frac{1}{2}}$
WITH THE EXPERIMENTAL RESULTS FOR
THE NON-ALUMINIZED X301 PROPELLANT
AT 1000 PSIA
r_o = .426 IN/SEC

Note: The critical acceleration, G_o, = 100G
K = 0.137, K' = 1.05

DISTRIBUTION LIST

		No. Copies
1.	U. S. Department of the Interior Bureau of Mines 4800 Forbes Avenue Pittsburgh, Pennsylvania 152133 Attn: M. M. Dolinar, Repts. Librarian Explosives Research Center	2
2.	Central Intellingence Agency 2430 E. Street, N. W. Washington, D. C. 20505 Attn: OCD, Standard Dist.	1
3.	Office of the Director of Defense Research and Engineering Washington, D. C. 20301 Attn: Dr. H. W. Schulz, Office of Asst. Dir. (Chem. Technology)	1
4.	National Aeronautics & Space Admin. Lewis Research Center 21000 Brookpark Road Cleveland, Ohio 44135 Attn: Library	1
5.	John F. Kennedy Space Center NASA Cocoa Beach, Florida 32931 Attn: Library	1
6.	National Aeronautics & Space Admin. Manned Spacecraft Center P. O. Box 1537 Houston, Texas 77001 Attn: Library	1
7.	National Aeronautics & Space Admin. Langley Research Center Langley Air Force Base Virginia 23365 Attn: Library	3

8. National Aeronautics & Space Admin. 1
Washington, D. C. 20546
Attn: Office of Technical Information &
Educational Programs, Code ETL

9. National Aeronautics & Space Admin. 1
Washington, D. C. 20546
Attn: R. W. Ziem (RPS)

10. National Aeronautics & Space Admin. 1
Goddard Space Flight Center
Greenbelt, Maryland 20771
Attn: Library

11. Defense Documentation Center 20
Cameron Station
Alexandria, Virginia 22314

12. Naval Ordnance Systems Command 2
Department of the Navy
Attn: ORD 9312
Washington, D. C. 20360

13. Naval Ordnance Systems Command 2
Department of the Navy
Attn: ORD-0331
Washington, D. C. 20360

14. Naval Air Systems Command 2
Department of the Navy
Attn: AIR-330
Washington, D. C. 20360

15. RTD(RTNP) 1
Bolling AFB
Washington, D. C. 20332

16. Arnold Eng. Development Center 1
Attn: AEOIM
Air Force Systems Command
Tullahoma, Tennessee 37389

17. AFRPL (RPC) 1
Edwards, California 93523

18. AFSC (SCTR) 1
Andrews AFB
Washington, D. C. 20331

19. AFRPL (RPR) 1
Edwards, California 93523

20. AFFTC (FTBPP-2) 1
Technical Library
Edwards AFB, California 93523

21. Office of Research Analyses (OAR) 1
Attn: RRRT
Holloman AFB, New Mexico 88330

22. Air Force Office of Scientific Research 1
Washington, D. C. 20333
Attn: SREP, Dr. J. F. Masi

23. Wright-Patterson AFB, Ohio 45433 1
Attn: AFML (MAAE)

24. FTD (TDBTL) 1
Wright-Patterson AFB, Ohio 45433

25. Commanding Officer 2
Ballistic Research Laboratories
Aberdeen Proving Ground, Maryland
Attn: AMXBR-I 21005

26. Department of the Army 1
U. S. Army Materiel Command
Washington, D. C. 20315

27. Commanding Officer 1
U. S. Army Research Office (Durham)
Box CM, Duke Station
Durham, North Carolina 27706

28. Commanding Officer 1
Frankford Arsenal
Philadelphia, Pennsylvania 19137
Attn: Propellant and Explosives
Section, 1331

29. U. S. Army Missile Command — 4
Redstone Scientific Information Center
Redstone Arsenal, Alabama 35808
Attn: Chief, Document Section

30. Commanding General — 3
White Sands Missile Range
New Mexico 88002
Attn: Technical Library

31. Naval Air Systems Command — 2
Department of the Navy
Attn: AIR-604
Washington, D. C. 20360

32. Naval Air Systems Command — 2
Department of the Navy
Attn: AIR-5367
Washington, D. C. 20360

33. Naval Ordnance Systems Command — 1
Department of the Navy
Attn: ORD-0624
Washington, D. C. 20360

34. Naval Air Systems Command — 1
Department of the Navy
Attn: ORD-0624
Washington, D. C. 20360

35. Commander — 2
U. S. Naval Missile Center
Point Mugu, California 93041
Attn: Technical Library

36. U. S. Naval Ordnance Laboratory — 1
Corona, California 91720
Attn: P. J. Slota, Jr.

37. Commander — 2
U. S. Naval Ordnance Laboratory
White Oak
Silver Spring, Maryland 20910
Attn: Library

38. Commander (Code 753) 6
U. S. Naval Ordnance Test Station
China Lake, California 93557
Attn: Technical Library

39. Superintendent 1
U. S. Naval Postgraduate School
Naval Academy
Monterey, California 93940

40. Commanding Officer 2
U. S. Naval Propellant Plant
Indian Head, Maryland 20640
Attn: Technical Library

41. Commanding Officer 1
Office of Naval Research
1030 E. Green Street
Pasadena, California 91101

42. Department of the Navy 1
Office of Naval Research
Washington, D. C. 20360

43. Director 1
Special Projects Office
Department of the Navy
Washington, D. C. 20360

44. Commanding Officer 1
U. S. Naval Underwater Ordnance Station
Newport, Rhode Island 02844
Attn: W. W. Bartlett

45. Commander 1
U. S. Naval Weapons Laboratory
Dahlgren, Virginia 22448
Attn: Technical Library

46. U. S. Naval Weapons Quality Assurance Office 1
Regional Patent Department
Naval Weapons Plant
Washington, D. C. 20360
Attn: Code QAO-8 (Mr. C. Funkhouser)

47. Aerojet-General Corporation 2
P. O. Box 296
Azusa, California 91703
Attn: Librarian

48. Aerojet-General Corporation — 1
11711 South Woodruff Avenue
Downey, California 90241
Attn: F. M. West, Chief Librarian

49. Aerojet-General Corporation — 3
Attn: Tech. Library 2484-2015A
P. O. Box 15847
Sacramento, Claifornia 95809

50. Aeronutronic Div. Philco Corporation — 1
Ford Road
Newport Beach, California 92600
Attn: Dr. L. H. Linder, Manager
Technical Information Dept.

51. Aeroprojects, Inc. — 1
310 East Rosedale Avenue
West Chester, Pennsylvania 19380
Attn: C. D. McKinney

52. Aerospace Corporation — 2
P. O. Box 95085
Los Angeles, California 90045
Attn: Library-Documents

53. Allied Chemical Corporation — 1
P. O. Box 70
Morristown, New Jersey 07960
Attn: Security Officer

54. American Cyanamid Company — 1
1937 W. Main Street
Stamford, Connecticut 06902
Attn: Security Officer

55. IIT Research Institute — 1
Technology Center
Chicago, Illinois 60616
Attn: C. K. Hersh, Chemistry Division

56. ARO, Inc. — 1
Arnold Engrg. Dev. Center
Arnold A F Station, Tennessee 37389
Attn: Dr. B. H. Goethert
Chief Scientist

57. Atlantic Research Corporation 2
Shirley Highway and Edsall Road
Alexandria, Virginia 22314
Attn: Security Office for Library

58. Denver Seminary 1
University of Denver
University Park
Denver, Colorado 80205

59. Batelle Memorial Institute 1
Columbus Laboratory
505 King Avenue
Columbus, Ohio 43201
Attn: Report Library, (CPIA)

60. Bell Aerosystems 1
Box 1
Buffalo, New York 14205
Attn: Technical Library

61. The Boeing Company 1
Aero Space Division
P. O. Box 3707
Seattle, Washington 98124
Attn: Ruth E. Peerenboom,
Library Processes Supervisor (1190)

62. Chemical Propulsion Information Agency 2
Applied Physics Laboratory
8621 Georgia Avenue
Silver Spring, Maryland 20910

63. Douglas Aircraft Co., Inc. 1
Santa Monica Division
3000 Ocean Park Boulevard
Santa Monica, California 90405
Attn: Mr. J. L. Waisman

64. The Dow Chemical Company 1
Security Section
Box 31
Midland, Michigan 48641
Attn: Dr. R. S. Karpiuk, 1710 Building

65. E. I. duPont deNemours and Company 1
Eastern Laboratory
Gibbstown, New Jersey 08027
Attn: Mrs. Alice R. Steward

66. Esso Research & Engineering Co. 1
Process Research Division
P. O. Box 8
Linden, New Jersey 07036
Attn: Dr. J. R. Lovett

67. Lockheed Missiles & Space Co. 1
Technical Information Center 50-14
Palo Alto Library
3251 Hanover Street
Palo Alto, California 94304
Attn: Propulsion Engineering 55-11

68. Ethyl Corporation 1
Research Laboratories
1600 West Eight Mile Road
Ferndale, Michigan 48220
Attn: E. B. Rifkin, Assistant Director,
Chemical Research

69. General Dynamics/Astronautics 1
P. O. Box 1128
San Diego, California 92112
Attn: Library and Information Services (128-00)

70. Allison Division 1
General Motors Corporation
4700 W. 10th Street
Indianapolis, Indiana 46208
Attn: Plant 8, Tech. Library
Mr. W. H. Richardson

71. Hercules Powder Company 1
Allegany Ballistics Laboratory
P. O. Box 210
Cumberland, Maryland 21501
Attn: Library

72. Hercules Powder Company 1
Research Center
Wilmington, Delaware 19899
Attn: Dr. Herman Skolnik, Manager
Technical Information Division

73. Institute for Defense Analyses — 1
400 Army-Navy Drive
Arlington, Virginia 22202
Attn: Classified Library

74. Jet Propulsion Laboratory — 1
4800 Oak Grove Drive
Pasadena, California 91103

75. Lockheed Propulsion Company — 2
P. O. Box 111
Redlands, California 92374
Attn: Miss Belle Berlad, Librarian

76. Martin Company — 1
Baltimore, Maryland
Attn: Science - Technology
Library - Mail 398

77. Martin Company, Denver Division — 1
P. O. Box 179
Denver, Colorado 80201
Attn: Res. Library, 6366

78. Martin-Marietta Corporation — 1
Sand Lake and Kirkman Roads
Orlando, Florida 32805
Attn: Library

79. Minnesota Mining & Manufacturing Co. — 2
900 Bush Avenue
St. Paul, Minnesot 55106
Attn: Code 0013 R&D
VIA: H. C. Zeman
Security Administrator

80. New York University — 1
Research Building No. 3
233 Fordham Landing Road
University Heights, New York 19468
Attn: Document Control

81. North American Aviation, Inc. — 1
Space & Information Systems Div.
12214 Lakewood Boulevard
Downy, California 90242
Attn: Technical Information Center
D/096-722 (AJol)

82. Rocket Research Corporation — 1
520 South Portland Street
Seattle, Washington 98108

83. Rocketdyne — 3
6633 Canoga Avenue
Canoga Park, California 91304
Attn: Library, Dept. 596-306

84. Rohm and Haas Company — 1
Redstone Arsenal Research Division
Huntsville, Alabama 35808
Attn: Librarian

85. TRW Systems — 2
1 Space Park
Redondo Beach, California 90200
Attn: STL Tech. Lib. Doc. Acquisitions

86. Texaco Experiment Incorporated — 1
P. O. Box 1-T
Richmond, Virginia 23202
Attn: Librarian

87. Thiokol Chemical Corporation — 2
Alpha Division, Huntsville Plant
Huntsville, Alabama 35800
Attn: Technical Director

88. Thiokol Chemical Corporation — 1
Elkton Division
Elkton, Maryland 21921
Attn: Librarian

89. Thiokol Chemical Corporation — 1
Reaction Motors Division
Denville, New Jersey 07834
Attn: Librarian

90. Thiokol Chemical Corporation — 2
Wasatch Division
P. O. Box 524
Brigham City, Utah 84302
Attn: Library Section

91. Thompson Ramo Wooldridge — 2
23555 Euclid Avenue
Cleveland, Ohio 44117
Attn: Librarian

92. Union Carbide Corporation — 1
Plastics Co. Div.
1 River Road
Bound Brook, New Jersey 08805
Attn: Librarian

93. United Aircraft Corporation — 1
United Technology Center
P. O. Box 358
Sunnyvale, California 94088
Attn: Librarian

94. United Aircraft Corporation — 1
Corporation Library
400 Main Street
East Hartford, Connecticut 06118
Attn: Dr. David Rix

95. United Aircraft Corporation — 1
Pratt & Whitney Fla. Res. & Dev. Ctr.
P. O. Box 2691
W. Palm Beach, Florida 33402
Attn: Library

96. General Electric Company — 1
Apollo Support Department
P. O. Box 2500
Daytona Beach, Florida 32015
Attn: C. Day

97. Stanford Research Institute — 1
Propulsion Sciences Div.
Menlo Park, Calif. 94025
Attn: Document Custodian

98. British Defense Staff, British Embassy — 4
3100 Massachusetts Avenue
Washington, D. C. 20008
Attn: Scientific Information Officer
VIA: Agency Int'l Programs Offices

99. Defense Research Member — 4
Cannadian Joint Staff (W)
2450 Massachusetts Avenue
Washington, D. C. 20008
VIA: Agency Int'l Programs Offices

100. Commanding Officer — 1
Ammunition Procurement & Supply Agnecy
Joilet, Illinois 60400
Attn: Engr. Library

101. Commanding Officer — 1
Radford Arsenal
Radford, Virginia 24141

102. Department of Commerce — 1
Office of Export Control
Washington, D. C.
Attn: Chief, Chemistry & Fuels Section
Paul M. Terlizzi

103. AFRPL (RPCE) — 1
Edwards, California 93523

104. Callery Chemical Company — 1
Research and Development
Callery, Pennsylvania 16024
Attn: Document Control

105. Ethyl Corporation — 1
P. O. Box 3091
Baton Rouge, Louisiana 70805

106. Hercules Powder Company — 1
Bacchus Works
Magna, Utah 84044
Attn: Librarian

107. Olin Mathieson Chemical Corporation — 1
Research Library 1-K-3
275 Winchester Avenue
New Haven, Connecticut 06511
Attn: Mail Control Room,
Mrs. Laura M. Kajuti

108.	Olin Mathieson Chemical Corporation Marion, Illinois 62959 Attn: Research Library Box 508	1
109.	Pennsalt Chemicals Corporation Technological Center 900 First Avenue King of Prussia, Pennsylvania 19406	1
110.	Purdue University School of Mechanical Engineering Attn: Dr. B. A. Reese Lafayette, Indiana 47907	1
111.	North American Aviation Rocketdyne Division McGregor Plant McGregor, Texas 76657	1
112.	Shell Development Company 1400 53rd Street Emeryville, California 94608	1
113.	The University of Utah College of Engineering 1400 E. Second South Salt Lake City, Utah 84112 Attn: Prof. M. L. Williams	2
114.	Texaco, Inc. P. O. Box 509 Beacon, New York 12508 Attn: Dr. R. E. Conary, Manager	1
115.	Aerospace Corporation 1111 Mill Street San Bernadino, California 92402 Attn: Mr. John S. Wise	1
116.	Los Alamos Scientific Laboratory University of California P. O. Box 1663 Los Alamos, New Mexico	1

117. Scientific and Technical Information Facility 2
P. O. Box 5700
Bethesda, Maryland 20014
Attn: NASA Representative

118. Library 2
Naval Postgraduate School
Monterey, California 93940

119. Department of Aeronautics 2
Naval Postgraduate School
Monterey, California 93940

120. Dr. Roy E. Reichenbach 10
Department of Aeronautics
Naval Postgraduate School
Monterey, California 93940

DOCUMENT CONTROL DATA - R&D

(Security classification of title, body of abstract and indexing annotation must be entered when the overall report is classified)

1. ORIGINATING ACTIVITY *(Corporate author)*
Naval Postgraduate School
Monterey, California 93940

2a. REPORT SECURITY CLASSIFICATION
UNCLASSIFIED

2b GROUP

3 REPORT TITLE
AN INVESTIGATION OF THE EFFECT OF ACCELERATION ON THE BURNING RATE OF COMPOSITE PROPELLANTS

4 DESCRIPTIVE NOTES *(Type of report and inclusive dates)*
Technical Report

5 AUTHOR(S) *(Last name, first name, initial)*
Anderson, James B. and Reichenbach, Roy E.

6. REPORT DATE	7a. TOTAL NO. OF PAGES	7b. NO. OF REFS
July, 1967	129	11

8a CONTRACT OR GRANT NO.

b. PROJECT NO.
NAVORDSYSCOM Req. No.
c. 17-7-5073

d.

9a. ORIGINATOR'S REPORT NUMBER(S)

9b. OTHER REPORT NO(S) *(Any other numbers that may be assigned this report)*

10. AVAILABILITY/LIMITATION NOTICES
This document has been approved for public release and sale; its distribution is unlimited.

11. SUPPLEMENTARY NOTES

12 SPONSORING MILITARY ACTIVITY
Naval Air Systems Command
Navy Department, Washington, D. C.

13 ABSTRACT

The average burning rates of composite solid rocket propellant were measured in acceleration fields up to 2000 times the standard acceleration of gravity. The acceleration vector was perpendicular to and into the burning surface. Propellant strands were burned in a combustion bomb mounted on a centrifuge, and surge tanks were employed to ensure essentially constant pressure burning at 500, 1000, and 1500 psia. The burning rates of both aluminized and non-aluminized composite propellants were found to depend on acceleration. The effect of acceleration on burning rate was found to depend on the burning rate of the propellant without acceleration, aluminum mass loading, and aluminum mass median particle size. The relative burning rate increase was found to be greater for slow burning propellant than for faster burning propellants. The experimental results are compared to the analytical models proposed by Crowe for aluminized propellants and by Glick for non-aluminized propellants. The results indicate that these models do not adequately predict the observed relative burning rate increase with acceleration, and hence that more complex modeling will be required to explain the observed acceleration effect.

DD FORM 1 JAN 64 1473

14 KEY WORDS	LINK A		LINK B		LINK C	
	ROLE	WT	ROLE	WT	ROLE	WT
Solid Propellant, Burning Rate, Acceleration						

TL785 94029
.A6 Anderson
An investigation of the effect of acceleration on the burning rate of composite propellants.